UNIVERSITÀ DEGLI STUDI DI TRIESTE

XXX CICLO DEL DOTTORATO DI RICERCA IN

Scienze della terra, fluidodinamica e matematica

High resolution earthquake relocation along Idrija fault system in Western Slovenia and its application in understanding the deformation along the active faults of NW External Dinarides

Settore scientifico-disciplinare: Scienze della terra

DOTTORANDO / A
BLAŽ VIČIČ

COORDINATORE
PROF. PIERPAOLO OMARI

SUPERVISORE DI TESI
PROF. GIOVANNI COSTA
PROF. ABDELKRIM AOUDIA

ANNO ACCADEMICO 2016/2017

High resolution earthquake relocation along Idrija fault system in Western Slovenia and its application in understanding the deformation along the active faults of NW External Dinarides

By

Blaž Vičič

University of Trieste, 2017

A blank page

Astratto

L'Italia nordorientale e la Slovenia occidentale si trovano in una regione a moderata attività sismica. Rari sono i forti terremoti che, nel passato, hanno colpito questa regione; si possono citare ad esempio il terremoto di Idria del 1511 con magnitudo 6.9, la sequenza del Friuli del 1976 con magnitudo superiore a 6 e i terremoti della faglia di Ravne del 1998 e del 2004 con magnitudo rispettivamente di 5.6 e 5.2. Numerosi studi geodetici, geomorfologici e geologici hanno mostrato che il sistema di faglie dell'Idrija (IFS) è un sistema di faglie attivo, con movimenti che possono arrivare ai 3.8 mm/anni su tutte le faglie.

A partire dal 2006 l'area del IFS è stata coperta da una rete relativamente densa di stazioni sismiche broadband che registrano in continuo. Al fine di comprendere meglio il IFS stesso, in questo lavoro di tesi è stato condotto uno studio sismologico dettagliato.

Per migliorare la conoscenza della geometria del sistema di faglia, del processo di fagliazione e del suo comportamente temporale, sono stati analizzati i dati di tutte le stazioni presenti nella regione. Prima di tutto sono state analizzate le serie temporali usando il classico algoritmo STA/LTA per l'individuazione di terremoti. In seguito, dopo un iniziale esame del database, sono stati rivisti manualmente i tempi di arrivo delle fasi dei terremoti identificati al fine di ottenere un tempo di arrivo il più preciso possibile. La magnitudo di completezza del catalogo così ottenuto è di 0.9. Per ottenere una magnitudo minore di completezza è stata effettuata un'ispezione manuale delle forme d'onda. In questo modo, nuovi micro terremoti sono stati aggiunti al database esistente.

Per l'identificazione di terremoti con magnitudo anche molto piccola, tutti i terremoti di magnitudo superiore a 0.8 sono stati selezionati come modello. Sulla stazione selezionata è stata effettuata l'identificazione di terremoti *matched filter*. Assieme all'identificazione di terremoti è stato eseguito anche un'identificazione precisa delle fasi usando la tecnica di cross-correlazione tra le fasi P ed S definite sui modelli con quelle dei terremoti appena individuati. I terremoti così ottenuti sono stati aggiunti al database abbassando la magnitudo di completezza a -0.7.

I terremoti rilocalizzati manualmente e i terremoti ottenuti attraverso l'identificazione matched filter hanno evidenziato chiaramente le faglie attive del IFS, mostrando attività

lungo tutte le faglie del sistema. Attraverso sezioni perpendicolari al IFS si definisce chiaramente la geometria della parte centrale del sistema. Una delle sezioni mostra che i terremoti lungo la faglia di Ravne sono molto più superficiali che sulle altre faglie del sistema ed evidenza una faglia immergente a SO che probabilmente si connette, in profondità, alla faglia di Idrija. La faglia di Idrija, nel periodo analizzato, è stata attiva solo nella sua parte settentrionale, con terremoti profondi che evidenziano un piano di faglia verticale.

Le faglie di Predjama e Selce sono le più attive nella parte centrale e meridionale del sistema. I terremoti lungo queste due faglie mostrano faglie ad immersione verticale. Infine, l'attività dei terremoti lungo la faglia di Raša è presente soprattutto nella sua estensione centrale e meridionale e mostra un piano di faglia immergente a NE.

L'identificazione ad alta risoluzione di terremoti permette di conoscere meglio l'evoluzione temporale dei terremoti lungo il IFS. Un raggruppamento temporale è stato osservato negli anni 2009-2010 e verso la fine del 2017. Nel 2009-2010 la maggior parte del sistema mostra una grossa attività, con sciami che si verificano nella parte settentrionale e centrale del sistema di faglie e molteplici serie di scosse principali-scosse di assestamento nella parte meridionale. Analogamente, nel 2017 sciami multipli e serie di scosse principali si sono verificati nella parte meridionale del sistema.

Combinando i raggruppamenti temporali dei terremoti identificati con i dataset ottenuti dell'estensimetro posto sulla faglia di Predjama, si è osservato che, nello stesso periodo in cui si era verificata l'elevata attività sismica del 2009-2010, era presente anche una deformazione superficiale significativa. La deformazione della superficie e l'attività sismica sono state modellate utilizzando i cambiamenti dello stress di Coulomb. La migliore corrispondenza è stata identificata nelle modifiche degli stress normali lungo la faglia di Idrija, le quali portano allo sblocco delle faglie parallele alla faglia di Idrija, aumentando così il tasso di terremoti lungo queste faglie e causando le deformazioni della superficie in seguito dell'estrazione e dello spostamento di fluidi in profondità.

Abstract

Northeastern Italy and Western Slovenia lies in the region of moderate earthquake activity. In the past, rare strong earthquakes struck the region, namely 1511 Idrija M 6.9, Friuli 1976 series of M 6+ and 1998 and 2004 M 5.6 and 5.2 Ravne fault earthquakes. Multiple geodetic, geomorphologic and geologic studies show, that Idrija fault system (IFS) is an active fault system, with slip rates up to 3.8 mm/yr over all the faults.

Since 2006 area of IFS is covered by relatively dense network of broadband stations recording in continuous mode. To better understand the IFS itself, a detailed seismologic study was performed in this study.

To gain the knowledge of fault system geometry, physics of faulting and temporal behaviour, the data of all the stations in the region was analysed. First, time series were analysed using classic STA/LTA detection algorithm for the detection of earthquakes. After the initial scan of the database, arrival times of phases of detected earthquakes were manually repicked to obtain as precise arrival times of phases as possible. The magnitude of completeness for the catalogue obtained in such way was 0.9. To obtain lower magnitude of completeness, additional manual inspection of waveforms was performed. New micro earthquakes were added to the existing database.

For the detection of even lower magnitude earthquakes, all the earthquakes of magnitudes above 0.8 were selected as a template earthquake. Matched filter detection of earthquakes was performed on the selected stations with simultaneous picking of precise phases as obtained from cross correlation around the P or S arrival times between template earthquake and the detected earthquake. The newly obtained earthquakes were added to the database lowering the magnitude of completeness to -0.7.

Manually relocated earthquakes and earthquakes obtained from matched filter detection clearly illuminated active faults of IFS, showing activity along all the faults of the system. From cross sections perpendicular to the IFS clear geometry was defined for the central part of the system. Cross section showed that earthquakes along Ravne fault are much shallower than on other faults of the system and illuminate a SW dipping fault which probably connects to Idrija fault at depth. Idrija fault was only active in its northern extend in the analysed period, with deeper earthquakes illuminating vertical fault plane.

Predjama and Selce fault were mostly active in the central and southern part of the system. Earthquakes along these two faults show vertically dipping faults. Finally, earthquake activity along Raša fault is mostly present in its central and southern extend and show a fault plane dipping towards NE.

High resolution detection of the earthquakes also gave a better understanding of temporal earthquake evolution along the IFS. Temporal clustering was observed in the years 2009-2010 and in the late 2017. In 2009-2010 majority of the system shows high activity, with swarms taking place in northern and central part of the system and multiple mainshock-aftershock series in southern part. Similar, in 2017 multiple swarms and mainshock series happened in the southern part of the system.

Combining the detected temporal clustering with the datasets of extensometer mounted on Predjama fault we observed that in the same time period as the 2009-2010 elevated activity happened, also a notable surface deformation was present. We modelled the surface deformation and earthquake activity using Coulomb stress changes. Best fit was given to the changes of normal stresses along the Idrija fault, which led to the unclamping of the faults parallel to Idrija fault, increasing the earthquake rates along these faults and causing the surface deformations due to the extraction and migration of fluids at depth.

A blank page

TABLE OF CONTENTS

TABLE OF FIGURES

A blank page

1. Introduction

1.1 Motivation and objectives

Damaging earthquakes are rare phenomena in NW External Dinarides in W Slovenia and easternmost part of Italy. From current knowledge, only one major earthquake is known to be associated with active faulting in the NW External Dinarides domain, the 1511 Idrija earthquake, which happened along the Idrija fault, the major active fault, consisting of multiple parallel active faults such as Ravne, Predjama and Raša fault. Together, they form so called Idrija fault system (IFS) of mostly right-lateral strike-slip faults.

In the past, few stronger earthquakes happened, mostly in the northern part along Ravne fault and southern part of IFS, but the extend, geometry and behaviour of the faults in southern part are not well constrained. The strongest earthquakes in the region were 1511 Mw 6.9 Idrija earthquake (Fitzko et al. 2005; Kastelic et al. 2004) in the central part of IFS, Bovec 1998 Ms 5.7 and 2004 Ms 5.4 (Bajc et al. 2001; Borghi et al. 2009) in the northern part of IFS and 1956 M_L 5.1 (Ribarič 1982) and 2014 Mw 4.5 earthquakes in southern part of IFS.

The IFS is not the only seismogenic source in the area of W Slovenia and NE Italy. The most important source is located in the Southern Alps with the major damaging earthquakes happening along the active thrusting Alpine front. Strongest sequence happened in the Friuli region in 1976 with extensive damage and life loss.

In this thesis we will only explore the IFS domain since it was never studied in detail from the seismological aspect. Due to the fact that IFS is capable to produce large earthquakes, the area should be studied in detail and continuously monitored in all possible geophysical manners, especially since the population is relatively high with major and important cities (Trieste and Udine in Italy, Koper, Postojna, Nova Gorica and Ljubljana in Slovenia) in its near vicinity.

Objectives of this thesis are:

- Define the most active faults of Idrija fault system by means of earthquake detection and location if possible and connect them with the surface expressed faults of the Idrija fault system
- Define the geometry of the faults from relocated earthquakes
- Explore temporal and spatial behaviour of the Idrija fault system if any behaviour can be derived for such a short time scale (2006-present)

1.2 Geology and tectonic setting

The studied area lies in W Slovenia and NE Italy, in the transition zone of two orogens – the Alps and the NW-SE trending Dinarides (Figure 1). Geographically it represents the transition from the mostly flat Po plain in N Italy, towards Julian Alps (southernmost part of Southern Alps) in the northern part of the studied area and Dinarides and Dinaric Karst in the S, SE part of the area. From the geotectonic point of view, area lies in the north easternmost corner of the Adria-Europe convergent margin, at the contact of two geotectonic units, Southern Alps in the north and External Dinarides in the southern part of the studied area (Placer 1999, 2008; Placer et al. 2010) as seen on Figure 2.

Area represents the north-easternmost margin of Adria microplate. Major tectonic features of the area are E-W striking N dipping thrust systems of the Alps and from NE part of the region, all along the central part of the area to its SE, NW-SE striking dextrally transpressing Dinaric fault system. To the west of the studied area, external front of the Southern Alps is characterized by a system of SE-verging NE-SW striking thrusts, that are intersected by strike slip and normal faults with the direction of NW-SE and NNE-SSW, inherited from older tectonic phases (Bressan et al. 2007). Towards E, the area is boarded by Ljubljana Basin.

Area is mostly built by Mesozoic carbonate and clastic rocks in the N part of the region and Mesozoic carbonates and Tertiary clastic rocks (flish) in the S part. Pull-apart basins along the Dinaric fault system are mostly filled with Quaternary sediments (Buser 2009).

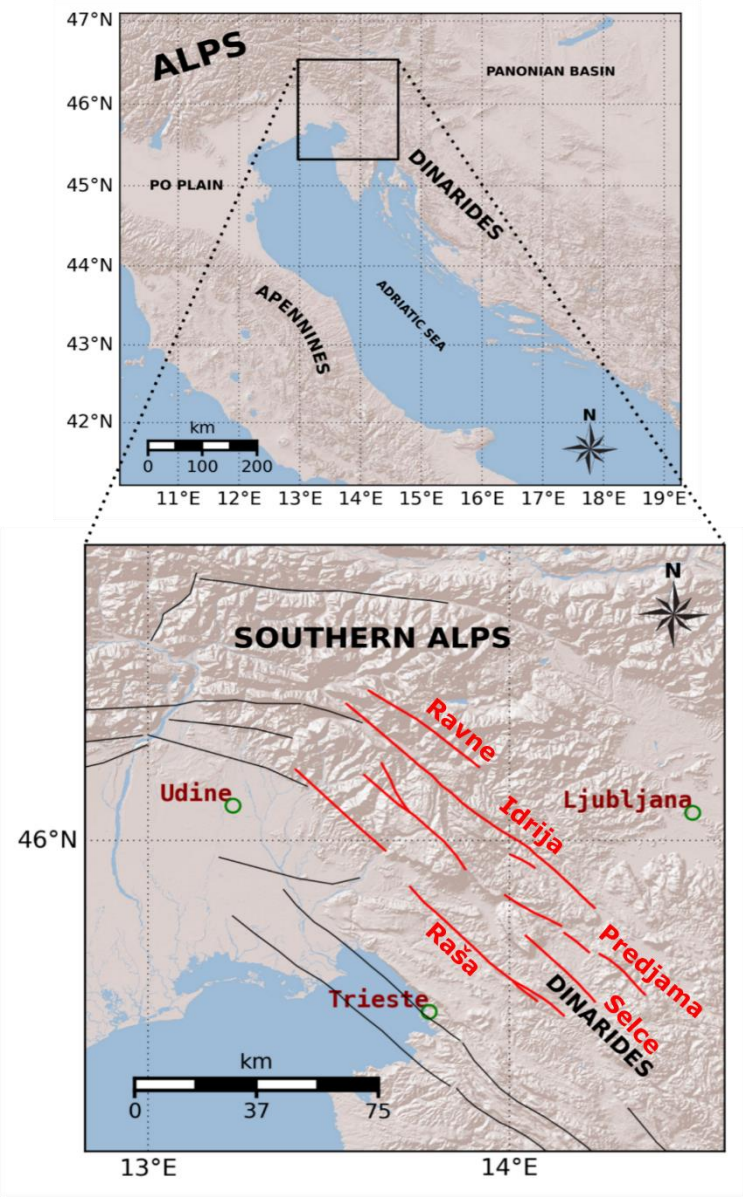

Figure 1: Location of the studied area between two mountain chains, Alps and Dinarides in the Western Slovenia. Black are active faults from the DISS database (Basili et al. 2008) *while in red, active faults of the Idrija fault system are shown as a compilation from this work and Moulin et al. (2016).*

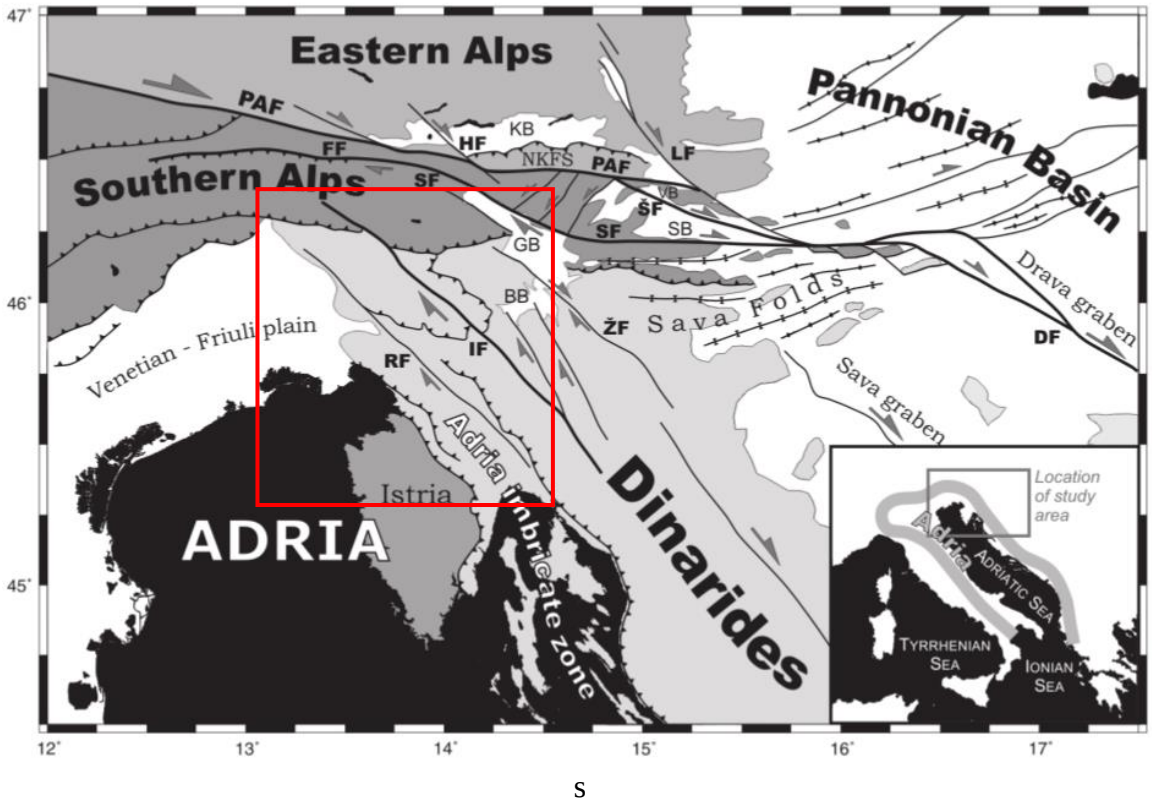

s

Figure 2: Simplified tectonic map of the north-eastern corner of the Adria-Europe collision zone. For work done in this thesis important annotations are: RF – Raša fault, IF – Idrija fault. From (Vrabec and Fodor 2006). Studied area is in the rectangle.

Regional active tectonic processes in the area are mostly driven by the convergence between Africa and Eurasia. The convergence initiated about 140 Myr ago due to the processes related to opening of the Atlantic Ocean (Stampfli et al. 1998; Stampfli and Borel 2002). Between 67-35 Myr ago, African promontory began to move independently of African plate, carving Adriatic microplate between European plate to the north, Iberian microplate to the west and African plate to the south (Handy et al. 2010). Collision between Adria microplate and European plate initiated around 40-35 Myr ago (Lippitsch 2003; O'Brien 2001; Stampfli et al. 1998; Stampfli and Borel 2002), forming two orogens, the Alps at the northern margin and the Dinarides at the north-eastern margin of the Adria microplate.

Precise geodetic measurements of the earth surface using GNSS technology gave us insights into recent geodynamic processes of the region. Africa is actively converging with Europe at the rate of 4-6 mm/yr (Nocquet 2012) (Figure 3). Adriatic plate, since the time it started to move independently of Africa is moving N-NW relative to the stable

Eurasia. This causes localized deformation on the plate boundaries and earthquake activity connected with it (Anderson and Jackson 1987). As discussed in (Nocquet 2012), GPS vectors of the stations located north of the Apennines, in the Dinarides and in Southern Alps, all indicate N movement. This fact suggests counter clockwise rotation of the Adriatic microplate, predicts NE-SW extension along Apennines and transition from N-S shortening in the Southern Alps to NE-SW shortening along the Dinarides. Rate of the deformation is increasing from north to south (Nocquet 2012). Inversion of the GPS vectors constrained the position of the pole of rotation of Adriatic microplate relative to stable Eurasian plate to the Western Alps with angular velocity of 0.297 ± 0.116º / Myr as seen on Figure 4 (Weber et al. 2010). In the area of interest majority of N-S shortening is absorbed in Southern Alps (2-3 mm/yr) up to Periadriatic line, where velocities drop to 0.5 mm/yr (Bechtold et al. 2009; Caporali et al. 2013; Grenerczy et al. 2000). Along the NE External Dinarides comparison between single site RADO in N Slovenia with sites along Adriatic coast shows up to 3 mm/yr dextral motion along NW-SE direction. Around 1 mm/yr is accommodated in the Raša fault in W Slovenia (Caporali et al. 2013).

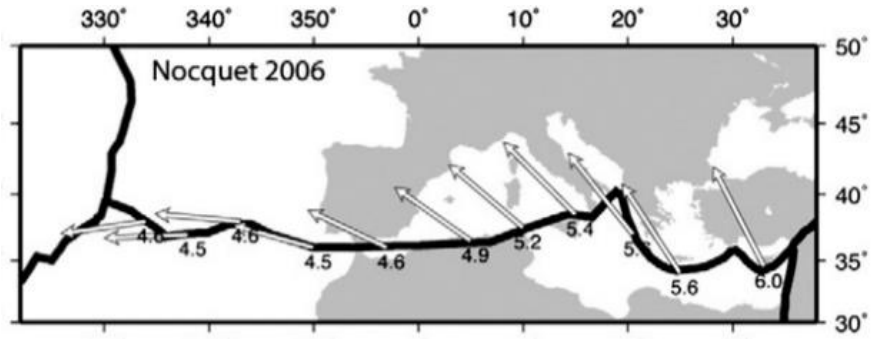

Figure 3: Motion of Africa with respect to stable Eurasia from the geodetic datasets (Nocquet 2012). *Black lines represent plate boundaries, arrows represent motion vector of Nubia plate in respect to Eurasia plate in the last 3.16 Ma as predicted from the geological motion models.*

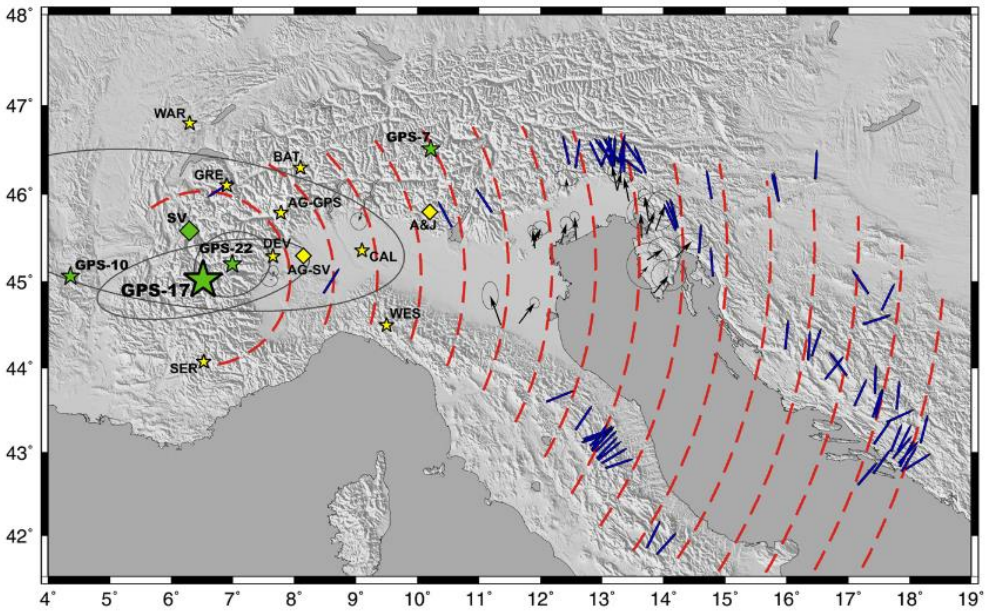

Figure 4: Counter clockwise rotation of Adria in respect to the stable Eurasia from GPS vectors and earthquake slip vectors (Weber et al. 2010) *with approximate axis of rotation in the Western Alps.*

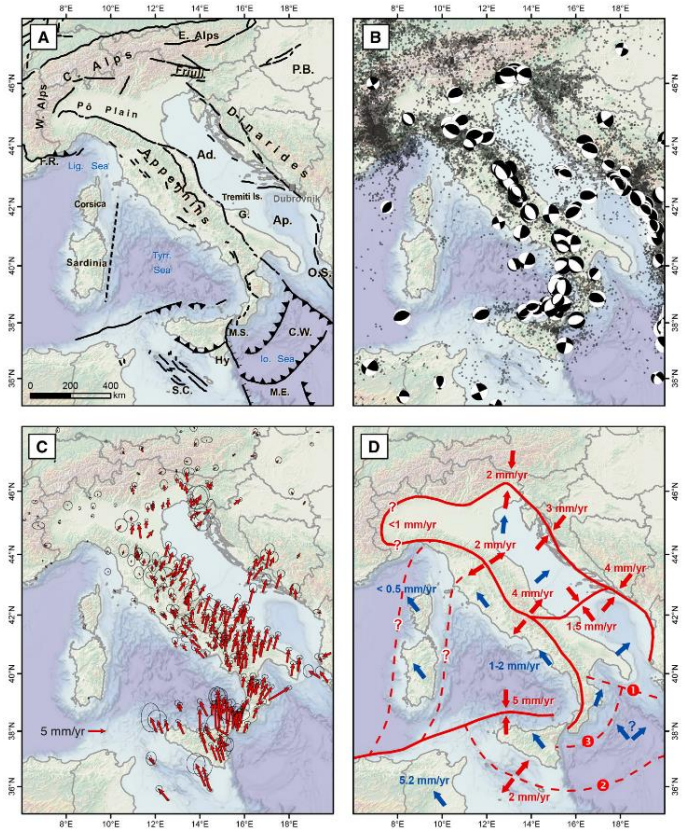

Figure 5: a) tectonic map of the broader region, b) earthquake distribution and their focal solutions, c) velocity field with fixed Eurasia, d) kinematic model of the Adria microplate (Nocquet 2012).

1.3 Active faulting, fault geomorphology and slip rate

Focal mechanisms of stronger and destructive earthquakes that happened in the region of interest in the past suggest recent activity of E-W trending N dipping thrust faults in the Southern Alps and NW-SE trending strike slip right-lateral faults in the Dinarides (Aoudia et al. 2000; Bajc et al. 2001; Basili et al. 2013; Benedetti et al. 2000; Burrato et al. 2008; Fitzko et al. 2005; Galadini et al. 2005; Kastelic et al. 2004, 2008; Poljak et al. 2000; Ribarič 1982; Vrabec and Fodor 2006; Zupančič et al. 2001).

Dinarides in the most northern part consist of older thrust faults, oriented in the NW-SE direction, dipping towards NE, and younger, sub-vertical active strike slip faults with the same direction of NW-SE which was inherited from the older structures (Kastelic et al. 2008; Placer 2008a). In the literature the faults are named »Dinaric faults« due to their orientation being parallel to the older structures present in the Dinarides, mainly NW-SE oriented NE dipping thrusts, but their origin is not related to the Dinaric thrusting episode (Vrabec and Fodor 2006). Whole system is 150 km long and stretches between 46.3ºN and 45.2ºN along a N315 direction. Faults are separated from one another by 10 to 15 km with 10 to 18 km long segments (Moulin et al. 2016).

Number of strike slip faults are geomorphically expressed on the surface and show recent geomorphologic activity, but only few can be directly connected with recent earthquake activity in the region. From the satellite and DEM datasets numerous faults were identified as were their geomorphologic markers of recent activity. Displacements along identified faults range from a few meters to several kilometres. Longest strike slip faults of the northern part of Dinarides (from NE towards SW) are Ravne fault, Idrija fault, Predjama fault and Raša fault (Figure 6) which are all recently active in the geomorphologic sense. Predjama fault splits in two branches with a bend in the fault strike but overall tend to be parallel with Idrija fault, suggesting that Predjama and Idrija fault could merge at depth (Moulin et al. 2016).

Geological slip rate along the Idrija, Predjama and Raša fault is estimated at 1.15, 1.45 and 1.3 mm/yr (Figure 8) as an average over last 255 ka (inferred age of displacement that could be used for dating) with overall slip rate along the fault system of 3.75 ± 0.6 mm/yr. The slip rates changes along different sites of the same segment, which could imply

decrease in the amount of slip towards the tips of the activated fault segment (Moulin et al. 2016).

Geodetic measurements (Figure 7) done over the tectonic structures of W Slovenia (Rižnar et al., 2007) and measurements done along the faults of the Dinaric fault system with tensiometers (Briestensky et al., 2015; Gosar et al., 2011; Gosar et al., 2009) all agree that some of the faults along the IFS are currently active both in horizontal and vertical direction.

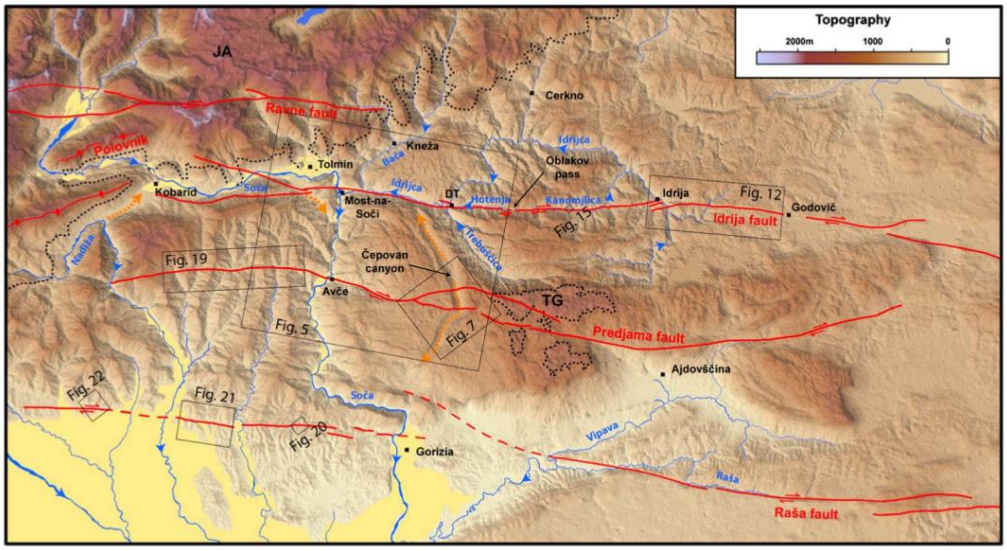

Figure 6: Location of active faults within the Dinaric strike slip system. From top to bottom are Ravne, Idrija, Predjama and Raša fault as discussed in (Moulin et al. 2016). *All these faults were defined as active faults from the geomorphological aspect which is in agreement with geodetic studies.*

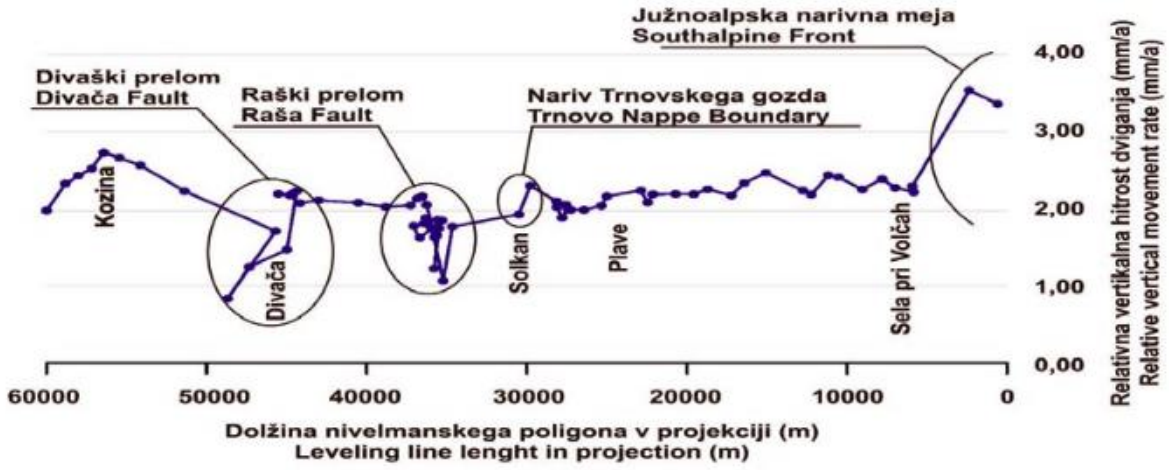

Figure 7: Relative vertical movement rate over a part of the active faults of the Dinaric strike slip system derived from levelling line (Rižnar et al. 2007). *Clear changes are observed over so called Divača fault, Raša fault Trnovo Nappe thrust fault and Southern Alps thrust front. From earthquake activity only Raša*

fault can be described as active, since no earthquakes could be associated with the levelling changes on other faults in this figure.

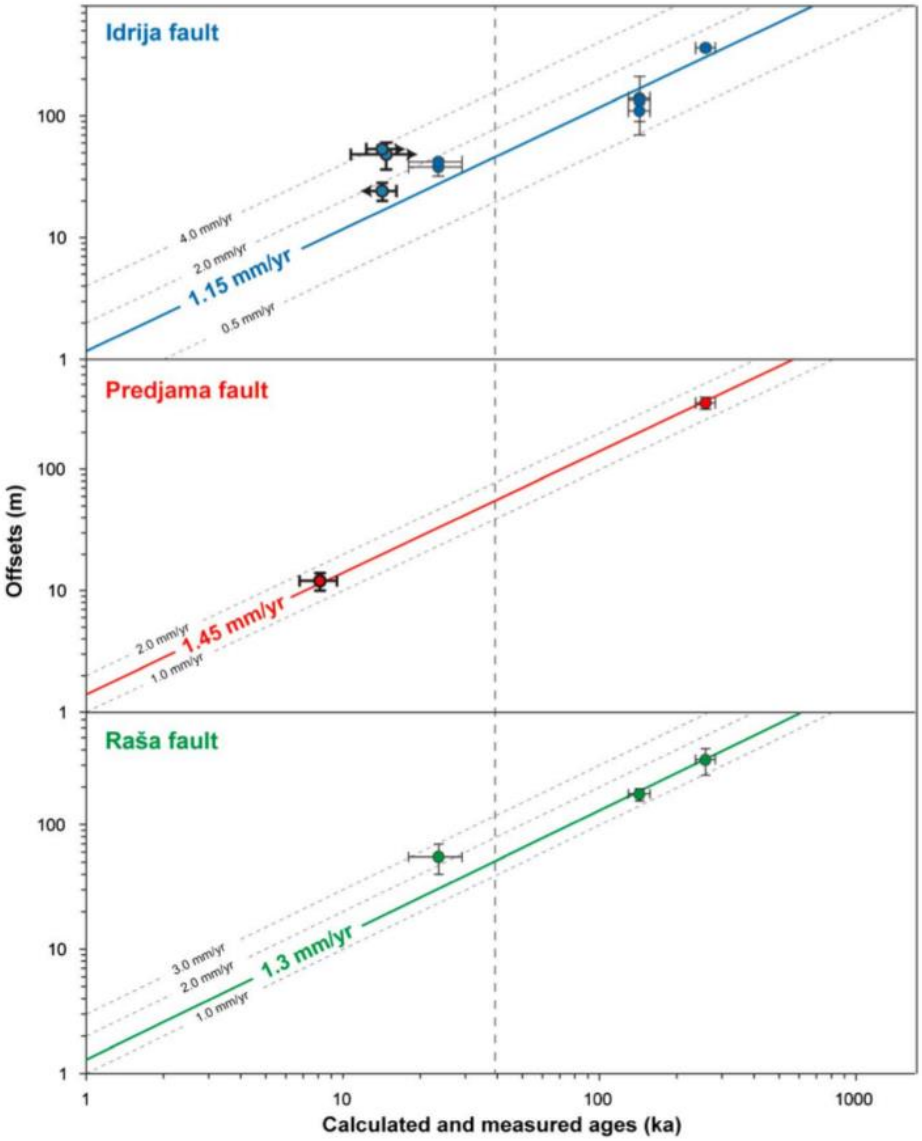

Figure 8: Slip rate assessments along the Idrija, Predjama and Raša fault from offsets measurements. Points represent offset of ^{36}Cl-determined ages, thick coloured line represents mean slip rate, vertical line represents the maximum age supported by the smallest offset (Moulin et al. 2016). *The Predjama fault seems to be the fastest slipping fault in the system followed by Raša and Idrija fault.*

1.4 Seismology

1.4.1 Past earthquakes in the near vicinity of Idrija fault system

The area studied in this thesis was in the past struck by numerous M > 3 earthquakes. In the time period between 1000 AD and 1899 AD (Stucchi et al. 2013) there were 175 earthquakes whose locations were determined approximately with historic data that was available, mostly using the intensity reports from the local population. The strongest and most important earthquakes that happened in and close to the region of interest between 1000 AD and 2006 are described here from earliest to latest. Historic earthquakes are represented on Figure 9.

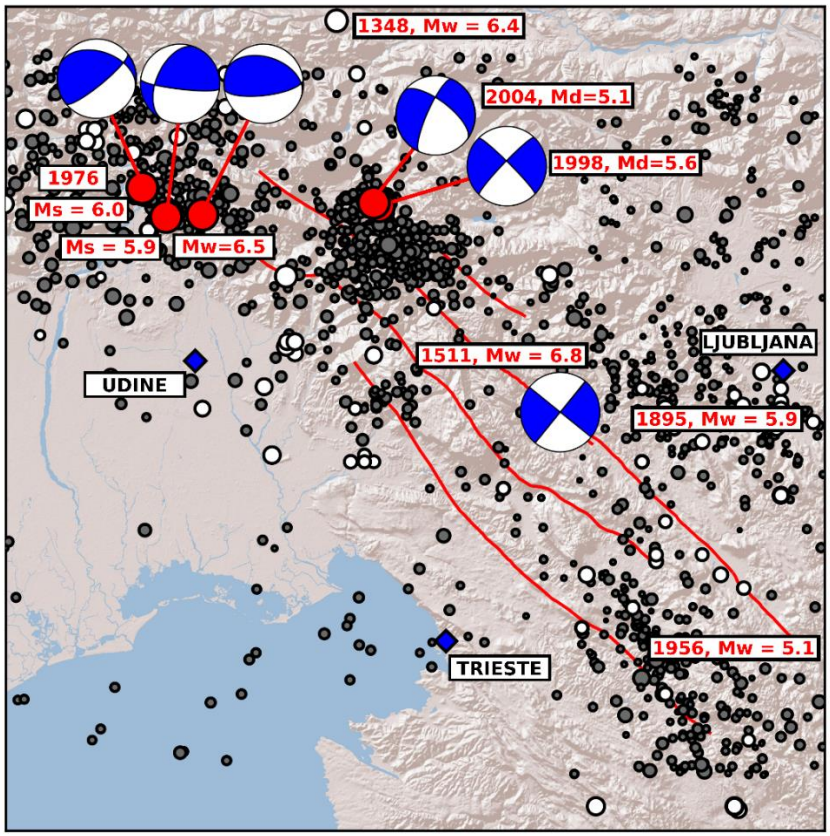

Figure 9: Locations of earthquakes from SHEEC catalogue (Stucchi et al. 2013) *are shown as white dots and rectangles with magnitude and date (aproximate location for 1348, 1895 and 1956 earthquakes) with representation of focal mechanisms. Gray dots represent earthquakes detected in the area of interest by USGS between 1977 and 2006. Clearly majority of earthquakes happened in the Friuli region, Bovec region in the northern part of Idrija fault system and in the southern part of Idrija fault system.*

1348 Villach earthquake

On 25th of January 1348, between 2 and 3 pm UTC, city of Villach, Austria was destroyed by a M_W 6.4 earthquake (intensity X EMS-98). Its depth is estimated to 7 km. It caused up to 40.000 casualties in the region of Austria, Italy and Slovenia and was later followed by numerous fires, floods and rockfalls (Merchel et al. 2014), biggest one with estimated volume of 1 km^3 on the Dobratsch mountain W from Villach. Earthquake was followed by up to 2 yearlong aftershock series felt by local population. The location of the event is still a matter of discussion, with some researches locating the earthquake in Austria, close to Villach (Ambraseys 1976) and some in Friuli, Italy (Gutdeutsch, R and Lenhardt 1996). In the study by Tiberi et al (2014), best fit and source of the fault is obtained from source modelling with comparison with intensity datasets for a bilateral rupture with uniform seismic moment distribution, located west from Villach, along Sava fault.

1511 Idrija earthquake

Next, strong earthquake that shook area of N Dinarides was 1511 Idrija earthquake. Earthquake happened on 26th of March 1511 between 3 and 4 pm local UTM. As reported in Ribarič (1979), two strong earthquakes happened one after the other, the first one NW from the town Tolmin, on the border between Slovenia and Italy, with M 6.9 and second, stronger that happened east of the city of Gemona in Friuli, Italy, with magnitude 7.0 – 7.2 but this was the only work, where two events were reported. The problem of one or two events was later solved by Košir and Cecić (2011) and was due to the wrong interpretation of available historic information. Macro seismic intensities were reported up to intensity X. In Fitzko et al. (2005) problematics of two mainshocks or one mainshock were addressed. Using synthetic earthquake modelling techniques and comparing the results obtained with reported intensities, best fit scenario was selected. The best source candidate was right lateral strike slip earthquake along the Idrija fault with M_W 6.9 with a 50-km long rupture, propagating towards NW. Similar final outcome was obtained by Tiberi (2014). A surface rupture was observed as discussed in Bavec (2013).

1895 Ljubljana earthquake

On 14th of April 1895 at 10:17 pm, earthquake happened close to the Ljubljana, capital city of Slovenia. Hypocentral depth was estimated to 16 km with M_L 6.1 (Vidrih 1995). Intensities between VIII and IX EMS were reached in the area of Ljubljana. Ljubljana was badly damaged with 21 fatalities. This earthquake means a turning point in Slovene seismology, since two years after, first seismic observatory was built in Austro-Hungarian empire. Detailed study by Tiberi et al. (2017) was performed to find the best fault candidate of the 1895 earthquake. Using the PGV estimations different ground motion scenarios were introduced, varying in selected fault, rupture dimension and seismic moment value. No final solution was proposed, but the data did show towards a strike-slip faulting located S of Ljubljana with the rupture propagating towards NW and with M_W 5.4, lowering the estimated M_L 6.1.

1956 Ilirska Bistrica earthquake

On 31st of January 1956 at 2:25 am UTM, town of Ilirska Bistrica, in the southern part of studied area, was damaged by an earthquake with M = 5.1. Highest intensities were reported at VII, EMS, with focal depth of 7 km (Ribarič 1982). 30 % of the town was badly damaged.

1976 Friuli earthquakes

On 6th of May 1976, Friuli area was struck by first (M_s = 6.5) of a series of strong, M > 6 earthquakes. Earthquakes damaged broad area of Italy, Austria and Slovenia. Maximum intensities were reported at X EMS, with strongly damaged buildings in all the region. The mainshock was preceded by a M 4.5 foreshock and followed by a strong aftershock sequence. The largest aftershock was a 15th September 1976 event (Ms 6.0) at 3:15 GMT and a 9:21 GMT (Ms 6.1) earthquake.

Aoudia et al. (2000) relocated the mainshock and strongest aftershocks and inverted surface waves for depth and focal mechanisms for mainshock and two strongest aftershocks. Relocation was done by JHD method (Dewey 1971).They found out that relocated aftershocks cover a surface of 25 km long and 15 km wide, which is comparable to expected fault source. Unilateral and west propagating rupture was proposed due to the aftershock distribution. For the mainshock, propagation of the rupture was proposed at the

constant speed of 70% shear wave velocity, with 18.5 x 11.2 km big area of rupture. Top of the fault plane was set at 1.5 km depth and the nucleation of the earthquake at 7 km.

Perniola et al. (2004) calculated Coulomb stress changes for the strongest of the Friuli 1976 earthquakes. They found a good correlation between calculated Coulomb stress increase and various fault segments that ruptured during the sequence. They discuss that static stress changes due to the mainshock promoted a later, M_W 5.1 earthquake that happened on 9th of May and M_W 5.2 that occurred on 11th September. Second, M_W 5.6 earthquake of 11th September was located in the area of increased Coulomb static stress due to the previous dislocations. In the area of M_W 5.9 earthquake that happened on 15th of September, Coulomb stress change was decreased and increased where M_W 6.0 of 15th of September happened.

Moratto et al., (2012) proposed new models of ruptures for few selected Friuli earthquakes. For the 11th of September earthquake they proposed two different models, first with one asperity, a bilateral rupture and the parameters proposed by Slejko et al. (1999), while the second one has two asperities and a unilateral E-W rupture using parameters from (Burrato et al. (2008)). The 2nd event of 11th of September was best fitted to the E-W propagating, unilateral rupture with two asperities. The 2nd event was shallower then the first one. September 15th event was best fitted to the pure thrust focal mechanism, a bilateral rupture and two asperities with fault striking in SW direction. All the events show migration from E to W.

As it is discussed in Caruli et al. (2005), Friuli area was struck by numerous stronger earthquakes in the past with strongest earthquakes close to Belluno and in Central Friuli.

Poli et al. (2002) relocated aftershocks and sequences after the Friuli 1976 earthquakes. They found out that most of the earthquakes lay between 5 and 12 km depth with the northernmost limit coinciding with the Fella-Sava fault and southern most limit at Friuli plain. They propose two seismogenic zones in this volume of seismic activity. First is around 3 km thick and 10 km wide area that gently dips towards N, with bottom located at 12 km depth. The second is located between 5 and 8 km. The zones seem to be separated by low seismicity zone. These two zones can be related to hanging wall of Pozzuolo thrust and Susans-Tricesimo and Buia thrust systems. Also, third zone was proposed as a presence of a high-angle south dipping structure, which could be related to the minor contractional structures.

Another set of interesting observation related to the Friuli 1976 sequence comes from the Grotta Gigante horizontal pendulum. In the 3 years preceding the Friuli 1976 sequence, instrument recorded numerous »tremor« signals. Bonafede et al. (1983) interpreted this signal as a silent earthquake originating in the deep portion of the fault in an unbrittle regime. In the same time period, anomalous southward tilting was observed (Dragoni et al., 1984; Rossi and Zadro, 1997).

1998 and 2004 Bovec earthquakes

On the 12th of April 1998 at 10:55 am UTC, earthquake with M 5.7 happened in the NW Slovenia, along the Ravne fault. Intensities up to VIII EMS were reported in the area. Depth was estimated at 8 km. Number of buildings were damaged and numerous rockfalls happened in the region, due to the high relief of the mountains. Earthquake was followed by a number of aftershocks, strongest of them with M 4.2 that happened on 6th of May 1998. In the same area, a M 5.1 earthquake happened on 12th of July 2004, along the same fault. Intensities reported were up to VII EMS.

Bajc et al. (2001) relocated the 1998 sequence using Joint Hypocentre Determination method for teleseismic events by adapting the method to the local earthquakes. With the method, they successfully relocated 45 best recorded events having at least 45 P or S wave arrival times. They found out that relocated events are in well-organized along a trend of N125, in good agreement with the computed focal mechanism of the mainshock. The depth of the mainshock was estimated to 7.6 km. With the inversion of strong motion data, they studied the source processes of the main shock. They propose a fault rupture with top at 3 km, length of 13 km and with of 7 km. Its strike is 315º, dip 82º and rake -171º. Seismic moment released in the mainshock was estimated at 4.5 x 10^{17} Nm, with average slip of 18 cm. Rupture propagated in bilateral direction which is also compatible with the aftershock distribution.

Bressan et al. (2008) discussed static stress changes, focal mechanisms and aftershock pattern of 1998 and 2004 earthquakes. From tomographic imaging of the area with use of local earthquakes, they suggest that the fault zone is characterised by mechanical heterogeneities. From across-fault tomography they observe sharp lateral P-wave velocity contrasts, branching of the fault and minor splay faults. Apparently, aftershock of both mainshocks are located inside a high velocity body, characterized by P-wave velocity in range between 6.2 and 6.8 km/s. 2004 mainshock was located into the area of smaller

number of aftershocks of the 1998 event. Both sets of aftershocks were distributed along the sharp Vp and Vp/Vs variations. Variable focal mechanism they obtained were interpreted as interaction between the stress field generated by the mainshock and the variations of strength revealed by tomography. They explored the perturbation of the stress field from the 1998 main shock by calculating Coulomb stress change. They found out that the largest after shock of the 1998 happened in the region of positive stress change, but 2004 main shock happened in the region of negative stress change. Apparently, the distribution of the stress around the region is due to the 1998 mainshock and region stress field. Similar are the conclusions of Ganas et al. (2008).

The area was studied also from the geomorphological point of view by Cunningham et al. (2006) using LiDAR datasets. With LiDAR data they found numerous splays along the Ravne fault with not so apparent strike-slip offsets. Tolminka Springs basin (epicentral area of the two earthquakes) was defined as a transtensional basin constructed in overall transpresional system. Field mapping done by Kastelic et al. (2008) showed there is no evident continuous surface trace of the Ravne fault, instead at the surface they observed a fault zone of moderate to steep NE dipping fault planes demonstrating thrust/reverse mechanisms.

After the 2004 earthquake no strong earthquakes happened in the region. The ISC catalogue between 2006 and 2015 – the same period as was analysed in this work, for W Slovenia contains 7147 earthquakes and quarry blasts. The maximum magnitude earthquake that happened in the area of W Slovenia was M_W 4.3 with epicentre at 45.65 and 14.23 and reported depth at 16.1 km.

1.4.2 Velocity models

Crustal and upper mantel structure of W Slovenia was, until recently not well resolved. Mostly, older studies consider this area in a regional scale, so detailed structures are lost. Despite the availability of a dense seismic network, classic tomography studies are limited, due to the non-uniformity of the geographical distribution of earthquakes in Southern Alps and Dinarides. From the studies available, some were done using surface waves, body waves and, latest, ambient noise tomography methods.

In 2002 the TRANSALP programme (TRANSALP Working Group, 2002), produced seismic profiles for the Eastern and Southern Alps using seismic reflection data. Profiles revealed double vergence of the Alps, with European Moho dipping south at an angle of 7º. Adria was observed to be dipping north at a shallower angle. From the P-wave velocity model, obtained from active source travel time tomography, Bleibinhaus & Gebrande (2006) found that Adriatic crust shows higher P-wave velocity then European crust. They suggested the existence of a S-directed subduction od European plate and a deep thrust fault in the Southern Alps at about 25 km. Brückl et al (2007) suggested that European Moho dips towards south with depths down to 47 km below the transition from Eastern to the Southern Alps, while the Adriatic Moho continues further south at shallower depths, suggesting a southward subduction of European lithosphere. Brückl et al. 2010 explained the results obtained from the controlled source seismic experiments with the subduction of the Europe below Adria from north to south and under thrusting of Adria below Pannonian from southwest to northeast. They suggested that fragmented Moho plays strong role in the active tectonic processes at the surface.

Bressan et al. 1992 inverted arrival times of local earthquakes to produce a 3D velocity model of the N part of Friuli, considering in the area also part of the NW Slovenia. To obtain 3D velocity structure, they simultaneously inverted travel-time residuals from local earthquakes by linearizing the time integral of the source-receiver paths. Solutions were obtained by iteration process, first solving for the hypocentres and then calculating velocity anomalies. Peak of seismicity vary from 7 to 11 km. Deeper earthquakes are rare, with no earthquakes beneath 20 km. Their conclusions were that in the central part of the studied area, majority of earthquakes is related to a thrusted uplifting wedge basement. The wedge is characterised by a branching structure of active faults with prevailing thrust component. Shallower earthquakes that happened in the sedimentary cover are rarer than in the basement and they seem to be induced by local stress inhomogeneities. Deeper earthquakes are again rarer than in the wedge, with no earthquakes deeper than 20 km. Sharp decay in seismicity was observed with depth in correspondence with the passage to low-velocity zone, detected at 10 -12 km.

Michelini et al. 1998 simultaneously inverted earthquake travel-times for velocity structure and hypocentres for whole region of Slovenia. They used P-wave first onset readings from the seismic network of Slovenia, Italy, Croatia, Austria and Friuli network for the period 1988-1996. For inversion, 166 earthquakes were used with at least 10 P

arrival times and rms misfit lower than 0.4 s and epicentral distance less than 150 km to avoid Moho refracted wave paths. In conclusions they show a presence of NNW-SSE oriented high-velocity body in W Slovenia. The position of the high-velocity body coincides with the outer part of External Dinarides. They interpreted this feature as the upper-crustal signature of the Adria-Eurasia collision at depth.

Gentile et al. 2000 produced a 3D V_p and V_p/V_s tomographic images of Friuli area, similar to Bressan et al. They showed that upper crust is characterised by marked heterogeneities related to the complex tectonic pattern. The proposed that V_p/V_s anomalies and sharp V_p/V_s lateral heterogeneities are effect of the faulting geometries. Again, they found that central part of the area consists of high-velocity body at the depth of 6 km bounded by V_p/V_s gradients. They interpreted this zone as a tectonic wedge, accommodating large amounts of crustal shortening associated with Alpine tectonic phase. Majority of the earthquake activity, together with the strongest earthquakes of 1976 sequence are located inside this wedge.

In 2011, Stipčević et al. constructed a crustal and uppermost mantle structure of External Dinarides from teleseismic receiver functions. For the analysis, 8 permanent broad-band stations of Croatian network were used with the data between 18 months and 10 years, depending on the station. Stations used in the study are all located in the coastal region of Croatia, on the border between Adria and External Dinarides. For the receiver function estimation, earthquakes with $m_b > 5.5$ and epicentral distances between 30º and 90º were used. After data preparation, between 42 and 108 earthquakes, depending of the station were used. First, initial and intermediate velocity models were constructed for each site and later the intermediate model was refined by Monte Carlo search of model parameters to obtain final velocities and thickness of layers. Station RIY, close to the town of Rijeka, Croatia is located in the southernmost part of the area of interest of this thesis and covers a part of the External Dinarides. The inversion they obtained match very well with the Alp07 DSS profile. They found two layered crust with a 3-km thick layer of low seismic velocities above upper crust. Upper crust has higher constant velocities that decrease slightly until the transition to the lower crust at the depth of 26 km. Lower crust velocities are higher and are rising towards crust-mantle boundary at the average depth of 39 km. Similar results are present also at the NVLJ station on the island of Pag, with a bit more complex structure.

A recent study by Guidarelli et al. (2017) was performed to obtain tomographic image of the region studied in this thesis using ambient noise. Findings from this study will be discussed in chapter 3.

1.5 Swarms globally

As will be discussed in the later chapters, area of active faults of the NW part of External Dinarides was affected by both, main shock - after shock activity and swarm activity. In this chapter a quick review on earthquake swarms will be given since swarms are a new kind of earthquake behaviour discovered in this region, confined to the southern part of the study area, on Predjama, Selce and Raša fault.

Classic main shock after shock sequences can be generally described with modified Omori law:

$$\lambda(\mathrm{c} + \mathrm{t})^{-p}$$

where *t* is the time elapsed since the mainshock, p is close to 1 and c is a small time constant (Utsu et al. 1995). Spatial distribution of aftershocks is correlated with the static stress field changes of the main shock, suggesting major role in triggering from stress changes (Stein 1999). To explain the time delay of aftershocks, additional mechanisms need to be considered. Such mechanisms are rate-state friction law (Dieterich and Kilgore 1994) post-seismic relaxation (Savage and Svarc 1997), after slip (Perfettini and Avouac 2004) and locally induced fluid flows (Nur and Booker 1972).

Earthquake swarms in the other hand, are groups of earthquakes defined as a sequence of gradually increased and then decayed activity in time without distinct mainshock. Activity can last from days to months (Sykes 1970). Laboratory measurements agree (Mogi 1963; Scholz 1968), that swarm activity patterns are limited to the regions of heterogeneous distribution of material properties, while regular main shock sequences are related with regions of homogeneous distribution of material properties and uniform stress field. In the literature, swarms are connected to different tectonic settings and different physical processes. Majority of swarms are related to the volcanic processes like magmatic intrusion and magmatic fluids migration (which are not in our interest, since the area of research is far from active magmatism), followed by non-magmatic fluid migration reducing the resistance of faults, pore pressure changes, static stress drop changes and aseismic deformation along the active faults, both at the tectonic plate boundaries as in the intraplate settings. Temporal evolution cannot be simply described by the Omori law and each earthquake in the series can play a role in the redistribution of the stress, which may in turn influence the subsequent swarm evolution (Main 1996).

As reported by Crescentini et al. (1996), swarm activity occurred in the area with radius of 200 km from the geodetic interferometer used to detect strain changes on an active fault. Interferometer is located 1400 m underground in the seismically active region of Apennines, central Italy (42º28'N, 13º34'E). During the time of the study, 180 strain changes were observed in the period between 1997 and 1998, before the Ubria-Marche earthquake sequence. The swarm activity started in the March 1997, after one year of diffuse background seismicity. The swarms reached magnitudes up to 4.1 and were concentrated in three sub regions named Matese, Massa Martana and Colfiorito. The Colfiorito sequence was also the beginning of Umbria-Marche destructive earthquakes. In the paper they discuss the presence of »slow« earthquake as the main driving mechanism of the elevated swarm activity in the region. The »slow earthquake« was located in the vicinity (less than 100 km away) of the interferometer.

Similarly, Segal et al., (2006) proposed a silent slip event as the driving mechanism of swarm of earthquakes happening at Kilauea volcano, Hawaii. As detected by a local GPS network, on the 10-11 November 2000, up to 1.5 cm of displacement happened in about 36 hours, along the fault with favoured depth between 4-5 km. Similar pattern of displacement and location of displacement was later recognised also in the 1998, 2003 and 2005 at the same area. In all 4 cases, area exhibited elevated swarm like microearthquake activity. They proposed 2 explanations for the microearthquake activity related to the slow slop event: (1) the earthquakes unpinning the fault, allowing slow slip to occur, or (2) the slow slip stressing the adjacent fault and increasing the seismic rate. Since the slow slip of 2005 as observed on GPS stations started well before the increase in earthquake activity, the 2nd option is preferred in this case. Swarm activity in the case of 2005 slow slip was interpreted as co-shocks and aftershocks of the »silent earthquake«.

Heinzl et al., (2006) proposed a model of earthquake swarm patterns due to fluid intrusion and stress triggering. They observed the earthquake swarm, that occurred in the Vogtland/NW Bohemia, Central Europe in 2000. Region is well known for episodic occurrences of earthquake clustering. Previous research suggests that the swarm activity of the region is induced by fluid overpressure (Winlich et al., 1999, Brauer et al, 2003). Same idea is supported by the observations that during the swarm activity, hypocentres migrate in a fluid diffusion like spreading (Parotidis 2003). In the paper they proposed that both, fluid diffusion and stress triggering influence the pattern of seismicity. Fluid diffusion is reflected as a spatiotemporal hypocentre migration but is the primary

triggering mechanism of the swarms. However, after the fault patch has been brought into the critical state by increase in pore pressure, stress triggering becomes dominant. The most important characteristics for the short-term clustering are post-seismic stress changes due to the after slip.

In research by Shelly et al. (2016), analysis of the swarm of 2014 in the Long Valley, California was performed. Swarm lasted from 31th of May until 1st of November 2014. More than 18,634 earthquakes were detected with magnitudes up to 3.5. The sequence exhibited repeated episodes of migration, beginning with small events in small source zone, expanding dramatically outward with time. Expansion with time was explained as consequence of triggering by fluid pressure diffusion from water and CO_2 migration from deeper areas towards surface, away from the magmatic body at depth. Since the migration is rapid, they excluded direct involvement of the intrusion of magmatic body. Analysis showed that as fluid pressure would rise, first earthquakes would occur on faults already stressed near failure. With faulting, permeability is expected to increase, and faulting could act as a »valve«, causing differing fluid pressure regimes to equilibrate. Increase of fluid pressure would reduce the effective normal traction on the fault and reduce the critical shear traction needed for failure according to the Mohr-Coulomb failure criterion. Another fluid related cause for swarm activity comes from the study by Vavryčuk et al. (2017). They proposed that interaction between fault zone with fluids can cause the fault zone to alternate and fault to slowly erode, gradually weakening the fault itself.

Swarms are also present in the intraplate seismic zones, away from plate boundaries or active volcanic areas. As discussed in Bisrat et al. (2012) one of such areas is the New Madrid Seismic Zone in the USA. The area was struck by numerous destructive earthquakes in the past, with 3 M>7 earthquakes in 1811 and 1812. In the study they rule out possibilities of magmatic origin of swarms and since there is no migration of the events, directional fluid migration induced seismicity or earthquakes induced by aseismic slip are also ruled out. They propose the driving mechanism of swarm to be pressure changes of the fluids inside the highly fractured crust.

Aseismic creep in either shallow or deeper portions of the active fault also contributes to the earthquake swarm activity. Lohman & McGuire (2007) observed shallow aseismic creep in southern California. In August 2005 the Californian network detected elevated number of earthquakes in the Brawley Seismic Zone near the southern termination of the

San Andreas Fault. In the same time, surface deformation was observed on two GPS stations and by InSAR. They found out that combined recorded seismicity alone is not enough to explain magnitude of surface deformation from InSAR, which was equivalent to M_W 5.3 earthquake. By modelling, they found out that surface deformation would be consistent with m M_W 5.75 earthquake, when they explained as a creep event that increased the stressing rate in the region. Creep event started few hours before the strongest earthquake of the swarm series.

As described in this chapter we clearly see that majority of the swarm activity is connected directly to fluid circulation at the seismogenic depths, in some areas in the shallow portions of the crust and in others in the deeper parts. In specific cases the involvement of the fluid can be directly observed (Davis et al., 2004), but not always. Also, aseismic creep has a big role in the swarm activity, either as a cause of the elevated earthquake rate, or as an effect due to the fluid circulation and its roll on the strength of the faults. These two processes are hard to distinguished, but with combination of space geodesy and seismic monitoring we are able to observe these two processes.

1.6 Transient deformation

A group of process commonly associated with the swarm activity over a region is most often described as a transient deformation. Transients related to post-seismic (after slip) deformation are well studied (Cheloni et al. 2017; Perfettini and Avouac 2007). But transients can also be associated with the completely aseismic processes, only observable from geodetic measurements or associated with various seismic processes like non-volcanic tremor, low frequency earthquakes and elevated regular earthquake activity either as normal mainshock-aftershock activity or swarm activity on a longer time scale, happening before bigger earthquakes which can have big influence on the seismic hazard of the region if we are able to monitor the transient deformation. Majority of the transient deformation in shape of aseismic slow slip events and slow slip events accompanied by tremor and low frequency earthquakes is normally associated with subduction zones such as Japan, Cascadia, Mexico, New Zealand and Costa Rica (Roger eat al., 2003, Ozawa et al., 2002, Wallace et al, 2013, Pritchard et al., 2006, Villegas-Lanza et al., 2016, Miyazaki et al., 2006). Similar quasi-static slips have also been documented along

creeping sections of large faults, like San Andreas Fault in California, Kilauea volcano in Hawaii and North Anatolian Fault in Turkey (Rousset et al., 2016, Linde et al., 1996, Segall et al., 2006).

In next few paragraphs a short description of the important studies regarding the phenomena associated with transient deformations are given.

In Linde, 1996 a slow earthquake along the San Andreas fault, at the transition between locked and stably sliding segments of the fault, is described in detail. Slow earthquakes are events of release of stored energy that happens in time scales of hours, even months in contrast to almost instantaneous release through regular earthquakes. The fault to the north ruptured in a M_W 7.8 earthquake, while to the south, slip occurs as creeping and small $M_L < 3$ earthquake series. The area is being also monitored by different strain meters which were used in the detection of the transient deformation. In December 1992, strain meters recorded a strain excursion. The change started rapidly on 11th of December. It was followed by slow, exponential-like change over next 8 days, with two interruptions on the 12th and 14th December. About 2 hours before the start of the deformation, a local M_L 3.1 earthquake happened, followed by 2 additional M_L 3.3 and 3.2 earthquakes few hours later. Next day few smaller earthquakes happened before another change in strain, with two M_L 3.7 earthquakes happening at the time of the change and few after the change. Calculated coseismic strain changes are few orders of magnitude smaller than the change detected by the strain meters. As proposed by Linde, observations suggest a relation between the redistribution of stress and the size of the related earthquakes.

Deformation aseismic transients were also observed on normal fault system of the Pollino range in Southern Italy. Through combination of geodetic (GPS, InSAR) and seismic observations, Cheloni et al., 2017 documented a transient aseismic slow slip that happened during a yearlong swarm sequence, that occurred between October 2010 and beginning of 2014. Both GPS and DInSAR showed that transient displacement started on July 2012, before the 25 October 2012 M_W 5.1 main shock of the activity and lasted until mid-2013. The transient deformations showed the cumulative displacement up to 10mm in this time period while M_W 5.1 alone showed only 2 mm. They observed high correlation between accelerating and decelerating phases of the deformation and the seismic rate. Around 70% of all the deformation was aseismic, with the maximum

cumulative slip reaching up to 250mm and the moment release equivalent to a M_W 5.5 earthquake, while combined moment release of earthquakes only reaches M_W 5.17.

Areas most prone to the transient deformations are subduction zones. Along the megathrusts different transient observations take place – aseismic, deep tectonic tremor and low frequency earthquake transients. Seismic signals are in general hard to locate, due to lack of distinct P or S phases. Low frequency earthquakes, which are most likely present in majority of deep tectonic tremor signals (Kao et al. 2005) can be distributed over broad range of depths or more constrained to the depth of the transient signal. The transient deformation in form of slow slip events is estimated to happen at the down-dip regions from the locked part of the megathrusts. Stressing in the up-dip zone is increased episodically, and each transient can make megathrust more prone to the failure in a large earthquake (Mazzotti and Adams 2004).

Rogers et al., 2003 reported on the episodic tremor and slip detected in the Cascadia Subduction Zone. In the northern part of Cascadia, the slip events were detected at depths between 25 and 24 km at the subduction zone interface using continuous GPS monitoring. These events are happening at the down dip of the locked portion of the fault and repeat every 13 to 16 months. The slip is accompanied by tectonic tremors, with low frequency content (1 – 5 Hz), while small local earthquakes show frequencies above 10 Hz. They named the slow slip events and associated tremors as Episodic Tremor and Slip (ETS). Time length of such tremors was reported between few minutes to several days.

Shelly et al., 2006 discovered that low frequency earthquakes, found to exist at the plate interface and sometimes build up the tremor itself, are in fact generated by shear slip during the aseismic transient, rather than the fluid flow that can also generate similar signal to the tectonic tremor, but normally in the areas of magmatic processes. They located the tremor within a belt that follows the strike of the subducting plate (Rogers et al., 2003). As proposed by Shelly, slow slip, low frequency earthquakes and tremor are all coupled phenomena, representing a mode of failure in the transition zone between locked and continuously creeping fault.

Tremor has been discovered also outside of the subduction megathrusts, under the San Andreas fault system, south of Parkfield (Nadeau 2005) and more recently tremor and low frequency earthquakes revealed slow slip on the Alpine Fault, New Zealand (Chamberlain et al. 2014; Wech et al. 2012) . Chamberlain presented the first evidence of

low frequency earthquakes (LFE) within the Alpine Fault, and that the tremor is indeed composed of swarms of LFE and that LFE also occur on its own, not connected to tremor or slow slip events.

In the area of W Slovenia and NE Italy, rare observations are done in regard to detect possible deformations connected to the transient episodes along the active fault system. The observations are derived from GPS monitoring of the region and from the Grotta Gigante Earth tide station.

Chiarutinni, 1976 reported on a series of interesting readings from the Earth Tide Station prior to the Friuli 1976 series of earthquakes. In January 1973 both E-W and N-S components of the pendulum recorded permanent deflections towards E and S, with perturbation happening for next 6 hours. More perturbations were observed later in 1973 happening for some hours per day until 1976. Bonafede et al. (1983) interpreted these phenomena as slow earthquakes, originating in the non-brittle part of the crust. At present it is not known if these perturbations of the signal are indeed connected to the Friuli earthquake sequence and they represent a transient deformation in time span of few years or are they connected to some unknow process.

From the GPS studies of the region Borghi et al. (2009) observed that strain-rate variations happened in the region of Bovec 2004 M_W 5.5 earthquake in the different scales of observation – long term covering time before and after the earthquake, short term prior to the earthquake and short term after the earthquake, giving us the insight in the strain-rate changes. They found out that strain-rates change in size and direction prior to the earthquake and after the earthquake.

2. Methodology

In seismology, when dealing with earthquakes of all sizes, the most important properties of the single earthquake are its location, magnitude and focal mechanism. From these properties we can build on our tectonic models of the area, earthquake hazard and risk or can monitor different human activities that affect Earth's crust directly, such as mining, fluid pumping and extraction, etc. When interested in earthquakes and their application to hazard, our goal is to detect and identify as many meaningful events as possible, through different methods, some of which were used also in this thesis and are described in detail in this chapter.

In this thesis, for detection and analysis of earthquake activity in the region of Idrija fault system, virtual network, spanning through different countries was used. For analysis of the earthquake activity in the N part of the region of interest, seismic stations of different smaller networks of Italy and some from Austria were used, while for the majority of IFS area, seismic stations owned by Slovenian Environment Agency were used. Lastly, for the S edge of IFS, a station from Croatian agency was used. All these subnetworks, except Croatian, are part of a virtual seismic network CE^3RN – Central and Eastern European Earthquake Research Network, which spans over different countries (Italy, Slovenia, Austria, Albania, Ukraine, Czech Republic, Hungary, Romania, Bulgaria and Croatia) and institutions from before mentioned countries. The main goals of this trans boarder network is to intensify the cooperation between these institutions and enable extensive seismic monitoring of the region for scientific and civil protection purposes (Bragato et al. 2014; Lenhardt et al. 2016).

The virtual network is not spatially homogenised, but the station coverage in the area of IFS is good enough to detect earthquakes with $M_L < 0$ for specific cases. In general, network density in NW part of the area, in the region of Friuli – Venezia Giulia in Italy is much higher than in central part of the area of interest, Slovenia. For central part of IFS, there were around 10 stations that were close enough for the detailed analysis performed in this thesis, while in the NW part number of station is much bigger as seen on Figure 10. Stations in near vicinity of IFS all transmit data in real time to the local monitoring centres and are all broadband seismic stations with sampling rate 200 Hz except few stations operating at 100 Hz.

Figure 10: Station coverage in the region of Idrija fault system. Different colours represent different subnetworks managed by different agencies. Sharp change in station coverage is visible on the border between Italy and Slovenia, but the Slovenian network still allowed us to detect all the felt earthquakes. In blue, stations of different institutes but not used in this study are represented. For the matched-filter detection analysis stations of Seismic Network of the Republic of Slovenia were used since they cover all the IFS.

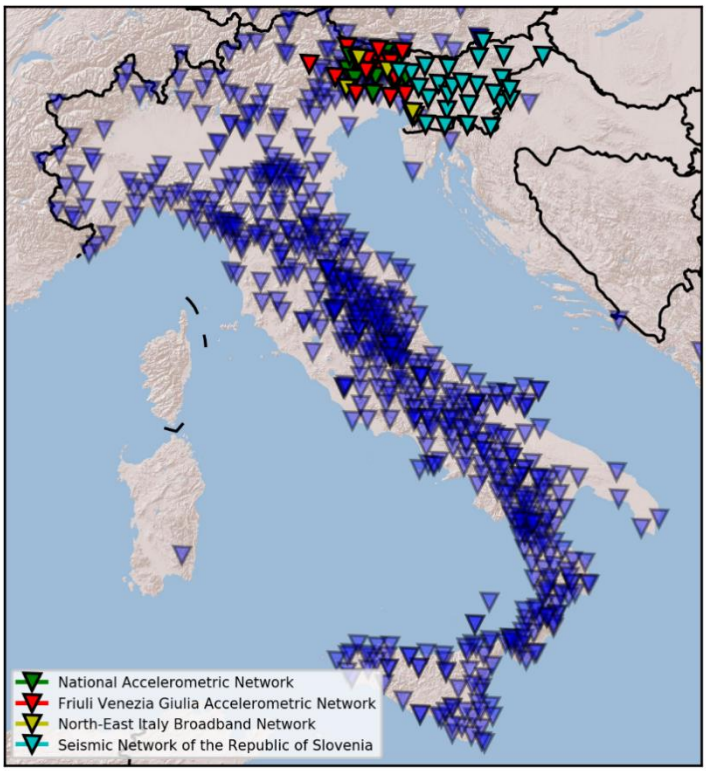

Figure 11: Area of interest is in the NE part of Italy (coloured seismic networks). Station density in Friuli, Italy is much higher than in surrounding areas, but the station distribution in Slovenia still enables us to detect micro earthquakes in real time. Blue stations represent the stations not used in this study but present in the area – of different institutions.

2.1 Earthquake detection

In next subchapters few of the detection methods used in this thesis will be described. Methods are used for the detection of all seismic events, earthquakes, seismic events connected to active mining and quarry blasts. Sometimes, distinguishing between these seismic events can be hard, but in this thesis, majority of quarry blasts that are common for this area were successfully filtered away by checking the frequency content of events, their location and timing, impulsivity and amplitude. Term »earthquake« will be used for natural seismic sources with broad frequency spectrum and release of energy from brittle failure of rock.

For the basis of this thesis, waveforms of all the stations of CE^3RN virtual network in the region of Idrija fault system were processed. First with automatic energy based detection algorithm and automatic location process, later with manual repicking of automatically detected events and by inspecting the data for missed events and lastly by means of cross-correlating of know signal with all available data to find similar repeating events.

2.1.1 Energy based detection

One of the most basic digital signal detector techniques used in seismology for seismic event detection within a continuous data are so called energy detectors. They are based on changes in amplitude of observed signal (Withers et al. 1998). For a successful detection declaration, a short increase in amplitude above the background noise of the single trace must be present in our data. The detection is declared by calculating average amplitude within two predefined moving windows over the data. First moving window is short-term average window (STA), which represents a possible signal of interest, and the second window representing long-term average background amplitude (LTA). A detection will be declared when the ratio of STA/LTA will reach certain present threshold. This technique can be used for different phases of the signal (P and S) with slight modifications. For reduction of false detections, a so-called network detection system must be applied to the data, so only detections declared on multiple station/channel pairs

will trigger a true detection. This enables us to filter the detections caused by near-station noise.

This technique is simple to use and due to the fact, that is not computational expensive can be easily run in real time. That is why most of the real-time monitoring agencies use energy based detection algorithms for real time monitoring.

For successful detection in normal conditions STA window length should be set to the length of a normal P-phase arrival, while LTA should be set to at least the period of the dominant background noise. In Figure 12 the STA/LTA detector is applied to 4 minutes of data on HHZ channel of CEY (Slovenia) station. We can observe 6 successful detections, one for the mainshock, that happened on 22. April 2014, with M_W 4.5, and five smaller aftershocks. A magnitude threshold for automatic detection in this area with STA/LTA parameters that are in use at Seisram group of University of Trieste is around M_L 0.8, meaning we are able to automatically detect all earthquakes with magnitude above this magnitude. For the detection of local earthquakes, STA/LTA parameters were tuned for the detection of high frequency local and micro events. As shown in chapter 2.1.3 the number of detections in the same time window can change dramatically using different detection algorithms.

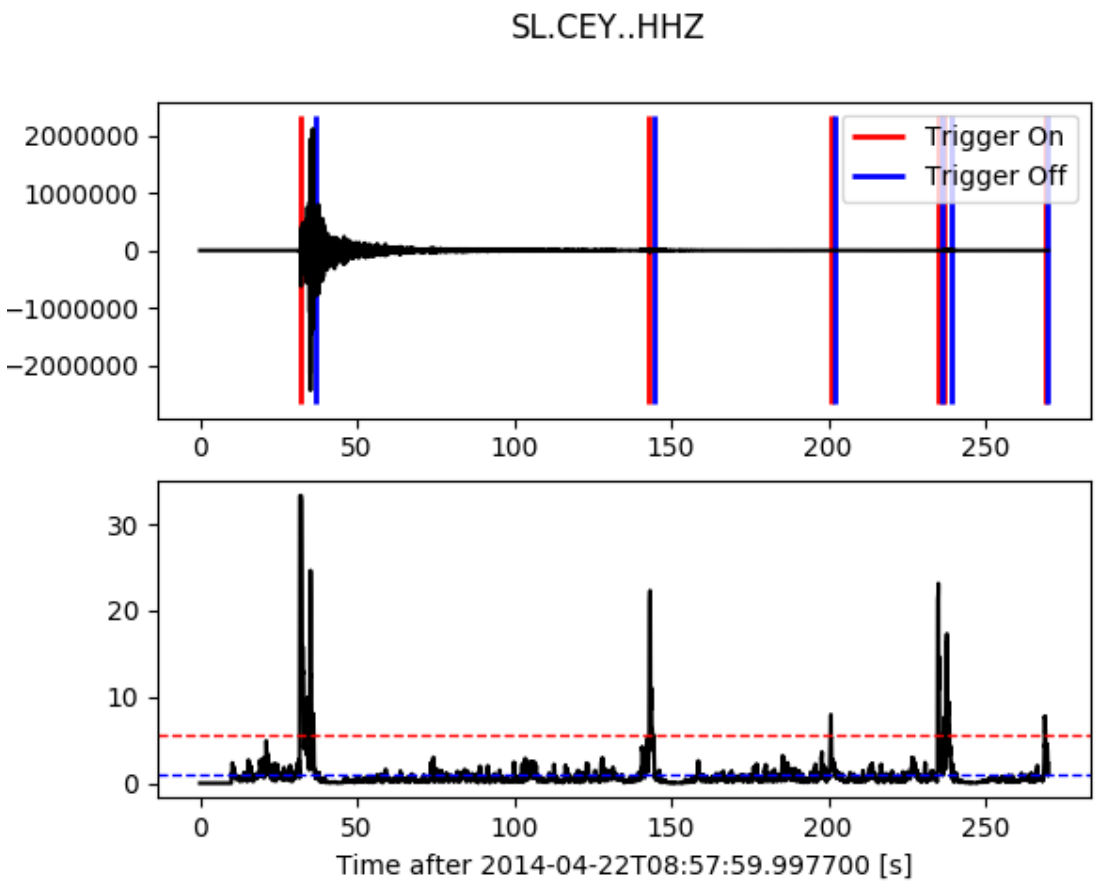

Figure 12: STA/LTA detector used on 4 minutes of data from CEY station, spanning from mainshock that happened on 22nd of April 2014 with M_W 4.5 in southern part of IFS. As seen on the figure, with STA/LTA we were able to detect 5 additional aftershocks. Upper panel shows waveform data band passed between 2-20 Hz with sampling rate of 200 Hz. Vertical lines are on/off times of the detector. STA window length is set to 0.3 s, LTA is set to 10 s. Trigger on ratio is set at 5.5 and trigger off ratio at 1.

2.1.2 Manual inspection of waveforms

For high resolution earthquake relocation and meaningful earthquake rates automatic detections were not enough. There are two main weaknesses of automatic detection, which were partially overcome by manual inspection of the waveforms:

1. Magnitude of completeness of the catalogue of the detected earthquakes in the region of interest is around M_L 0.9 meaning we are able to detect all the events above this magnitude. Most of smaller events are missed.
2. Automatically assigned P-phase or S-phase arrival times must be rechecked and assigned correctly, especially for smaller magnitude earthquakes since the automatic picker is biased at small amplitude changes.

In Figure 13 automatically detected earthquakes are analysed. Magnitude of completeness (Mc) for this catalogue is 0.9 with normal b-value = 1.06. Number of detected earthquakes is 7148 for the period between 2006 and 2015. In Figure 14 Mc of automatic detections using cross-correlation of waveforms with known signal is -0.73. Number of detected earthquakes for this catalogue is 11073. The change in number of detected earthquakes is mostly coming from powerful cross-correlation detection algorithm, that was used for detecting repeating micro earthquakes.

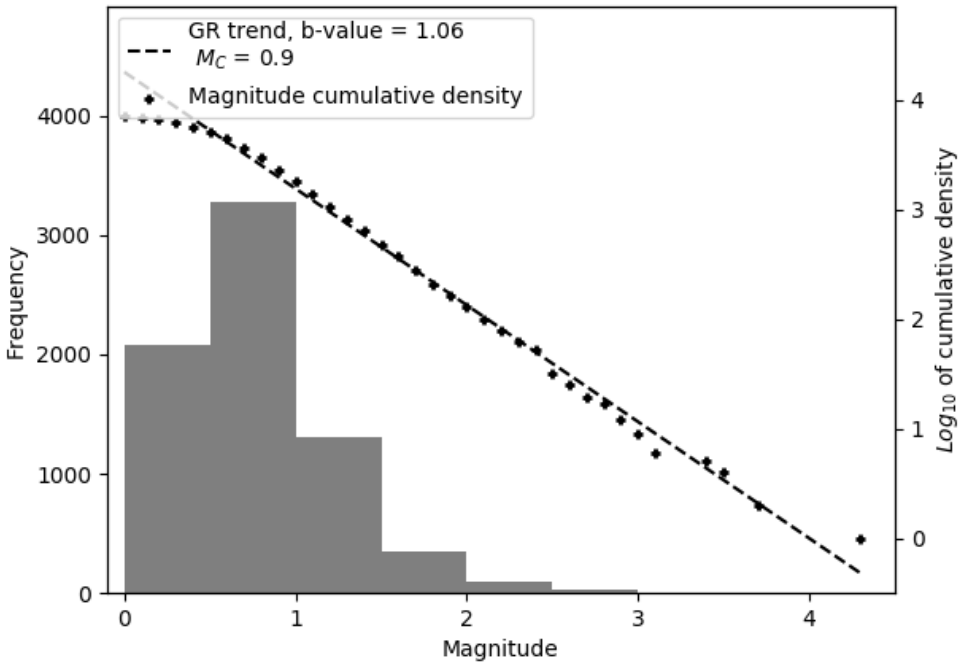

Figure 13: Magnitude of completeness for automatic detection of earthquakes in the area of IFS as reported by ISC (International Seismological Centre 2014). *As seen on figure, GR trend nicely follows the magnitudes of earthquakes until Magnitude of completeness of 0.9 where we can see that the network is not capable of detecting lower earthquakes.*

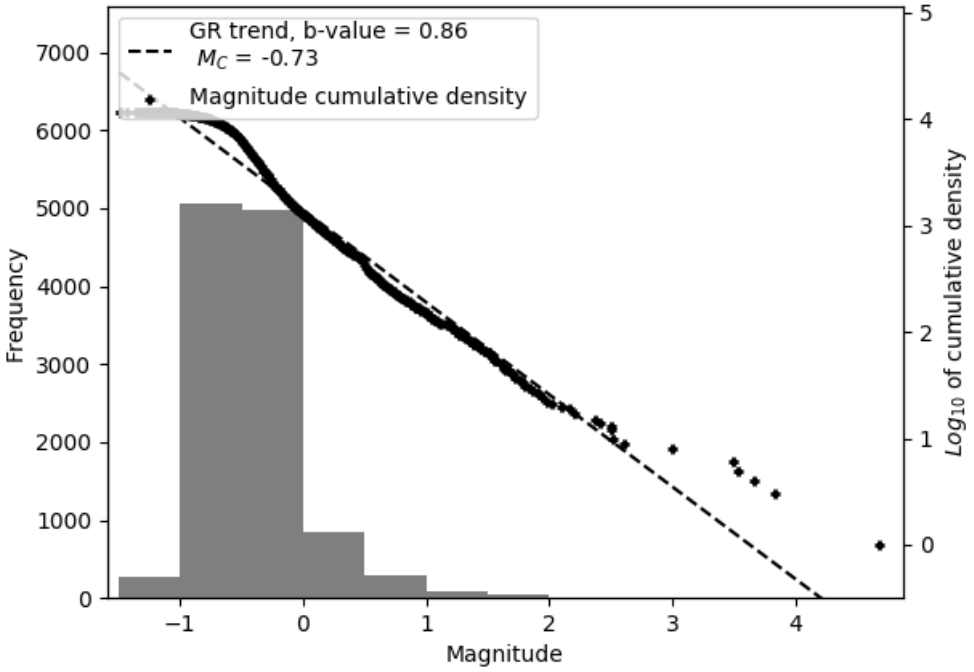

Figure 14: Magnitude of completeness for manual and similarity search algorithm for the same time period and same area as previous figure. Mc was lowered to -0.7 which means we were able to detect majority of micro earthquakes. From the trend we see that there is an elevated number of micro earthquakes with magnitudes below 0.

After the initial scan of all available data with STA/LTA detector, all the detected events had to be checked for false detections and precisely repicked (Figure 15), for better

location estimate. Since Mc for automatic detection is around 0.9, all the remaining data was manually checked, and new events were added to the catalogue with precise arrival picks to obtain good locations. During the manual inspection of the waveforms, numerous events were observed, especially those of aftershock and swarm series, that were too small (observed by less than 3 stations) for phase picking and their relocation. For detection of these events, cross-correlation algorithm was used in the later step.

With manually inspecting all the data available between 2006 and 2015, I was able to detect and better locate multiple new earthquakes, especially earthquakes from aftershock and swarm series, happening along the IFS.

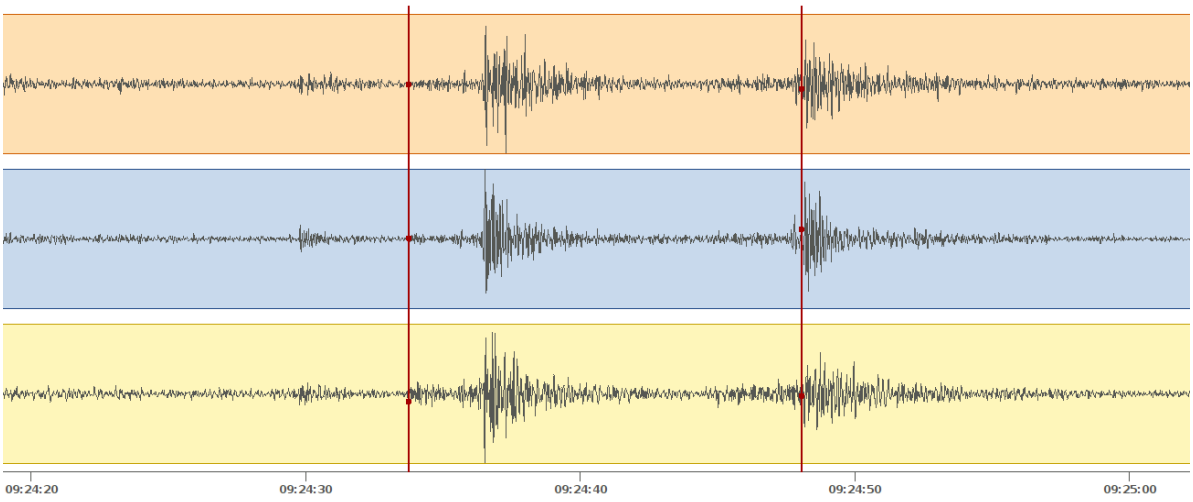

Figure 15: Example of automatic detection and phase association for two aftershocks of the 22. April 2014 M_W 4.5 earthquake on the 3 channels of the station CEY. As seen on figure, one small event was not detected, while the 2 stronger events were. For the first detected event it seems, that the P phase was assigned correctly, but closer inspection shows, that there are still small errors for the automatic trigger. This seen even better for the second detected earthquake which is hidden in the noise of the previous earthquake, so the P arrival time was picked on S and surface waves.

2.1.3 Cross-correlation detection and repicking

Cross-correlation of known signal with continuous signal is one of the most accurate ways for detecting repeating events (Chamberlain et al., 2014; Gibbons & Ringdal, 2006; Shelly et al., 2007). With cross-correlation of the signal even signals with amplitudes way below the signal to noise ratio (SNR) can be successfully detected if our, so called template, matches the part of continuous signal. In seismology, cross-correlation of the signal is known as matched-filter routine and is used in different disciplines of seismology, mostly for detecting repeating earthquakes, whose correlation values are above 0.7 (70% similarity) (Schaff and Richards 2011) in different tectonic settings (Dreger et al., 2007; Igarashi et al., 2003; Massin et al., 2013).

Matched-filter detection routine can be used as a detector of near repeating events on one station, where we rely on high single-channel correlation value for detection declaration (Schaff and Richards 2011). One station/channel pair detections can be observed on Figure 17. If we compare the same time window that is visible on Figure 17 and Figure 16 we clearly see the difference in STA/LTA method and matched-filter method. In the first case, STA/LTA method was unable to detect a micro earthquake that happened in the series of aftershocks to the mainshock of 22. April 2014, but with the match-filter we were able to detect 2 more earthquakes in the same time window.

In this way we can only detect self-similar repeating earthquakes that are happening at almost the same location of asperity, but we are not able to calculate its precise location. This is why matched-filter technique was adapted to seismic network scale, where detection is performed on multiple station-channel pairs at the same time using a network cross-correlation sum, giving us precise P and S arrival times, which we can directly use for the relocation of the detected event. Using network cross-correlation sum we can better detect events hidden in the poor SNR. The method is exceptional for detecting known explosions (Gibbons and Ringdal 2006) and detection of global seismic waves (Dodge and Walter 2015)

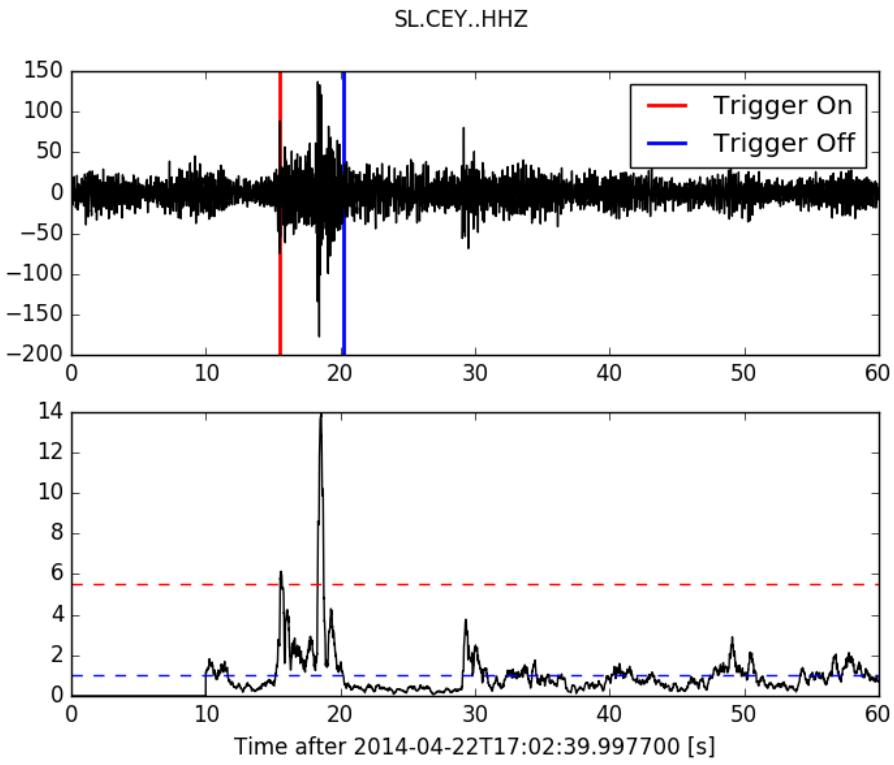

Figure 16: STA/LTA detection method (same parameters as before) was unsuccessful in detecting the micro earthquakes (aftershocks) except of the strongest one in the selected time window which happened later in the day as the mainshock of 22. April 2014. Manually we can clearly see one aftershock and we were able to identify even smaller events, but we were unable to pick the phases.

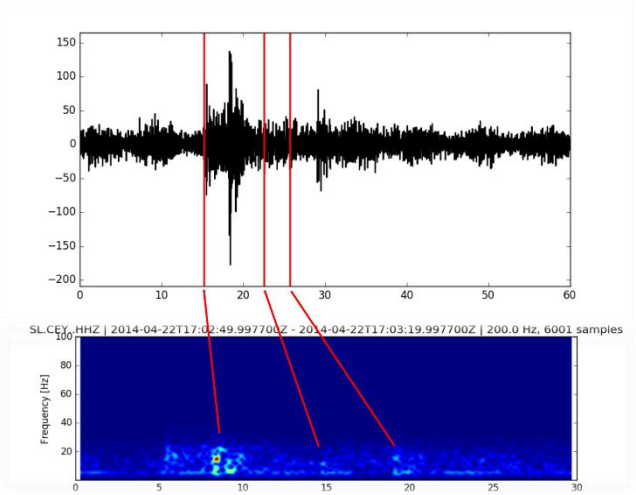

Figure 17: Same data as on previous figure. Red vertical lines represent detected P arrival time of earthquakes detected by matched-filter algorithm. First arrival is correctly set for the biggest of the three events. We were also able to easily obtain arrival of the third event, which was already identified before, but we were not able to set phases. For the second detection we are unable to see the phases at all, but the earthquake can be identified from the spectrogram of the signal. Due to the size this earthquake was not relocated.

Through this thesis, correlation methods were firstly used for the detection of nearly repeating earthquakes in a network configuration (at least 4 stations) and secondly, the method was used to obtain lag-time of arrival times of phases, for calculation of relative locations of the detected events. I used open source software EQCorrscan. For matched-filter detection of new events, EQCorrscan uses normalised cross-correlation values obtained with OpenCV computer vision codes, mostly the *matchTemplate* function from this library. Function is normally used for matching 2D images with R, G, B values for each pixel, but can also be used with 1D seismic data, where each sample represents a pixel with a single amplitude measurement. Normalised cross-correlation values of time series are normally calculated in the time domain (for use in seismology, it is done in frequency domain for faster calculations):

$$R(x,y) = \frac{\sum_{x',y'}\left(T'(x',y') \cdot I'(x+x',y+y')\right)}{\sqrt{\sum_{x',y'} T'(x',y')^2 \cdot \sum_{x',y'} I'(x+x',y+y')^2}} \qquad 1$$

where I' is the normalized source image, T' is the normalised template image and R is the result. (x, y) is a sample in the image (where (x, y) ranges from 0 to ($N_{(x,\,y)} - w_{(x,\,y)}$), with $N_{(x,\,y)}$ equal to the length of the image in x and y dimensions and $w_{(x,\,y)}$ equal to the length of the template in x and y dimensions. (x', y') is the sample position within the window being correlated. In the case of 1D seismic data, y values can be ignored simplifying Equation 1 to:

$$R(x) = \frac{\sum_{x'}\left(T'(x') \cdot I'(x+x')\right)}{\sqrt{\sum_{x'} T'(x')^2 \cdot \sum_{x'} I'(x+x')^2}} \qquad 2$$

here, the normalised template and image are computed as:

$$T'(x') = T(x') - \frac{1}{\omega} \cdot \sum_{x} T(x'') \qquad 3$$

and:

$$I'(x+x') = I(x+x') - \frac{1}{\omega} \cdot \sum_{x''} I(x+x'') \qquad 4$$

with x'' representing the position in the template or image being summed over for the normalization.

EQCorrscan uses implementation of the above algorithm in the frequency domain, since computing cross-correlation in the time-domain is slow for large datasets, meaning our data is transferred from time domain to frequency domain using Fast Fourier transform – from time series into a sum of sine waves of different frequencies.

When running our data in EQCorrscan, first our data of interest (daylong datasets) are padded with zeros and then re-cut at start and end of the day. Template waveforms are then cross-correlated with our data on the same station and channel pairs as the templates. To obtain network cross-correlation sum, the correlation vectors from single station channel pairs are summed.

After we obtain network cross-correlation sum, we need to find the correlated events. To find the events, a threshold based on median absolute deviation (MAD) value is set (normally to 8 x MAD). MAD is a robust statistic to outliers in otherwise normally distributed data, meaning that in the data of random noise, network cross-correlation values are randomly distributed, while in case of the detected event, outliers will be present in otherwise normal distribution as seen on Figure 18. If too low value for MAD is selected we will obtain much higher number of detections, due to the correlation in noise. Too high MAD on the other hand will remove low magnitude earthquakes and earthquakes hidden in the low SNR. With selected value at 8xMAD we obtained less than 5% of fake detections – mostly due to the quality of our templates which were all manually reviewed. Since we visually inspected all the detected earthquakes, fake detections were removed and did not affect this study.

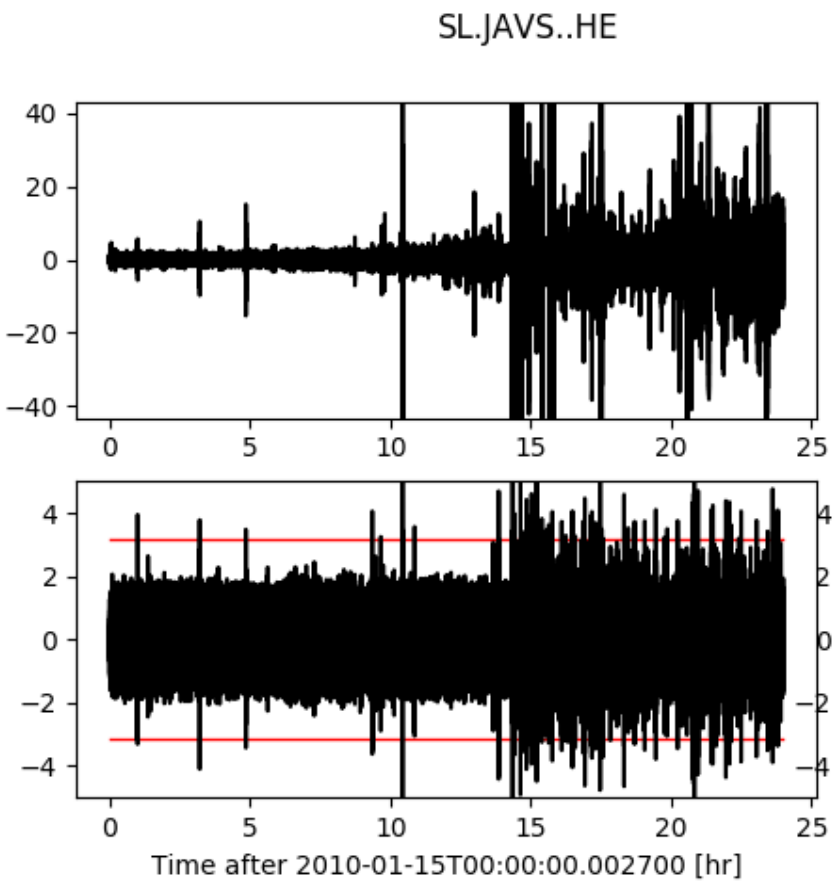

Figure 18: Example of one day of data. On top figure raw daylong (hours) data is shown. On the bottom figure cross-correlation sum of templates along this channel is displayed with red horizontal line set at 8xMAD. For each template a cross-correlation value for each sample (time window is advancing at 0.01s) is calculated then summed. Where threshold is reached, a detection is declared. Similarly, network cross-correlation sum is defined. Instead taking CC sum on only one station/channel, summation is performed along all the stations and all the channels used in templates.

In this thesis, templates were created for precisely repicked events with magnitudes above 0.8 for earthquakes in the N part of IFS, along Ravne and Idrija fault, for central part of IFS and for the southern part of IFS along Selce, Predjama and Rasa fault and for mainshock-aftershock sequences and swarm sequences. Templates were generated from catalogue of arrival times for different earthquakes, on four closest stations for sub region. For templates at least 4 P arrivals had to be present, while S arrivals were used where available.

After successful detection (Figure 19) of repeating and similar earthquakes was performed, repicking of the detected phases was performed by cross-correlating P and S time windows of the template earthquake with P and S time windows of the detected

events. At the highest cross-correlation value, new P or S arrival time was declared incorporating slight lag time that is later translated into slightly different location. With this method even changes smaller than one sample (if interpolation is used) of the two signals can be detected. The method for obtaining new arrival times in EQCorrscan package uses time-domain correlation from the seismological open source python package Obspy (Beyreuther et al. 2010). Module computes normalised cross-correlation for the master signal with its detections to find the optimal offset without padding our data. This is done by selecting time window around the detected P or S arrival time for each station channel pair. The correlation is done between template and original signal and where the peak of cross-correlation is found, new lag-time is declared, which can be then used for recalculation of absolute P or S arrival time:

$$T^i = t^i_{window} + \delta t^i + \tau^i \qquad 5$$

where T is the resultant absolute pick, t_{window} is the start of the window, δt is the lag time generated by our process and τ is the delay between the start of the template window and the known phase arrival.

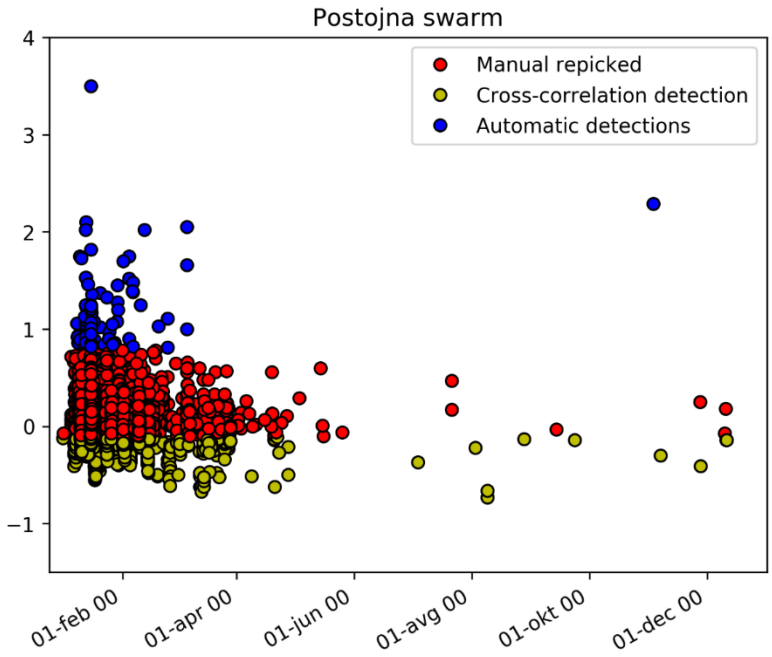

Figure 19: Differences in 3 techniques used in this thesis. In blue automatic detections are shown. Red are handpicked events. Handpicking can be time consuming and we are not able to locate all observed events. In yellow, automatic detections from matched-filter detection are shown. With this technique we were able to detect all the events visible on this figure in matter of hours, while handpicking can take months. For matched-filter detection only templates of the earthquake in blue were used, but all seen on the figure were detected.

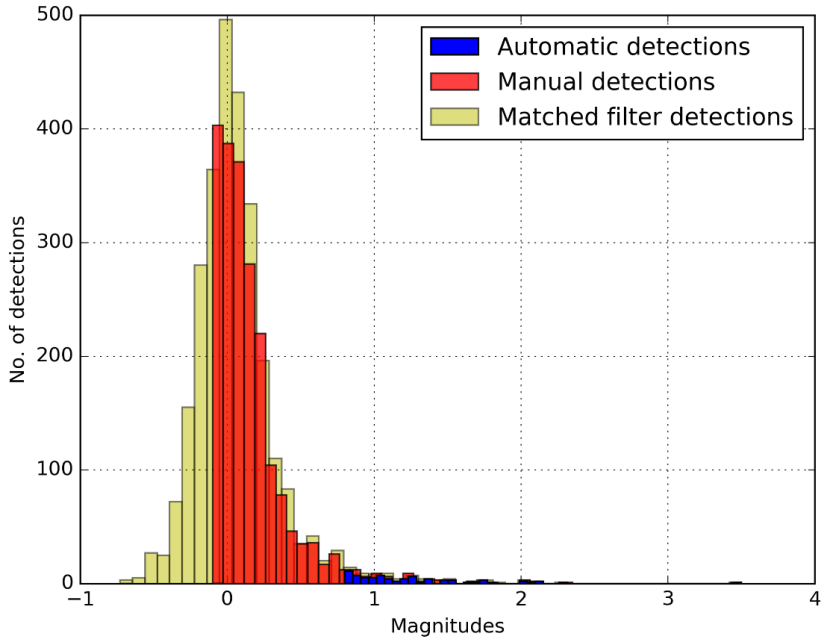

Figure 20: Similar to Figure 19, we can clearly observe the differences between automatic detections for the Postojna swarm (blue), manual inspection of the waveforms (red) and detections done by matched-filter technique (yellow). The biggest change is observed at the low magnitude earthquakes where SNR is low. Earthquakes detected automatically were repicked and used as templates.

	No. of automatic detections	No. of relocated and used for templates	No. matched-filter detections
Vipava 2006	54	22	699
Postojna swarm	99	67	3151
Ilirska Bistrica 2010	90	82	2336
Knežak 2014	47	45	1359
Bovec area	113	71	1874
Selce 2017	9	9	275
Rijeka 2017	52+27	52+27	748+453
Ilirska Bistrica 2017	6	6	29
Snežnik 2017	21	21	271

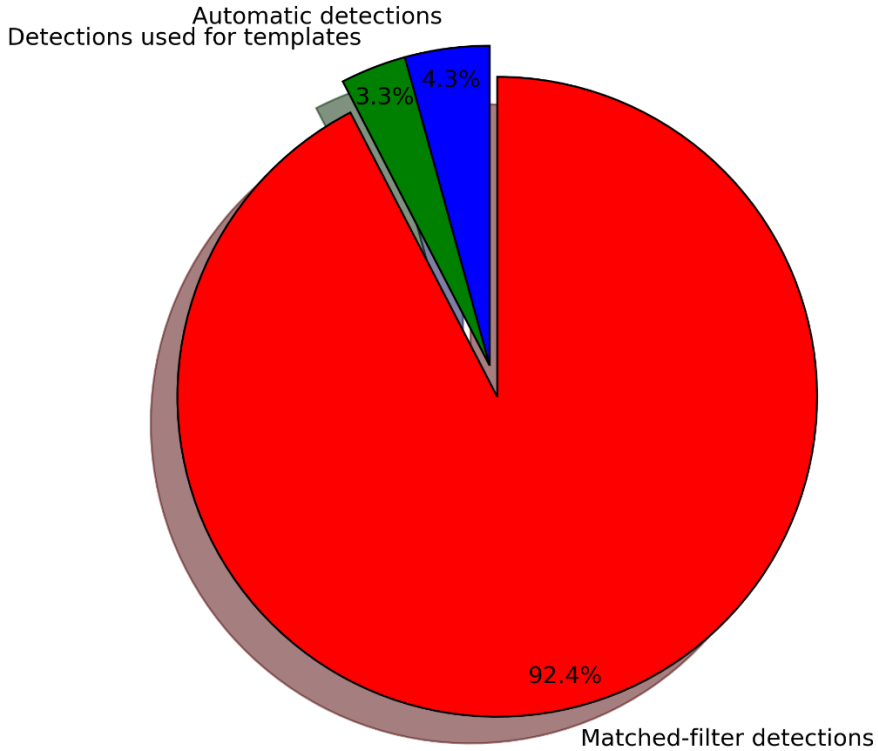

Table is showing number of automatically detected earthquakes for different sequences that happened in the study area in the time span of the datasets. For templates slightly lower number of the detected earthquakes was used, since we only used earthquakes above magnitude 0.8 and good SNR ratio. It is clear, that with the matched-filter detection technique we were able to detect much greater number of earthquakes.

2.2 Earthquake locations

Location of an earthquake is, together with magnitude its most important feature. Location gives us some constrains on the underlying geological structure of the area and in case of earthquake hazard, insight on what damage to expect in different regions of the area struck by an earthquake. Earthquake location can be obtained by forward modelling of source parameters or obtained from inversion of the raw signal from the seismic observations. Normally, location is given as a hypocentral location, which represents earthquake location in three dimensions, either in global or Cartesian coordinates. In these chapter three main methods used for the relocation of the events in the area of IFS will be described, starting with the simplest linear methods (not really used for the relocation of the events, but serves as a basis of understanding the earthquake location techniques). Later non-linear and relative methods will be discussed.

2.2.1 Linear methods

The simplest methods for earthquake location are linear methods. For a simple homogeneous half-space in Cartesian coordinate system (X, Y, Z), relation between origin time (T), arrival time (t) and hypocentre follows next equation:

$$t_i = T + \frac{1}{v}\sqrt{(X - x_i)^2 + (Y - y_i)^2 + (Z - z_i)^2} \qquad 6$$

Where $_i$ denotes the characteristics of i^{th} recording station and v is the velocity of the homogeneous half-space. By forward modelling, we can calculate travel time for a given station from a pre-chosen hypocentre and origin time. The best location (grid or some other) is then selected by minimizing residual (r_i) where residual is given by:

$$r_i = t_i^{calc} - t_i^{obs} \qquad 7$$

Contrary, the inversion approach of the above problem uses Geiger's location method (Geiger, 1910), later modified by Thurber (Thurber 1985). Inversion relies on the expansion of the first order Taylor series about a hypocentre and solving in a least squares fashion:

$$r_0 = \frac{\delta t_i}{\delta X}\Delta X + \frac{\delta t_i}{\delta Y}\Delta Y + \frac{\delta t_i}{\delta Z}\Delta Z + \Delta t_0 \quad (8)$$

where t_0 is origin time and term preceded by Δ are adjustments to be made on the model. Partial derivates are expressed below:

$$\frac{\delta t}{\delta X} = \frac{X - x_i}{vS} \quad (9)$$

$$\frac{\delta t}{\delta Y} = \frac{Y - y_i}{vS} \quad (10)$$

$$\frac{\delta t}{\delta Z} = \frac{Z - z_i}{vS} \quad (11)$$

where all terms are as before, with addition of a path length term (S).

To obtain all the earthquake location parameters, we would need at least four travel-time recording of the single earthquake. With more information also our accuracy will increase.

For more accurate results prior knowledge of the earth structure should be considered, which is why equation 6 include the velocity model modification. Changes in the model itself will give us better understanding of the fault geometries, since we will be able to obtain better earthquake location. Discussion on complexities (different seismic phases

due to the layered earth model) derived from the changes in velocity model is described in details in Thurber (1985).

The Geiger method relies on the approximation of a non-linear system (equation 6) to a linear system of equations (equation 8). This methodology is reasonable for local earthquakes in a simple medium but becomes unreasonable for more complex media or for distant earthquakes.

2.2.2 Non-linear methods

For complex media, we must include the second order term of the Taylor series, which takes the form of second order differentials (Thurber 1985) if we want to solve for more stable earthquake locations. Differentials can be calculated analytically as seen below with similar solutions for remaining x and y terms:

$$\frac{\delta^2 t}{\delta Z^2} = \frac{1}{vS}\left[1 - \frac{(Z - z_i)^2}{s^2}\right] \quad 12$$

$$\frac{\delta^2 t}{\delta Y \delta Z} = \frac{(Y - y_i)(Z - z_i)}{vS^3} \quad 13$$

$$\frac{\delta^2 t}{\delta X \delta Z} = \frac{(X - x_i)(Z - z_i)}{vS^3} \quad 14$$

Non-linear methods are useful for calculating location of sources whose depths are at similar depths as our receivers (shallow events) since for the case Z = z_i the first-order partial derivative for $\frac{\delta t}{\delta Z}$ vanishes and for the second-order partial $\frac{\delta^2 t}{\delta Z^2}$ is maximised. Also, if hypocentre of our source lies outside of our array of receivers, non-linear methods should be used, due to higher sensitivity of second-order partial derivates.

For non-linear inversion to work, we need at least 4 travel-time observations. For all the earthquakes that were automatically detected in the studied time period, we obtained more than 4 travel-time observations, while for some of the earthquakes found by manual waveform inspection this was not the case, so I was unable to locate those earthquakes. Automatic locations were obtained with Antelope package with grid locations, while manual locations were obtained with different locator, giving us better locations. For the initial locations Antelopes® dblocsat2 package was used, which uses non-linear iterative inverse technique performing the least-squares inversion via a singular value

decomposition method. Dblocsat2 calculates events location, confidence bounds, residuals, arrival times, azimuth and slowness for local, regional and teleseismic events.

In real Earth situations, we rarely deal with constant velocities, so we need to take in account changing Earth's structure either in 1D or 3D. In our work, both 1D and 3D velocity models were used. For first automatic and manual locations, 1D IASP (Kennet 1991) velocity model was used, while in the next step, I used NonLinLoc software (Lomax 2011) with which I used regional 3D velocity model. The use of linear methods is reasonable for local events in the simple medium (1D velocity model) but the problem quickly becomes unstable for more complex media (3D velocity model) or for distant earthquakes.

For non-linear solutions, software package NonLinLoc (Lomax 2011) was used. To obtain locations with NonLinLoc, package first generates travel time grid for every source in a chosen grid to each receiver. Picks are then compared to these grid travel times by non-linear inversion with a Metropolis-Gibbs method (Lomax 2011) which gives us the best possible location of the event through 3 main stages of localization – learning stage, equilibrium stage and saving stage. Learning stage is a step with relatively large and fixed step sizes and will explore the search volume globally, migrating towards regions of high likelihood. In the equilibrium stage, step size is adjustable in proportion to the standard deviations of the spatial distribution of all previous accepted samples. In the saving stage, step size is fixed again at the best size obtained in the equilibrium stage. The »walk« continues to explore regions of high likelihood, finally giving us the best probability density function of the x, y, z hypocentre location.

2.2.3 Relative methods

For final relative earthquake location estimation, double-difference method was used, as is provided in the HypoDD software (Waldhauser 2001). Input for the software were handpicked P and S arrival times of the local earthquakes and for the relocation of clusters, input were arrival times with lag-time added, obtained by match-filter detection.

For relocation of the events with relative methods, absolute travel time measurements and/or differential travel times obtained from cross-correlation of master event with its

family of events are needed. Travel times are used for generation of double difference equation in the form of:

$$dr_k^{ij} = \left(t_k^i - t_k^j\right)^{obs} - \left(t_k^i - t_k^j\right)^{cal} \quad 15$$

where dr_k^{ij} is the double difference residual for a pair of earthquakes, i and j. The method works only for the events that happened close in space and share a constant slowness vector. Location is obtained from expansion of previous equation into:

$$\frac{\partial t_k^i}{\partial x}\Delta x^i + \frac{\partial t_k^i}{\partial y}\Delta y^i + \frac{\partial t_k^i}{\partial z}\Delta z^i + \Delta\tau^i - \frac{\partial t_k^j}{\partial x}\Delta x^j - \frac{\partial t_k^j}{\partial y}\Delta y^j - \frac{\partial t_k^j}{\partial z}\Delta z^j - \Delta\tau^j = dr_k^{ij} \quad 16$$

with terms as the partial derivates of travel-times t with respect to the location (x, y, z) and origin times τ. Δx, Δy, Δz and Δτ are the changes required to make the model better fit the data. Computation of these changes is done by linear, least-square inversion for all the stations and hypocentral pairs with iteration.

With this method we allow for variations in the velocity structure that is not apparent in the original velocity data and we can obtain improved locations of the hypocentres according to the correlation limits derived from our repicking of phases by correlation. Final result gives us better understanding of the underlying geological structures with highlighting the activated structures (Waldhauser 2001). Differences in the location algorithms are presented on Figure 21.

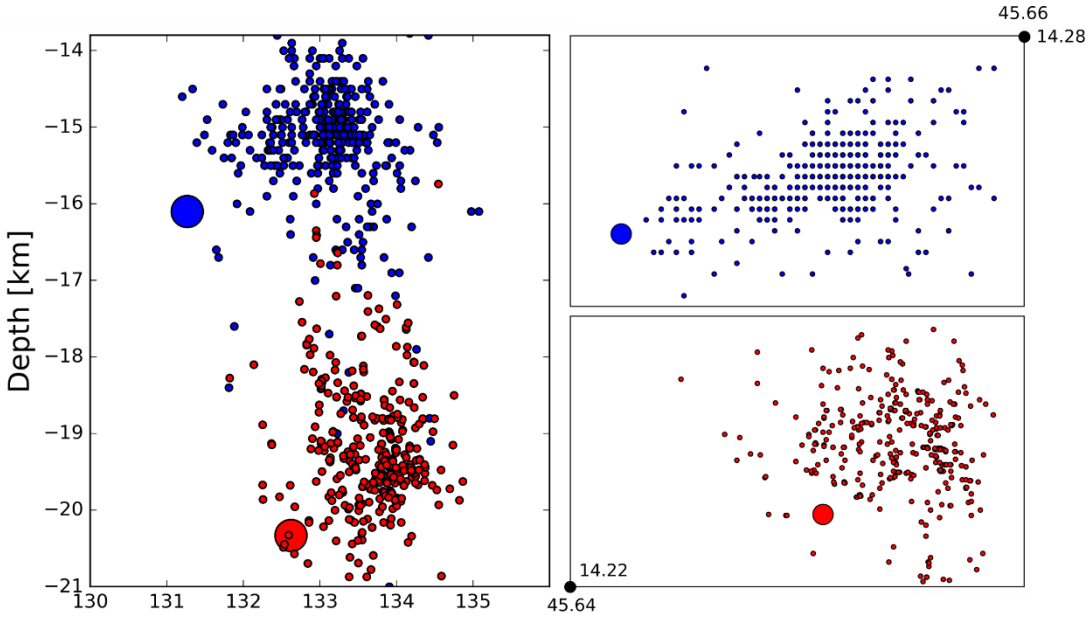

Figure 21:On the left figure a depth profile of 22. April 2014 mainshock aftershock (45.6467, 14.2534) sequence is presented. In blue, locations as reported in ISC bulletin are shown (relocated using IASP91 model) while in the red locations obtained with matched-filter detection algorithm and later relocated with hypoDD software and 3D velocity model are shown. ISC bulletin for this example uses grid search methodology for location of the earthquakes which is a fast method but masks possible reactivated faults. While the network density along IFS still does not allow us to observe structures in detail, it seems that a seismic gap is present (both on map view and cross section) at the location of mainshock, which could be explain with a location of freshly ruptured fault. The possible location of the main rupture becomes even more apparent if we select the right lateral strike slip event in NW-SE direction as the preferred solution. Aftershocks happen along smaller parallel structures stressed due to the mainshock. The difference in depths is present due to the 3D model being slightly faster in this region.

2.2.4 Earthquake location errors

When locating earthquakes we cannot go past the fact, that our earthquake location is only an estimate of a true location due to the several facts:

- Always present measurements errors of seismic arrival times,
- Errors due to the modelling co calculated travel times (errors of velocity model…)
- Nonlinearity of the earthquake location problem

All these errors will cause our locations to scatter all around the real location and their size will vary according to the previously specified problems. When dealing with errors we speak about errors in precision and errors in accuracy. Precision errors come from the measurement errors (our (in)ability for precise detection of phases that are not impulsive…) while accuracy errors are always present biases coming from unknowns in modelling of data.

Most common of the precision errors are errors of measurements of seismic arrival times. Seismic signal is always affected by some level of noise and the arrival phase is not a pure delta pulse, every seismic signal incorporates at least small uncertainty. We partially overcome this problem by manually checking all the detected earthquakes and reassigning the arrival times to their more precise timings. This was all done on the three component stations so also S arrivals were chosen with better precision. For the impulsive phases selecting “correct” time was easier than for gradual phase arrival, for which we had to choose a short time window of the arrival. For the smaller similar earthquakes that we detected using the matched-filter detection algorithm precise picks were derived from cross correlation of known signal with the detected one and selecting the arrival time of the phase at the highest cross-correlation value of normalized signals.

Very important uncertainty estimate comes from the station geometry criteria. We only selected earthquakes for which we had azimuthal gap less than 180° and were recorded on at least 4 stations (P phase). S phases were harder to detect, but for the majority of the earthquakes at least 1 read S phase was available.

The hardest spatial parameter of the earthquake to obtain is its focal depth. To obtain good estimate of depth we need to have many arrival times on the stations at different distances from the source. For larger earthquakes in our study this was not a problem,

since they were detected by multiple stations of the network. For the micro earthquakes this was not the case, since majority of them was only detected by closest 4 or less stations (for relocation only those detected by 4 stations were used). But since we knew the location of the earthquakes used for creation of templates (more than 4 stations) we could evaluate location of the detected micro earthquakes as good since after the relocation their location did not shift far away from the initial template.

With this constrain we were able to evaluate relative locations of the micro earthquakes to their bigger template originals. For evaluation of the absolute location, ground truth events were used (quarry blasts). We know the location of all the active quarries in the region and approximate timing of the detonations. When setting arrival times to the detonations, which were detected by multiple stations, we observed that our location was never more than 500m away from the quarry with depth always between 0 and 1km, depending on the network in the vicinity.

From the relocated earthquakes (before the matched-filter detection) we estimated our spatial errors to be relatively low, with maximum area of error ellipse for epicentre at less than 2km and maximum depth error at 3km (Figure 33).

Final workflow of the earthquake detection and relocation consisted from next steps:

- STA/LTA detection algorithm was used for the detection of local earthquake.
- Automatically detected and located earthquakes were manually inspected for the correction of arrival times set by previous run.
- The waveforms of the same time period were manually inspected for all the missed earthquakes for which we were able to assign at least 4 P arrival times. If this condition was not met, the event was not used.
- All the automatically detected and repacked earthquakes and all the manually picked earthquakes with $M_W >= 0.8$ were selected as template earthquakes and were pre-processed and cut accordingly.
- Template earthquakes were used for the detection of similar earthquakes with EQCorrscan package using cross-correlation as a detection method.
- The detected events were simultaneously shifted to the best match in correlation value to obtain more precise P or S picks.
- The newly detected earthquakes were relocated using NonLinLoc and HypoDD if the picks were done for at least 4 P arrivals giving us a better view on the geometry of the IFS.
- Magnitudes were calculated for real earthquakes; fake ones were discarded.
- Newly detected earthquakes were used for tectonic interpretation and interpretation of temporal evolution of the IFS.

2.3 Magnitude calculation

Magnitude is, together with the location of an earthquake one of the most important earthquake parameters. Correct estimation of magnitude is one of the most important estimations for seismic hazard since it helps to plan distribution of help after the earthquake and can be of help in estimation of other hazards, directly connected to the earthquake itself (tsunamis, landslides, ...). Multiple different magnitude estimation exists, with most important one being moment magnitude (M_W). M_W gives us a direct observation of physical properties of the rupture but can only be constrained for earthquakes with magnitudes above 2. M_W can be written as:

$$M_w = \frac{2}{3} log_{10}(M_0) - 10.7 \quad (17)$$

where M_0 denotes seismic moment:

$$M_0 = \mu AD \quad (18)$$

where μ means shear modulus of the crust, A is area of the slip on the fault and D is average displacement during the earthquake.

For local micro earthquakes, local magnitude (M_L) was calculated using next formula:

$$M_l = log_{10}(A) + corr \quad (19)$$

where *A* represents maximum amplitude of the signal in micrometres as read on any of the three components and *corr* represents station correction coefficient obtained from the epicentral distance between station and earthquake epicentre. Final magnitude was estimated as a median of magnitudes on all the stations used for the location of the event.

Important note here is, that the majority of the earthquakes detected and relocated with matched-filter technique is too small to even consider using any different kind of magnitude estimation. These earthquakes were normally detected just by four closest stations, which are maximum 50 km away from the epicentre. North-eastern Italy has a low attenuation values for the magnitude estimates (Di Bona 2016), but since all the stations used for micro earthquake detection are near source, attenuation should not play significant role for the magnitude estimation in any case. Big number of events detected using matched-filter detection algorithm show negative magnitudes. Negative magnitudes exists because M_L, when introduced in 1935 (Richter 1935) used a so called Wood Anderson seismograph to develop the magnitude scale. Scale was defined as a record of a magnitude 3 earthquake, that produced 1 mm amplitude reading at the epicentral distance of 100 km. A magnitude 0 earthquake had 0.001 mm amplitude at the same distance (Shemeta and Anderson 2010). Since the advance in equipment design in seismometers and shorter distances between sources and receivers, much smaller events can be detected, whose baseline is lower than 0 originally designed by Richter (Richter 1935). Example of M_L magnitude calculation of earthquakes that happened close to the city of Rijeka in Croatia in summer of 2017 and of the swarm sequence happening not far away from Rijeka in 2017 can be seen on Figure 22.

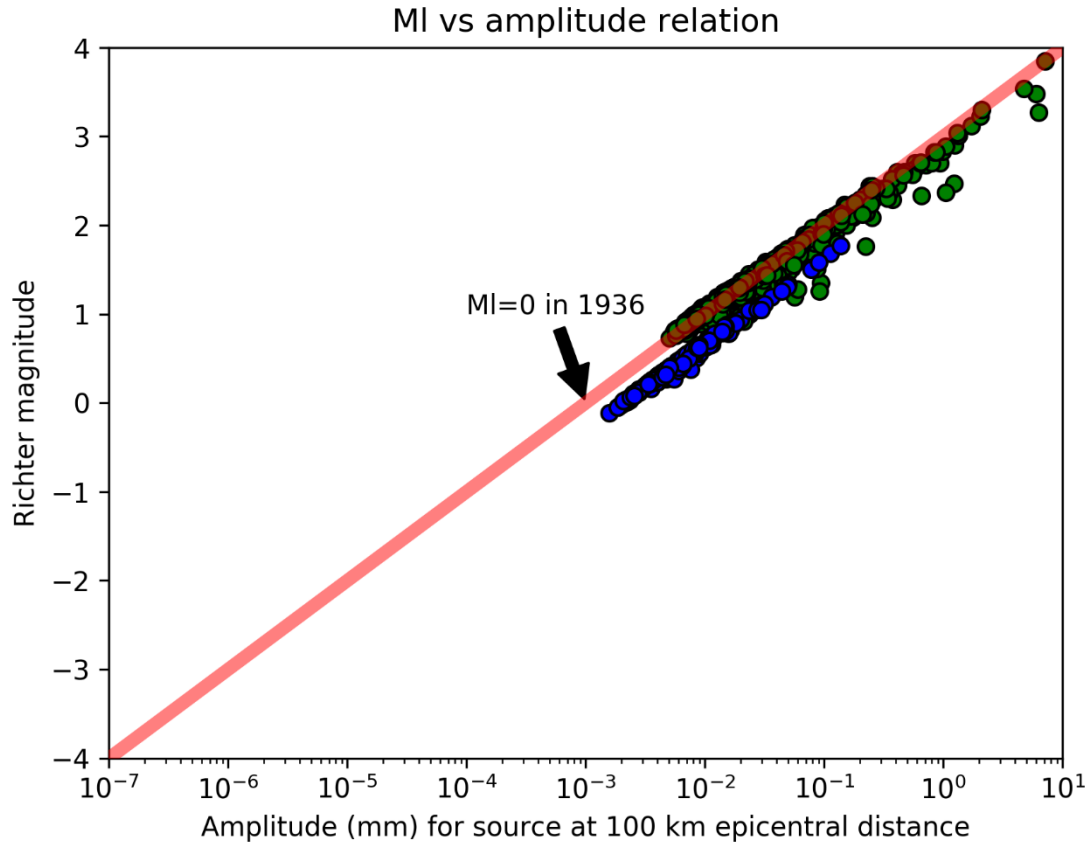

Figure 22: Richter magnitude versus the displacement recorded at the 100 km epicentral distance from the earthquake with Wood Anderson seismometer is represented by red line. Green dots represent calculated magnitudes for mainshock aftershock sequence of 2017, that happened close to the city of Rijeka, Croatia. Because the closest station RIY is very noisy and records only at 50 Hz, we miss all the micro events below magnitude 0.7, but we can clearly observe that M_L calculated in this thesis nicely follows Richter magnitude law. Blue dots represent a 2017 swarm, happening along Selce fault. We were able to detect lower magnitude events, due to better network geometry and fact, that closest stations were much less noisy and are recording at 200 Hz, as in the Rijeka case. Slight shift away from Richter magnitude is observed, probably due to the small number of stations, used in the calculation of the magnitudes.

Magnitudes for earthquakes, detected with matched-filter detection method were calculated only on the 4 closest stations, due to the size of earthquakes, which was small enough, for earthquakes not to be visible on the stations further away. To compute the magnitude, waveforms of all three channels of all stations were ordered by epicentral distance. For each station, I broadband filtered the waveforms between 2 and 20 Hz and remove the response of the station. Waveforms were transferred from raw data to displacement seismograms. After this step, waveforms were detrended and then, detection times of the earthquakes obtained with matched-filter were taken, and the waveforms were cut for 0.1 second prior to the detection time and few seconds after, changing from

cluster to cluster, depending on the location of the seismic cluster. Signal was cut in such way, that all the earthquake was present in the cut waveform. After cutting, 0.5% taper was applied to remove artefacts at the beginning and end of the cut waveform. The maximum amplitudes were read on all 3 channels, not only horizontal, from where only the maximum amplitude reading was kept. After this step, magnitude of station was calculated applying the correction factor depending on the epicentral distance obtained from the study of earthquakes in Southern California (Hutton and Boore 1987). The same factor can be applied in my case (Di Bona 2016). Lastly, median of all the station magnitudes was selected as final magnitude, to remove big outliers. The station corrections are between 1.4 for 0 km epicentral distance to 3.0 at 110 km epicentral distance as it is shown in Table 1.

Correction	Epicentral distance [km]
1.4	0 - 5
1.4	5 – 10
1,5	10 – 15
1.6	15 – 20
1.7	20 – 25
1.9	25 – 30
2.1	30 – 35
2.3	35 – 40
2.4	40 – 45
2.5	45 – 50
2.6	50 – 55
2.7	55 – 60
2.8	60 – 65
2.8	65 – 70
2.8	70 – 75
2.9	75 – 80
2.9	80 – 85
3.0	85 – 90
3.0	95 – 100
3.0	100 – 110

Table 1: Station correction factor used in magnitude calculations with respect to the epicentral distance in kilometres between the source and station.

In the same way, also magnitudes of the automatically detected earthquakes, using STA/LTA method and earthquakes, manually picked from the waveforms, were calculated. For the calculation of these earthquakes, software package Antelope was used.

2.4 Focal mechanisms calculation

Focal mechanism of an earthquake gives us insight in geometry and sense of the displacement that happened during the earthquake in the source region that generates seismic waves. By calculating focal mechanism, we obtain orientation of the fault plane and slip vector. Focal mechanism can be obtained by full waveform inversion, but the method is limited to earthquake of magnitudes above 3, for which we can obtain full moment tensor solution. The second possibility of focal mechanism calculation, which was used in this study, is from polarity of first motion arrivals. In the first motion focal solution method, we directly observe sense of the first arriving P wave. The relative movement of the arrival will tell us either the station is located in the region of compression or in the region of dilatation. The radiation pattern is directly connected with the radiation pattern of a focal sphere. The focal sphere is defined by take-off angles and azimuth for the ray path leading to the station. The focal solution is now defined by quadrants of tension axes, which reflects the minimum compressive stress direction (coloured) and pressure axis, which reflects the maximum compression stress direction. When the focal mechanism is constrained, two orthogonal fault planes are possible. True fault plane must be selected by expert judgement.

Focal mechanisms, as shown in Figure 23 are routinely calculated by Italian agency »Instituto nazionale di Oceanografia e di Geofisica Sperimentale« using full waveform inversion (Dreger 1994) and by Slovenian agency »Agencija Republike Slovenije za okolje« using first arrivals polarity (Snoke 2003). Focal solutions from OGS, ARSO and those calculated during this thesis (not covered in the catalogues by OGS or ARSO) are shown in different colours, depending on which fault the focal mechanism was constrained on. The focal solutions calculated during this thesis were calculated from first arrival polarities since magnitude of earthquakes was not high enough to use some waveform inversion methods.

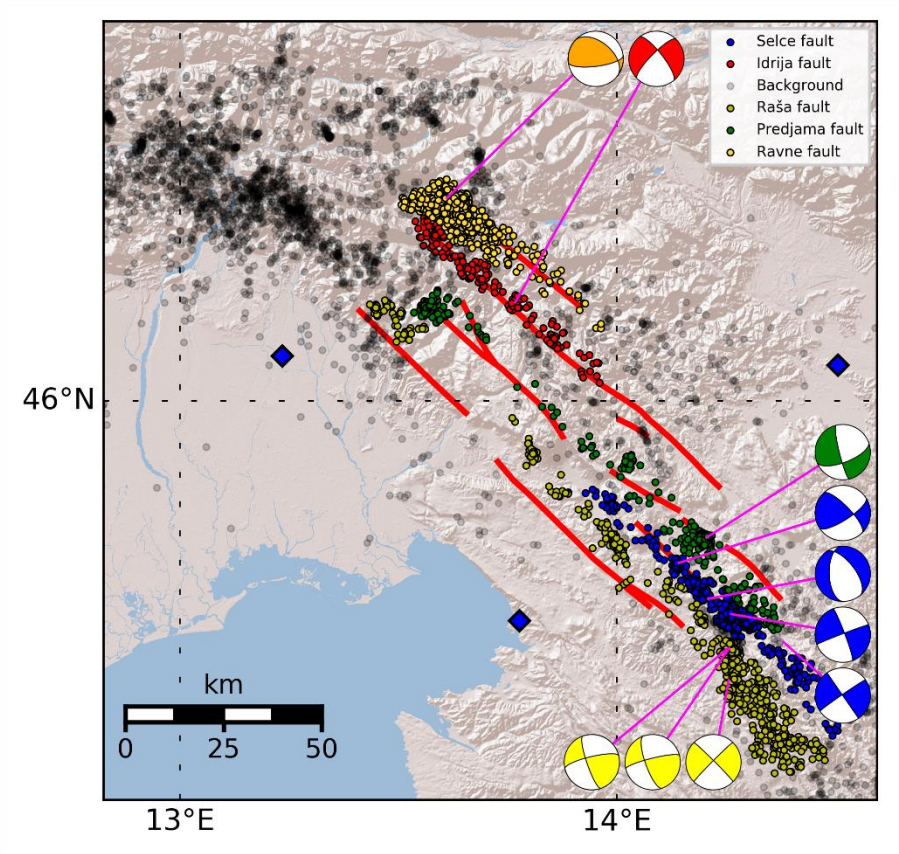

Figure 23: Focal mechanisms for the stronger events that happened between 2006 and summer of 2017 in the area of IFS. Focal mechanisms are coloured regarding the main fault they could belong to. The locations of earthquakes come from this study. As seen on the figure, majority of earthquakes that happened along IFS can be attributed to one of the faults and only small number cannot and are treated as background earthquake activity. Focal mechanisms were obtained from OGS and ARSO, while some of them where calculated in this work.

For the computation of focal mechanisms, a package of Fortran codes Focmec (Snoke 2003) was used. First, data was prepared by reading the polarities of the waveforms of vertical component for each station. Also, the impulsivity of the signal was checked. Next, the epicentral distances, azimuth between the event and station and take-off angles of phases for the event were calculated using the IASP91 velocity model. The data was inputted into Focmec software which calculated best possible fits of the input polarities. Since the station coverage for such small events is not optimal, errors in few degrees are possible, but the solutions were stable enough to decide on possible mechanism. Finally, two new focal solutions were added to the existing ones, one showing normal solution that happened in 2017 as a strongest earthquake of swarm sequence and one with strike slip solution, that happened in 2017, SE of previous swarm sequence.

3. Recent advances in understanding of Idrija fault system

To understand the behaviour of the active faults and the roll they impose on the seismic hazard of the region, faults need to be studied using combined methods such as seismology, geodesy and geology. Each methodology on its own can and will give us different insights into the earthquake cycle, but the results can be misleading if only one is used. In the recent years seismological studies enabled us to better constrain the geometry of the active fault in NW part of the External Dinarides, mainly geometry of the biggest Idrija fault. From geodetic studies slip rate along the active faults was estimated as well as the pre, co and post-seismic behaviour of the faults was observed. Geological data gave us slip rates along the main faults for the longer, geological times and occurrence of destructive earthquakes along of one of the segments of Raša fault and Idrija fault were obtained. Slip rates were also modelled by combining different geodynamic parameters. In this chapter quick overview of this studies is given with a discussion on implications of these studies on our understanding of recent active tectonics of the region and how these recent datasets contributed to the final model of the IFS and its behaviour in the short time interval since 2006.

The most recent geological research on the active faults of the NW External Dinarides was performed mostly in the geomorphologic view of the area (Moulin et al. 2014, 2016). The studies were done by combining digital elevation models with 5m resolution and digital elevation models obtained from LIDAR survey with resolution of 1m along the 20-km long portion of Idrija fault and obtaining slip rates along different segments of the Idrija fault from geomorphological markers and calculating slip rate from GPS stations (Basovica, east from Trieste, Italy and Ljubljana, Slovenia).

They observed that the Idrija fault exhibits right-lateral movement (offsets comprised between 35 and 360 m) as well as significant vertical motion in sense of uplift of the NE block compared to the SW block. The uplift rate was suggested at 2.5 mm/yr (Rižnar et al., 2007).

From the geomorphologic markers, slip-rate was calculated in different ways. From observation of late-Quaternary sedimentation rates decreases and incision of the streams,

right-lateral offsets between 32 and 58 m was observed at three study sites along the fault. Slip rate of 1.8 – 3.9 mm/yr was proposed.

From the ^{36}Cl dating performed on the karstified abandoned river channel, a slip-rate between 1.1 -2.5 mm/yr was obtained. Based on the correlation of the horizontal offsets and the three last glacial maxima, a constant slip rate was assumed over the last 350 ka. Slip-rate was estimated to be between 1.0 – 1.4 mm/yr.

Considering only the smallest offsets the estimated slip-rate of Idrija fault was set to be between 1.8 -3.9 mm/yr depending on the observed time window (Moulin et al. 2014).

By observing the GPS series of the Basovica and Ljubljana stations (Caporali et al. 2008), a slip-rate of 2.6 ± 2.0 mm/yr was proposed over the active faults of IFS.

In the work by Moulin et al., 2016, similar study was performed but on the broader scale, extending the research also over the Predjama and Raša fault, two major faults parallel to the Idrija fault, all composed of 10-18 km long segments. Large-scale morphology, fault geometry, long-term faulting and folding, offsets and slip-rates were obtained from the inspection of SPOT images, 12.5 and 5m resolution digital elevation models, topographic maps, 0.5 m resolution orthophotos and ^{36}Cl dating.

For Predjama fault, they propose that it merges with Idrija fault at depth, due to it being parallel to Idrija fault with only 10 to 15 km between the two of them. On the other hand, Raša fault is much more linear then Predjama fault, still merging with Idrija fault, but at much greater depth (Figure 24).

In this work, they propose different slip-rates for different sites along the Idrija, Predjama and Raša fault, ranging between 0.5 – 4.0 mm/yr for Idrija with weighted mean slip-rate of 1.15 mm/yr, between 1.0 – 2.0 mm/yr with weighted mean of 1.45 mm/yr for Predjama fault and between 1.0 – 3.0 mm/yr with mean of 1.3 mm/yr for Raša fault. Finally, they propose that the 3.8 ± 0.6 mm/yr of right-lateral motion as accommodated along the Northern Dinarides is equally distributed between the three active faults – Idrija, Predjama and Raša fault.

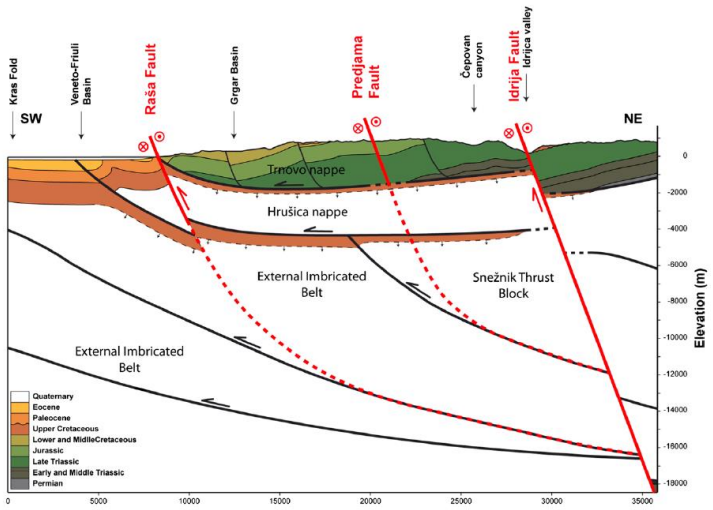

Figure 24: Proposed cross section over the IFS (red lines) (Moulin et al. 2016). *Black lines represent inactive thrusts at depth adapted from Placer et al. (2010). All the active strike slip faults are relatively shallow and change from near vertical to dipping at shallow depths.*

Along the Idrija fault paleoseismological trenching was performed in 2012 (Bavec et al., 2013). In the trench numerous fault planes were identified, with nine displacing the interface between the bedrock and Holocene sedimentary cover. They were able to trace them also into the Holocene units, confirming the coseismic deformation along the Idrija fault. They speculated one or two earthquakes along the main splay of the fault with one that could be the 1511 Idrija earthquake.

In 2016 and 2017 extensive trenching was performed along the Raša fault (Foroutan et al., 2018) giving the insight in the slip-rate, seismic behaviour and geometry of the Raša fault. In the different trenches, all along the same segment of the Raša fault similar coseismic displacements were found, with at least two earthquakes. Both earthquakes show similar horizontal and vertical offset, together giving 1.7 m of horizontal and 1 m of vertical offset. Calculated slip rate for particular segment of Raša fault was estimated below 1 mm/yr.

Kastelic et al. (2012) approached the slip-rate estimation for External Dinarides from the geodynamic modelling aspect (Figure 25), combining database of active faults and physical properties of the region (heat flow, crustal thickness, rheology, boundary conditions). Final model proposed much lower slip-rates for the active faults of the NW External Dinarides. For Idrija fault they proposed a slip-rate between 0.06 and 0.22 mm/yr, with mean at 0.1 mm/yr and for Raša fault slightly higher slip rate between 0.08 –

0.34 mm/yr with mean at 0.13 mm/yr. In the discussion they propose that these values underestimate the true slip-rates due to the unknowns in physical properties and influence of the boundary conditions such as the change from External Dinarides towards Southern Alps.

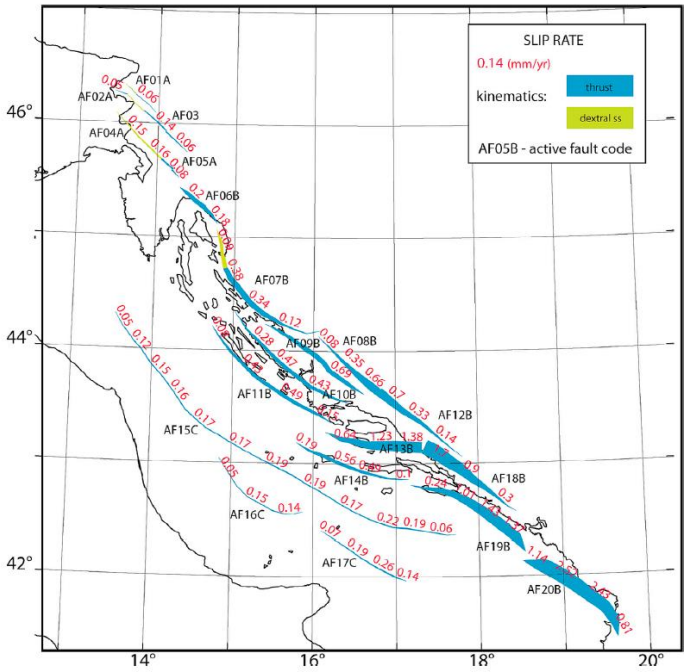

Figure 25: Slip rates calculated for different faults in the External Dinarides by geodynamic modelling (Kastelic and Carafa 2012). *The area studied in this work lies in the NW corner along faults named AF01A (Ravne), AF03 (Idrija) and AF04A (Raša).*

Wang et al. (2018) studied the active faults of NW External Dinarides using space-born InSAR datasets. By processing 75 radar acquisitions on the descending track and 45 acquisitions on ascending track they obtained 93 and 62 interferograms over the area (Figure 26). By using multi-interferogram method they constructed a rate map over the active faults in order to measure subtle interseismic deformations. With the best fit model (best agreement with GPS velocities and locking depth of the faults derived from seismology) they observed a dip-slip rate of 2 mm/yr which agrees with strike-slip slip rate and uplift rate from previous research. Interestingly, the biggest line of sight velocity change happens in the area between the Predjama and over the Idrija fault. They discussed that with such slip rate as observed by InSAR, already 1.4 meters accumulated since Idrija earthquake of 1511 with the coseismic displacement referred to be 1.2 meters (according to the scaling relationship for surface displacement to rupture length (Wells

and Coppersmith 1994)). Current moment deficit is large enough to be released in a large or in a series of medium sized earthquakes.

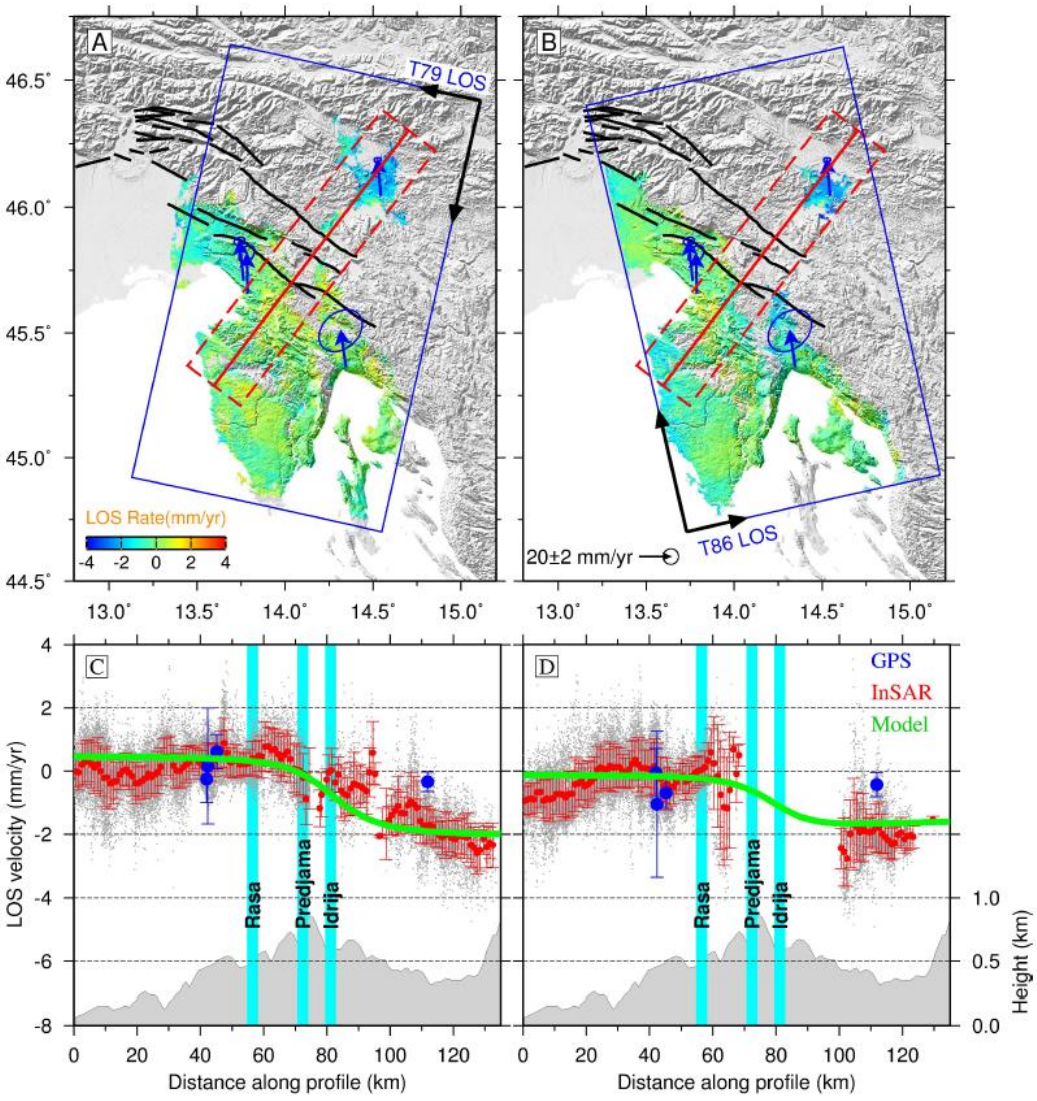

Figure 26: Line of sight (LOS) (A descending, B ascending) InSAR rate maps over IFS. On C and D red bars represent InSAR data, blue are GPS datasets and green represent modelled LOS. The maps show biggest change of slope over Idrija fault, while no change is visible over Raša fault.

From the recent seismological studies performed in the area (Guidarelli et al., 2017), the crust and the upper mantle of the region were studied using ambient noise tomography. In the study they obtained a new 3D shear wave velocity model of the region (Figure 27). For the NW External Dinarides they observed a sharp change of the group and phase velocities with the strike of NW-SE. They revealed a high angle dipping structure that corresponds to the mapped Idrija fault at the surface. The changes in velocities show a

clear change (Figure 28) in physical properties within the crust across the Idrija fault system. They interpreted the Idrija fault as a sub vertical fault sampling whole crust.

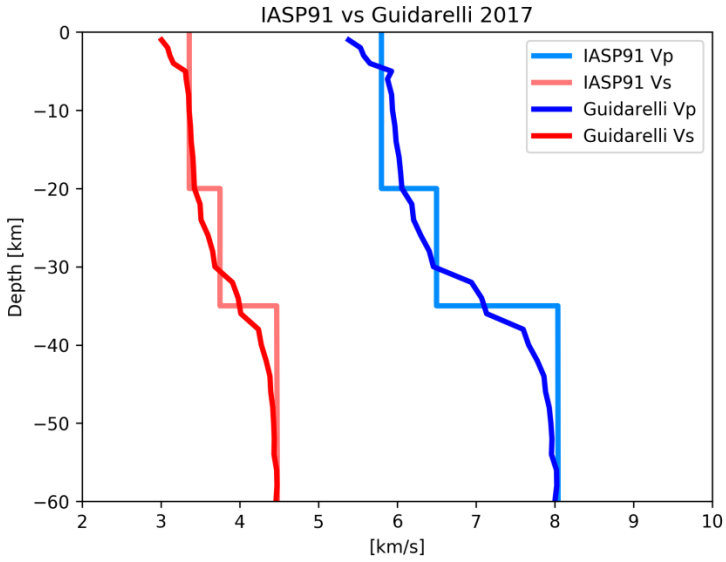

Figure 27: Comparison of IASP91 and 3D velocity model (Guidarelli et al. 2017) *for P and S velocities. Model represents just one part of southern IFS but in general reflex its properties over all the region, with 3D velocity model being slightly faster..*

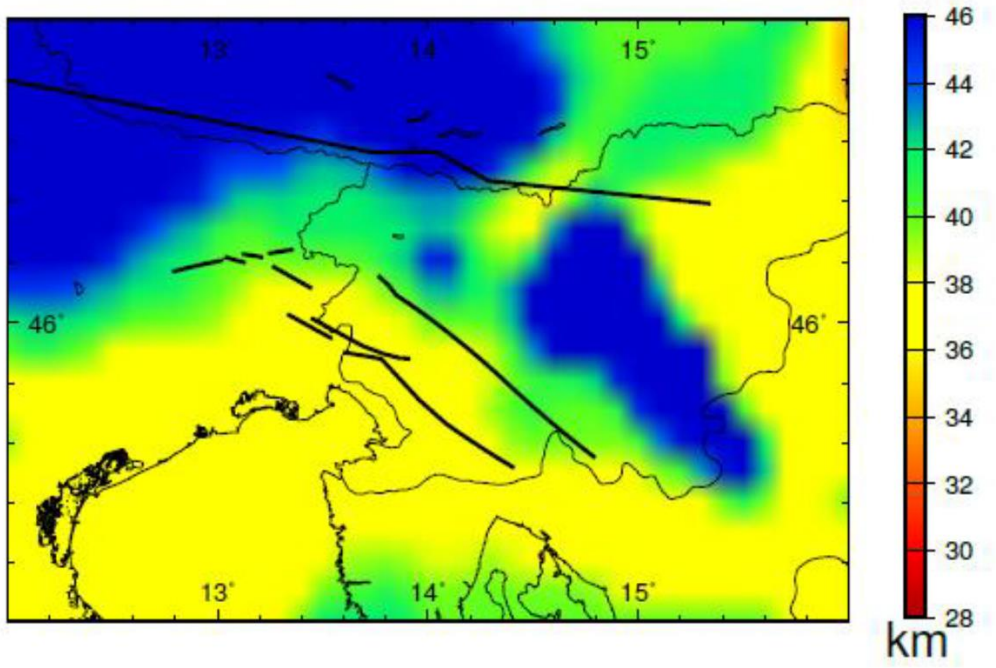

Figure 28: Depth of Moho as obtained from the 3D ambient noise tomography model (Guidarelli et al., 2017). *Black lines represent major fault of the region – our area of interest is in the central part of the figure with Idrija and Raša faults.*

The studied area is also monitored by a number of extensometer devices, mounted on the presumably active faults of the IFS (Gosar et al., 2011; Gosar et al., 2009; Šebela et al., 2005). Although the extensometers are mounted along different faults (Ravne fault, N part of Idrija fault, Predjama fault and Raša fault), only data from the Postojna cave extensometers (Predjama fault) was found useful for this study, due to its location in the cave, removing the environmental effects. According to Gosar et al., 2011, the extensometer in Postojna cave shows only measurements related to changes produced by tectonic effects, since no changes are observed during the high flood events, and the changes seemingly correlate with local earthquakes (Gosar et al., 2009)

In general, what they observed along the Predjama fault (Postojna cave extensometer) was dextral horizontal movement of -0.05 mm from 2004 to 2010 with extreme vertical movement in the period between 2009 and 2011, when NE block subsided for 0.07 mm in October – December 2009. It returned to slightly changed initial position somewhere after June 2010 (Figure 29). Similar, also changes along the xy rotation axis are observed in the same time period.

From the extensometers, mounted on other faults, slow slip rates were observed. For Idrija fault, six years average shows 0.24 mm/yr horizontal displacement, with short term rates reaching up to 0.54 mm/yr. Raša fault exhibited 0.07 mm/yr horizontal displacement and uplift/subsidence from 0.16 to 0.37 mm/yr.

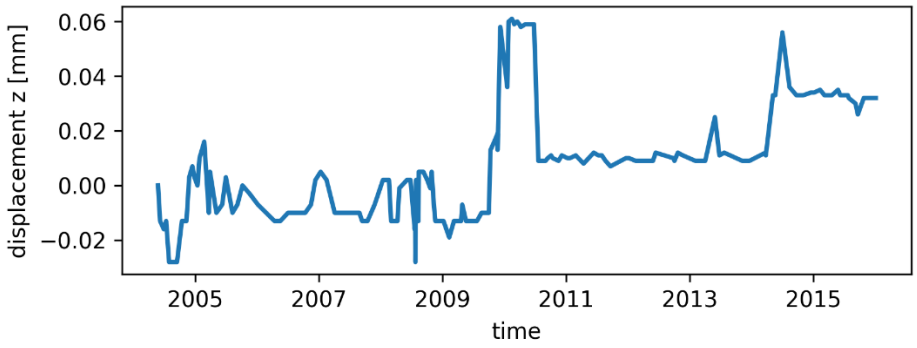

Figure 29: Vertical component of Postojna cave extensometer between 2005 and 2016. Clear changes are visible at the end of 2009 lasting until mid-2010. Another jump is associated with a M_W 4.5 local earthquake in April 2014.

Another recent work deals with possible transient deformation taking place along the NE Italy and NW Slovenia. In the study by Rossi et al., 2016, they analysed the timeseries data of group of GNSS stations along the northern margin of Adria microplate in NE Italy

and NW Slovenia. The data was corrected for seasonal and hydrological effects, to retrieve only signals related to the tectonic processes. They observed that the GPS time series show significant deviations from the regional linear trend in addition to effects by hydrological loading (Figure 30). Approximately 2.5 year long transient was observed, seemingly propagating in circular direction, causing initial upward movement in the direction of principal fractures. Location of origin of the transient deformation was obtained with principles used in tomographic inversion for Vp/Vs seismic velocities. The origin was located to the vicinity of Ravne fault where M_W 5.4 earthquake happened three and half months later. They proposed a porosity wave as a process of the deformation, observed on GPS stations, a process caused by presence of supra-hydrostatic gradients in fluid pressure across an active fault.

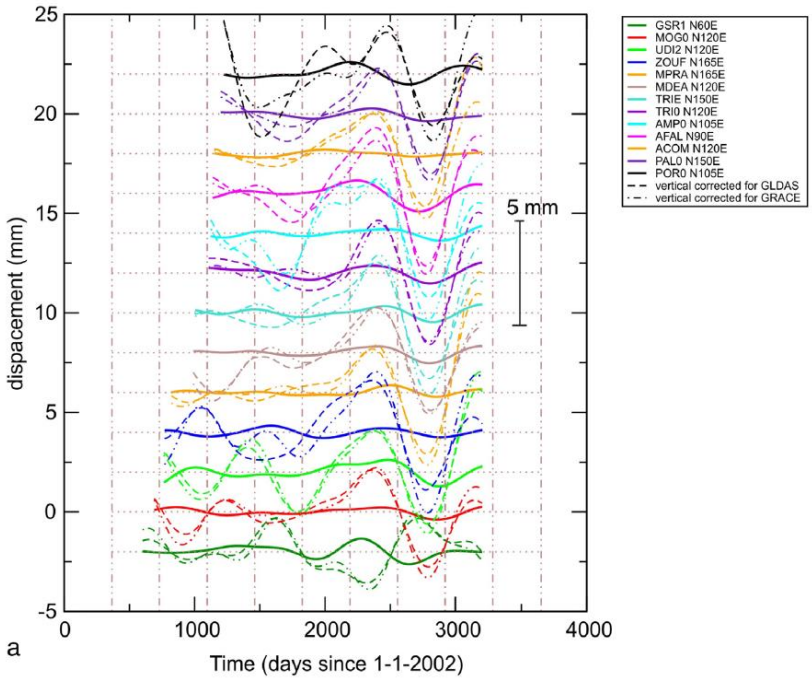

Figure 30: Strain transient as recorded on multiple stations in NE Italy. Dashed and dash-dot lines represent corrected vertical components, solid lines represent horizontal component.

3.1 Discussion on constrains used for Idrija fault system model

These findings helped us in constraining a reasonable model over the active faults of the NW External Dinarides which is discussed in the chapter 5. From them a new velocity model was used for precisely relocating the earthquakes in order to observe fault geometries and spatial extend of the seismogenic zones. The tomographic image and InSAR map of the area also constrained Idrija fault as sub vertical leading fault sampling all the crust.

As quickly described in the overview of recent studies of the area, fault slip-rates are not in strict agreement on the orders of slip-rate along different faults of the system. From the modelling (Kastelic and Carafa 2012) slip-rate is lower than from the slip-rates derived from the geomorphological markers and GPS measurements (Moulin et al. 2016). While modelling might underestimate the slip-rate on Idrija fault, it might in the agreement with InSAR datasets and paleoseismological show agreement along the Raša fault (Foroutan et al., 2018).

The slip-rates as proposed by Moulin et al. (2016) are equally distributed over all three bigger faults of the system – Idrija, Predjama and Raša fault. In the work done by Foroutan et al., (2018) the slip-rate derived from paleoseismological trenching along Raša fault shows that slip-rate along Raša fault is less than the one proposed by Moulin (Figure 31). This smaller slip-rate agrees with InSAR data, which shows almost no gradient in the line of sight of the satellite over the Raša fault. This would mean that slip-rate from InSAR along Raša fault is so small, that InSAR cannot be used for its observation, while when we go towards Idrija fault, velocity is big enough to be nicely observed on the rate maps.

From the observations and results proposed in the work of Moulin et al., (2016) especially when looking at the slip-rates ranging between 1.8 and 4.0 mm/yr in different time windows, idea that Idrija fault is exhibiting episodic seismic and tectonic behaviour, either on the fault scale or broader fault system scale, does not seem to be farfetched and agrees with episodes of elevated earthquake activity and transient deformation observed and discussed later in this work along the broader zone of active faults of IFS.

Similar proposal of episodic or transient deformations as proposed by Moulin, with origin along the Ravne fault few months before the 2004 M_W 5.4 Ravne fault earthquake, is also

given by Rossi et al., 2016. Currently, not enough data exists to verify whether this kind of transient deformation as they observed by GPS stations of the area was one of a kind or normal behaviour of the faulting in NW External Dinarides.

Another episode of transient deformation was observed on extensometer along Predjama fault, but similar to the work by Rossi et al., 2016, time window of observations is too short, to see if the deformation observed there are something we can observe multiple times on the longer time scales or not.

Correlating the transient obtained from GPS and transient observed on the extensometer, no clear connection is present. Proposed migration velocities from Rossi et al., 2016 (16.7 – 19.5 km/yr) are too large to explain strong transient displacement on the Predjama extensometer, if indeed what they observed on the GPS stations is a phenomenon, that could migrate from their proposed location to the area of extensometer, which is approximately 75 km SE.

Taking all this into account we can define the Idrija fault as the leading fault in the system of active faults of NW External Dinarides to which all the parallel faults merge somewhere at the depth. Idrija fault probably exhibits slip-rates higher than the Raša and Predjama fault which is observed from the InSAR datasets and disagreement between proposed slip-rates along the Raša fault derived from geomorphological markers and those observed in the paleoseismological trenching. From the seismological inspection performed in this thesis (chapters 4 and 5) spatial-temporal clustering of earthquake activity was observed agreeing with the proposal of Moulin and Rossi, that Idrija fault system exhibits episodes of elevated slip and earthquake activity.

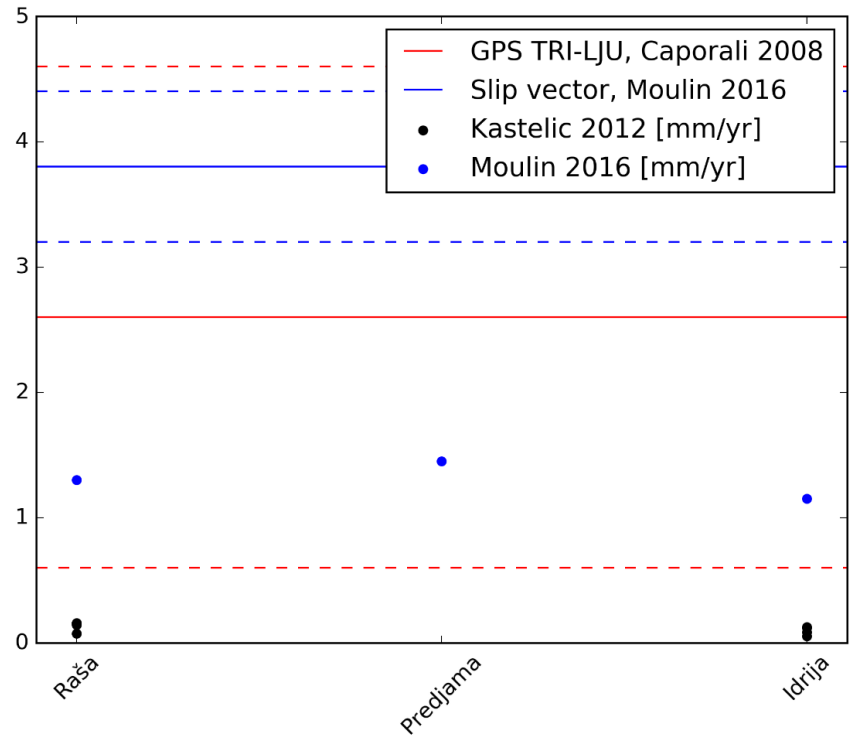

Figure 31: Proposed slip-rates along Raša, Predjama and Idrija fault from modelling, GPS observations and geological investigations. Black dots represent datasets obtained with geodynamic modelling, while blue dots represent data obtained from geomorphologic markers. Slip vector (blue lines) is constrained over all the IFS combined.

4. Research

We studied the earthquake activity along the active faults of NW part of External Dinarides along so Idrija fault system in the time period between 2006 and 2016 using all available seismic stations over the area of W Slovenia and NE Italy in order to model the active faults in their geometry as in their temporal behaviour, if present. Additional analysis was performed by using only matched filter techniques until the end of 2017 for all the area and additional seismic sequences (both swarm and mainshock – aftershock series) that happened in the second half of 2017 in the southern edge of IFS.

Data was first processed using STA/LTA detection methodologies with manual repicking of the associated phases, to obtain as precise locations as possible. After the automatic detection and repicking, manual inspection of the data between 2006 and 2015 was performed (data after this period was only checked with automatic detection techniques) in order to find additional earthquakes that were not detected in the previous, automatic run. New earthquakes were added to the existing database if detected and relocated using at least 4 phases. The initial relocation was performed using the Antelope® software package, while addition relocation was performed by NonLinLoc (Lomax 2011) and HypoDD (Waldhauser 2001) software using 3D velocity model (Guidarelli et al., 2017) of the region. For earthquake sequences detailed detection and relocation of detected earthquakes was performed using the matched-filter detection algorithm (open source package EQCorrscan (Chamberlain et al., 2017)), with precise picking of the arrival times using cross-correlation of the signal techniques.

Templates used for matched-filter analysis were chosen from the automatically detected earthquakes that happened in mainshock - aftershock or swarm sequences. The earthquakes found only by manual inspection were not used to form templates for matched-template detection due to the time and computer power limitations. After the successful detection and relocation of earthquakes, M_L was calculated for each of the earthquakes. The methods are described in detail in the chapter 2.3. The number of earthquakes detected in this way is much higher than number of earthquakes as published by Slovenian Environmental Agency, with greater precision in the location.

For template detection, earthquakes around Bovec region (1998, 2004 earthquakes), central region (1511 earthquake) and southern Postojna-Ilirska Bistrica region with $M_L >$

0.8 were chosen. The northern Bovec region and southern Postojna - Ilirska Bistrica regions were chosen since both are showing higher seismicity rates then the area between them and represent northern and southern edges of surface defined Idrija fault. For the central part, the template algorithm was used in hope to find some missing activity that would show us that the region is not so inactive as it seems.

For Bovec region, 71 template earthquakes with $0.8 < M_L < 4.2$ were chosen, mostly along the Ravne fault, which is the leading active fault in the area. Few template events happened along northern part of Idrija fault just south of town Tolmin and town Serpenica. This template earthquakes are deeper (12-15 km) than earthquakes distributed along Ravne fault (5-9 km). 110 template events used for region between the towns Postojna and Ilirska Bistrica with $0.8 < M_L < 4.5$ were chosen. Majority of events are happening along the Selce fault (Šebela 2005), which is the leading seismically active fault parallel to Idrija fault. Selce fault is probably causal fault of 2014 M_W 4.5 strike-slip earthquake, the strongest earthquake that happened along the active faults of NW External Dinarides since 1998 and 2004 Ravne fault earthquakes in the northern part. Templates do not cover the 2006 Vipava swarm and 2010 Postojna swarm-like activity that happened in the same area as other Postojna-Ilirska Bistrica templates. For 2006 Vipava swarm 30 templates were chosen with $0.8 < M_L < 2.7$ that happened in 2006 (majority), 2009 in the north of the 2006 swarm and in 2015 in the south of 2006 swarm. For Postojna swarm 67 templates were used, with $0.8 < M_L < 3.8$. The 2010 Postojna swarm is one of a kind in the years between 2006 and 2017 since 2010 is the only year when earthquake activity is present in this particular area, spanning from end of 2009 to beginning of 2011 with 2792 detected events. For the central part of NW External Dinarides, 32 templates with $0.8 < M_L < 1.7$ were created that represent shocks of randomly distributed earthquakes in this area.

Because of the fact, that all the continuous waveforms were processed in advance for all three regions, northern, southern and central, lower number of broadband stations was used (ROBS, CADS, VINO, GORS, VOJS, JAVS, CEY, KNDS, SKDS) which made a computational part relatively quick but still allowed us to use obtained detection for relocation of the events using the P and S arrival times computed from cross correlating the detection times with templates. Prior to running the template detection algorithm, waveforms were pre-processed which made run time shorter. Both templates and continuous waveforms were down sampled from 100 or 200 Hz to 20 Hz and bandpass

filtered between 3.0 and 8.0 Hz. All the local earthquakes in the region are high frequency earthquakes, but bandpass filtering lowers the computational cost, gives more coherent and higher number of detections but still provides us with ability to distinguish between individual families of earthquakes. Waveforms with length less than 0.8 of the 24 hours were discarded to not introduce artefacts in the detections. Length of templates was 5 s with 0.1 s pre-pick times with P arrival times set on vertical component and S arrival on horizontal component.

For the template detection EQCorrscan software package (Chamberlain et al., 2017) was used. All the channels in the templates are correlated with day-long continuous waveforms on the same stations and channels. For successful detection, normalized cross-correlation values for each day are summed on all the channels which gives us a network cross-correlation time series. When the network cross-correlation sum exceeds 8 x Median Absolute Deviation, a detection is declared. Value 8 x MAD introduces also detections that are not real events, but these events were later manually removed. For removing untrue detections, spectrograms of original signal were computed and visually inspected. Detections that were not clearly identified as an earthquake (observed on at least two stations) were removed.

The area was, in the studied time period, struck by numerous mainshock-aftershock sequences along all the length of the active faults and swarm-like sequences that are much more common in the southern part of the studied area. In fact, the northern part, along the Ravne fault, was only struck by one swarm-like sequence, happening along 20 long segments of the fault, while in the southern part, swarms in this time period happened along different faults, each swarm-like sequence occupying much smaller nucleation area.

The catalogue of automatic and manually detected earthquake (before the matched filter detection) consists of 7148 earthquakes with magnitude of completeness (Mc) set at 0.9 and normal 1.05 b-value. Much bigger number of events is present in the catalogue after the matched filter detection and consists of 11073 earthquakes for the period between 2006 and 2017. The Mc for this catalogue was lowered to -0.73 (Figure 32.)

Horizontal and vertical errors of manually and automatically (by using lag-time calculations) relocated earthquakes are quite constant with depth error between 2 and 3 km for majority of earthquakes. Horizontal errors were defined as area of error ellipse with 1-3 km^2 in size (Figure 33).

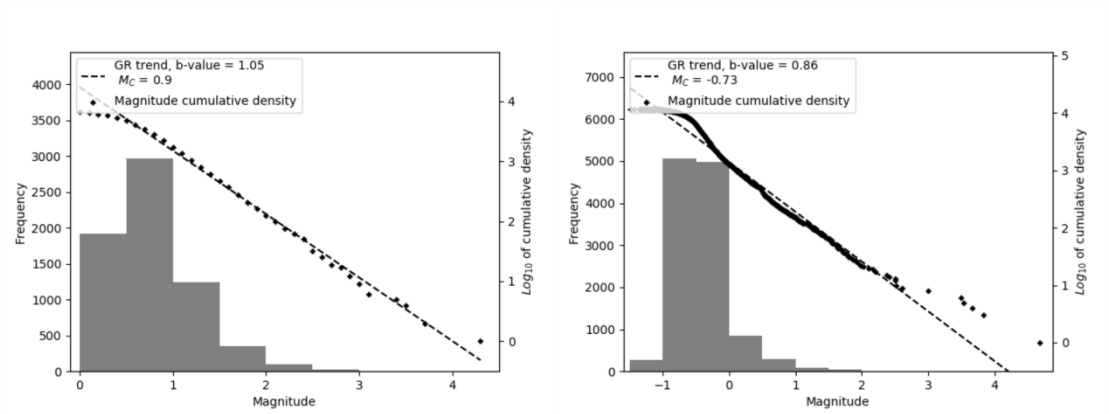

Figure 32: Differences in the catalogues. Automatic and pre-matched filter detection (left) and after matched-filter detection (right).

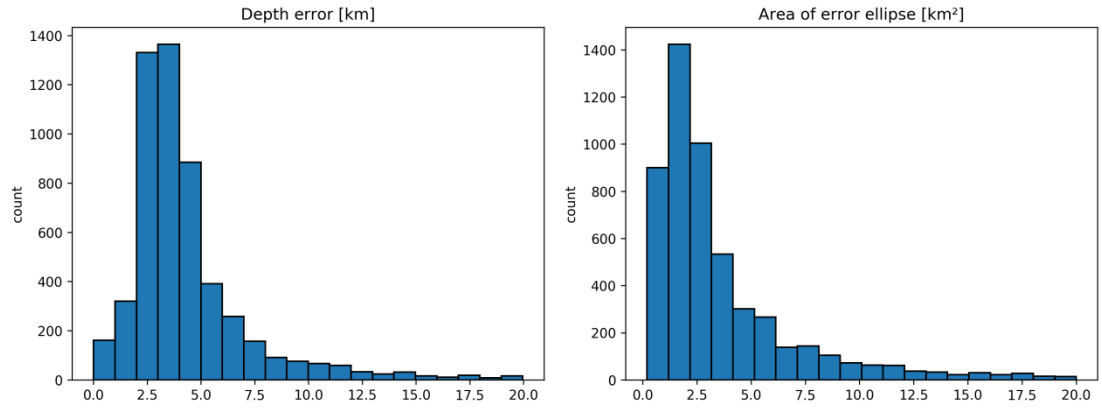

Figure 33: Depth error and area of error ellipse estimations for relocated earthquakes. Outliers comes from the events outside of the network but considered in the catalogue.

In the next sub chapter, analysis of earthquake clusters is given for the most interesting sequences that happened in the time span between 2006 and 2017. As is discussed later, two spatial-temporal clusters along the southern part of the studied area were observed, first in 2009-2010 and the second in 2017. Both comprise of both mainshock-aftershock activity and swarm-like activity. First one is spread over the northern part of the active fault system, central part of the system and southern part of the system, while the second one is more localized along the southern part of the active faults.

4.1 Description of earthquake sequences in the time period between 2006 and mid-2018

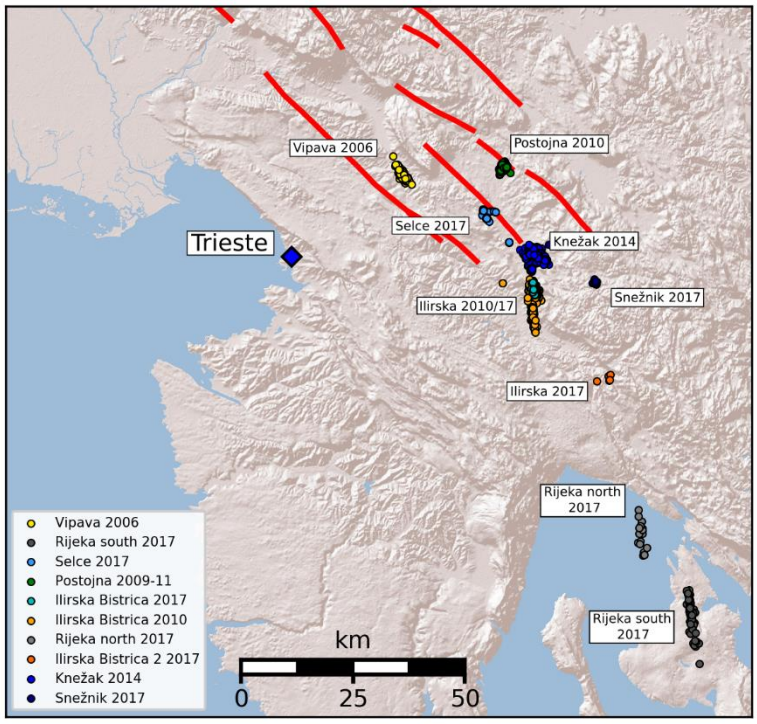

Figure 34: Map view of southern part of IFS with locations of analysed clusters (except of earthquakes happening along Ravne fault to the north of IFS)

4.1.1 Vipava 2006 swarm sequence

The Vipava 2006 swarm started on the 31. of August 2006 and finished in November of the same year. Prior to the end of August, no earthquake activity in this area was detected using nor STA/LTA method nor template detection method. The events that were detected in area few km to the W and SE from the epicentral area all come from quarry blasts from two big quarries southeast and to the west of the region.

Biggest tectonic feature of this area is NW-SE trending Raša fault which is clearly visible on the surface as a Raša valley. Along the central part of Raša fault, we can clearly observe around 3km long surface scarp. In the area of the swarm, Vipava fault was mapped when highway Koper-Ljubljana was being built but the fault is not really

expressed on the surface (Placer 2008b) and is probably not an active fault, but a fault related to past tectonic phases.

The size of the mainshock with M_L 2.3 and not so good network coverage in that time did not allow us to compute focal solution of the mainshock, so the swarm cannot be directly connected to the faults in its proximity. This earthquake could be connected to the NW-SE oriented Raša fault since the trend of scarce earthquakes continues towards NW.

The activity started again as a small mainshock-aftershock series on the NW edge of the 2006 swarm in 2009 and again as a small mainshock-aftershock series on the SE edge in 2015 which were not detected by 2006 templates. Vipava 2006 swarm initiated with a series of micro earthquakes which were followed by the M_L 1.0 earthquake only few days later 2nd of September 2006. Micro earthquakes continued with low magnitude earthquakes with only one earthquake reaching M_L 1.0 on 9th of September. On 21st of September, earthquake rate got elevated. The elevated sequence was finally followed by swarm's strongest earthquake that happened on 24th of September, reaching M_L 2.3. After this event, preceded by slightly elevated pre-shocks and aftershock series, earthquake activity slowly shut down, finally ending on 20th of November 2006. Altogether 698 earthquakes were detected with completeness of the catalogue at M_L 0.04, and with b-value = 1.46 (Figure 35 - right). After 2006, there were no earthquakes at the same place as the swarm took place.

The swarm is confined in the area of 30 km² at approximate location of latitude/longitude 45.777 13.995 with the depth ranging from 5 to 12 km (Figure 37 - left), with majority at around 10 km.

The similarity analysis of P windows between all the templates and between S windows (Figure 36) for all the detected earthquakes was performed in order to see if earthquakes are originating in the same place or not, as is observed from the elongate extension from NW to SE on the map. We observed that the correlation is not very high, which would mean that the earthquakes indeed nucleate along different part of the asperity during the swarm sequence.

The correlation between P windows of all selected templates was calculated for all the studied sequences. Similar calculations were performed around S windows of all the detected earthquakes with matched-filter technique. In the figures showing correlation matrices, it is clear that value of the similarity between templates (P window) or

similarity of detections (S window) may vary between -1 and 1. The differences could be due to the slight changes in focal mechanisms (inverse focal should show value of -1), and/or addition of the noise overprinting the signal of the earthquake (low SNR) – for the correlation matrices the signal also incorporates slightly higher frequencies as were used for the matched-filter detection itself. Focal solutions inside swarms can change slightly(Evangelidis et al. 2008; Shelly, Ellsworth, and Hill 2016; Yukutake et al. 2011), but we were not able to prove that due to the size of the detected earthquakes.

The alighment of the detection on P phase shows slight differences, mainly along S wave arrival (Figure 37 - right), showing that indeed, the rupturing is happening in the different places along the fault.

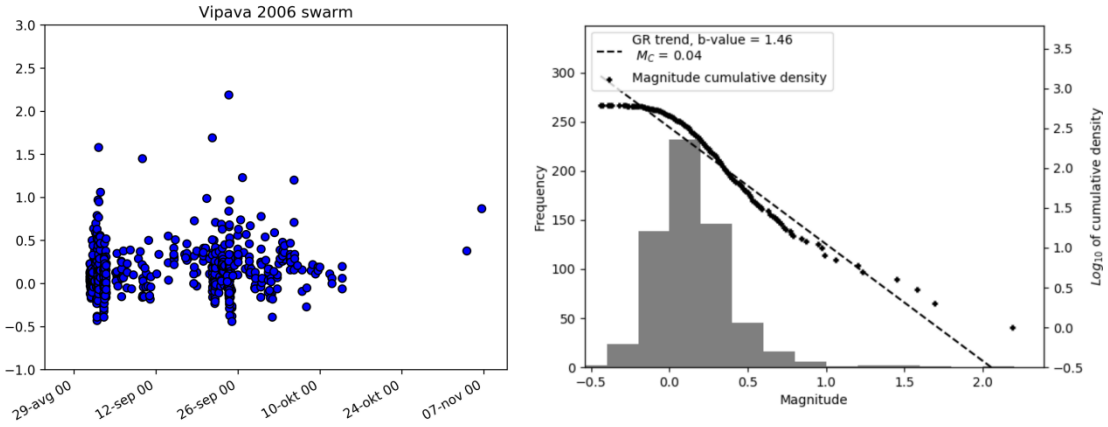

Figure 35: Magnitude vs time distribution (left) of the detected events for 2006 Vipava swarm. Mc and b-value of the swarm (right).

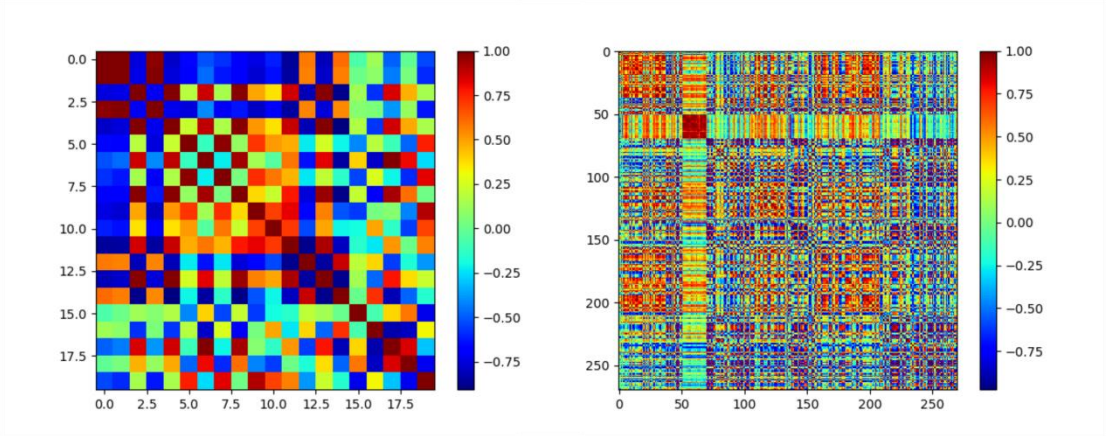

Figure 36: Correlation values of the selected templates around P arrival (left) and correlation values of all the detections around S arrival (right)- higher correlation means higher simillarity. As observed from the correlation values selected templates show all the range of values (from 1 to almost -1). Reason for this is in the missing waveforms data for the closest station, so the comparison is done on 2nd closest station. Additionally to slightly different locations of the template events, distance between the source and receiver and low magnitudes of the earthquakes introduce worse SNR conditions. On the other hand, the low values around S window for the all detected events (right figure), low correlations for later events is probably due to very low magnitudes overprinted by noise.

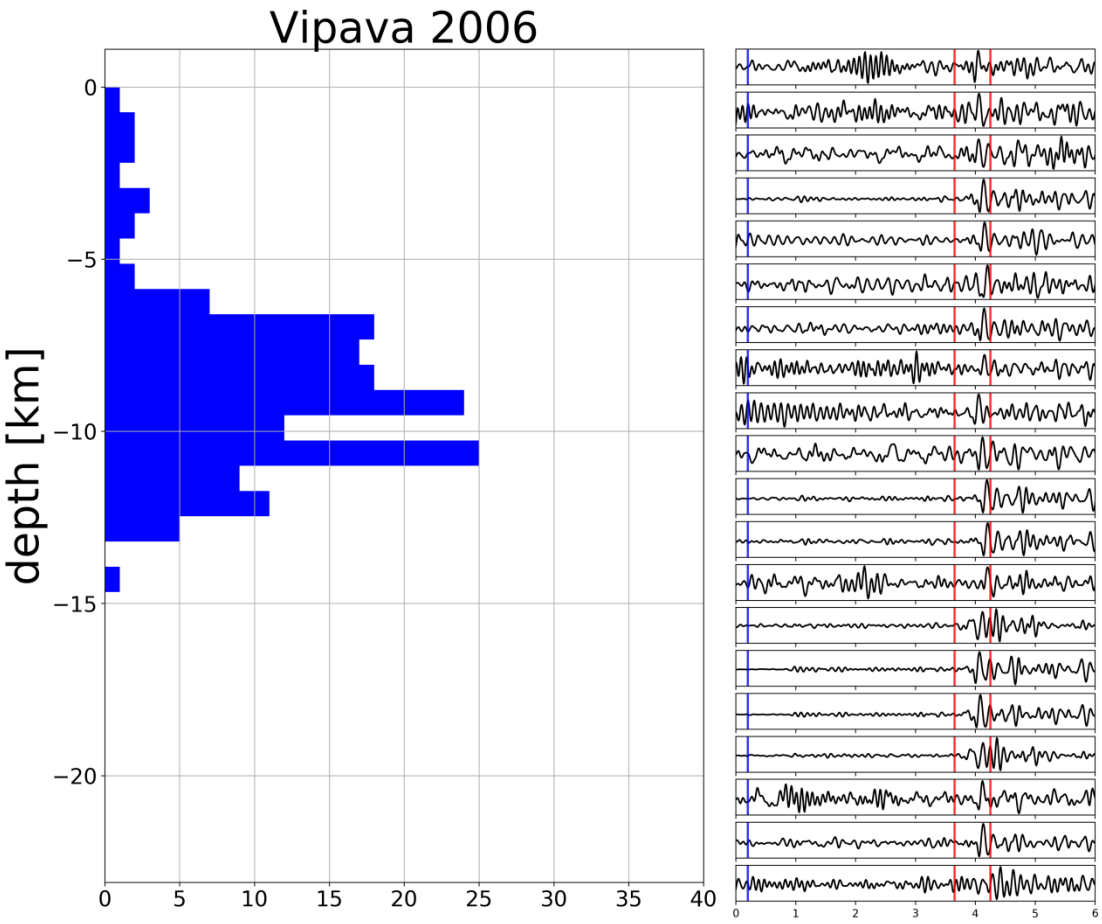

Figure 37: Depth distribution between 5 and 12 km for the Vipava swarm (left). On the right figure we can observe slight changes around S window after aligning the detections on P arrival time. Changes come from different locations and depth of the earthquakes.

4.1.2 Postojna 2009-2011 swarm sequence

Postojna seismic swarm sequence was longest, and by number of earthquakes the biggest cluster of earthquake activity along the IFS if we do not count the activity along Ravne fault, where 1998 and 2004 magnitude 5.7 and 5.4 earthquakes happened. The swarm started in the December of 2009 and lasted until June 2011. In this period 3151 earthquakes were detected with magnitudes ranging between M_L -0.73 and 3.5. The mainshock of the sequence happened on 15. January 2010, some 20 days after the initiation of the swarm. Earthquakes nucleated along a patch on the Predjama fault, beneath town of Postojna in the small epicentral area of 9.5 km² at latitude/longitude around 45.780, 14.202 with depth distribution between 10 and 17 km (Figure 40 - left), with majority happening at 15 km. Altogether 50 earthquakes of $M_L > 1.0$ happened during the swarm-like episode with 49 of them happening in the first 3 months of the episode and last one happening on 3rd November 2010. After 2011 the only occurrences of micro earthquakes along the same fault patch were on 19th May 2016 when a M_L -0.68 got detected with matched filter detection method and a M_L -0.47 earthquake that happened on 1st of January 2017. Completeness of the catalogue is at M_L -0.23, and with b-value = 1.29 (Figure 38 - right).

During the swarm sequence there was no migration of the events observed. Either no migration happened along the sequence or spatial error with the network configuration was too big to observe any kind of migration (closest station is 16 km away and no data from temporal stations deployed few days before the mainshock by local monitoring agency was included in this study).

For the two earthquakes with highest magnitudes focal mechanisms were computed by ARSO using first arrival of P waves and by OGS using waveform inversion for the strongest earthquake. For the mainshock, both solutions are similar, showing mostly strike slip faulting with some dip component. The second focal mechanism calculated from first arrivals shows similar strike slip solution, with slightly different strike.

From the comparison of the P windows of templates and S windows of detections (Figure 39), it is clear, that templates nicely represent overall detected earthquakes, and a big number of earthquakes shows high similarity. Events of lower similarity could represent earthquakes with different focal solutions, but their size do not allow as to explore this.

Similar as in Vipava 2006 swarm, alignment of the detections on P arrival shows slight variations in S arrival and the change of location related to this.

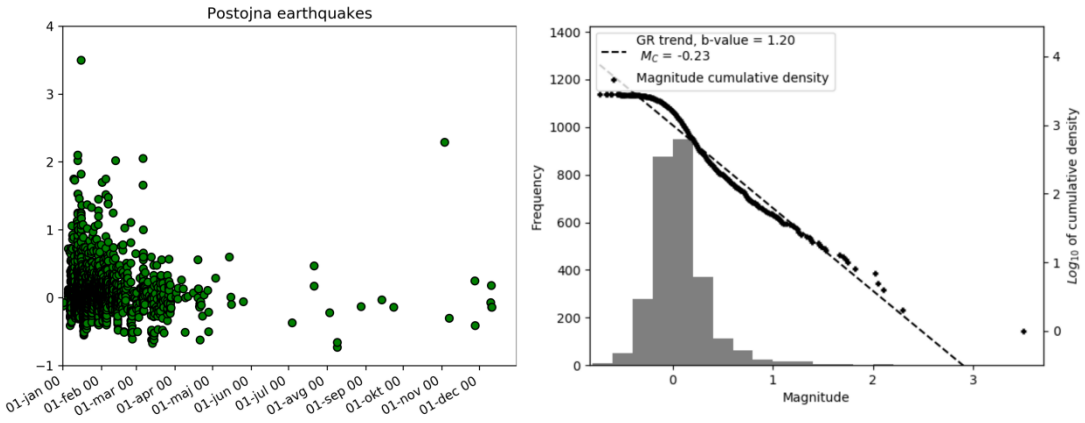

Figure 38: Magnitude vs time distribution (left) of the detected events for 2010 Postojna swarm. Mc and b-value of the swarm (right).

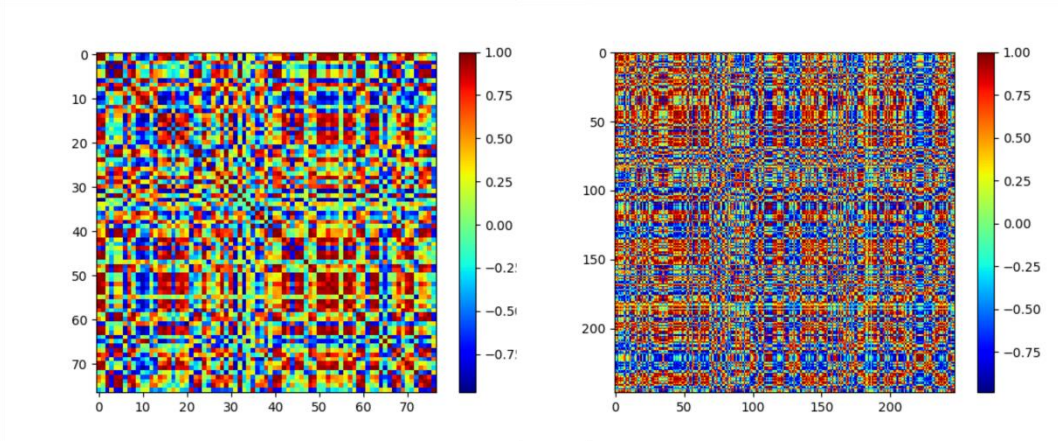

Figure 39: Correlation values of the selected templates around P arrival (left) and correlation values of detections around S arrival (right). Clear high similarity of detections is observed (both positive and negative). Negative could be due to slightly different focal mechanism (and noise) of a family of events, but these earthquakes are too small to compute focal mechanisms.

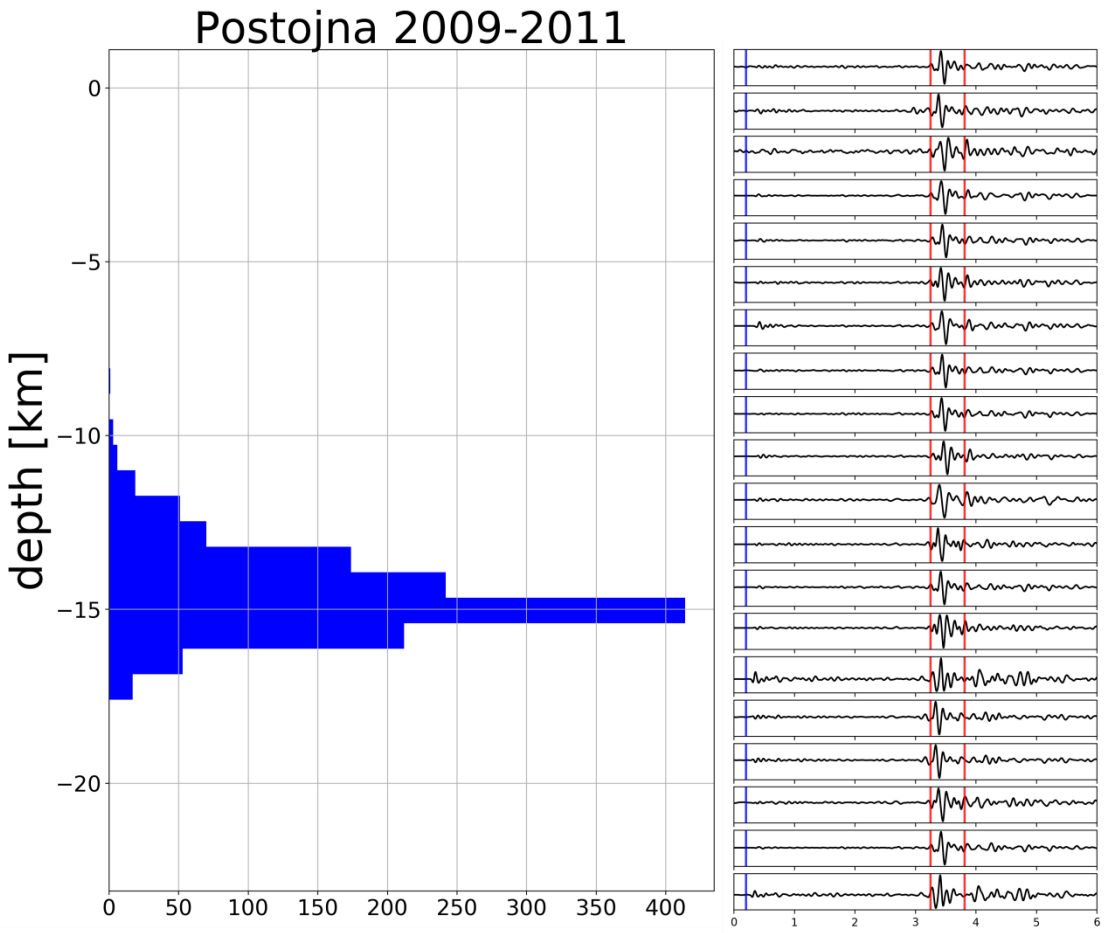

Figure 40: Depth distribution between 13 and 16 km for the Postojna swarm (left). On the right figure we can observe slight changes around S window after aligning the detections on P arrival time. Changes come from different locations and depth of the earthquakes.

4.1.3 Ilirska Bistrica 2010 earthquake sequences

In September 2010, Ilirska Bistrica earthquake sequence took place 3 km NE of the town Ilirska Bistrica. The epicentral area is located at the southern part of the area, in the area representing the Raša fault, the westernmost active fault of the IFS. Sequence started with two M_W 3.5 earthquakes 2 minutes apart and was later followed by 2335 aftershocks. The magnitude of completeness of the sequence is -0.65 while its b-value is 0.81 (Figure 41 - right), relatively normal value for mainshock-aftershock sequences. Epicentral area is quite large with more than 30 km², but since later we were able to distinguish 3 different sequences inside the main sequences, this agrees to the migration of the focal areas. Using matched filter detection method and relocation performed by HypoDD, we were able to separate the aftershock sequence into the sequence directly related to the 2 mainshocks and two smaller sequences related to their own mainshocks, which migrated from N to S during the months following the 2 mainshocks of September 2010.

Focal solutions for both mainshocks is very similar strike slip faulting, derived from waveform inversion by OGS and first arrivals by ARSO. For the 2nd smaller sequence, focal solution was obtained only from first arrivals and it shows strike slip faulting (Čarman 2011).

Migration was not only observed in the horizontal but also in the vertical direction, with the first and northernmost sequence being the deepest, between 13 and 16 km, the second one, that happened in the central part was shallower, with majority of earthquakes happening at the depth of 10 km, and the last, southernmost sequence was most shallow one, happening at around 6 km depth (Figure 43 - left).

Comparison of P windows of the template events maybe shows 3 different groups of earthquakes, as were relocated, migrating in time. Since focal solutions of first and 2nd group are very similar, clearly not much difference should be present. This is not the case in the comparison of S windows of the detection, where clearly, we can observe differences of three groups, migrating in time, with leading first mainshock series, between event 0 and 180, 2nd group between 180 and 210 and third, smallest group above number 210. Since in this case we are comparing S windows, the change in location should strongly affect the correlation coefficient, mostly due to the big changes in the depth of these groups (Figure 42).

Alignment of P arrivals and comparing the S arrivals clearly shows (Figure 43 - right), that indeed we were dealing with three groups of mainshock-aftershock series, different in depth as well as the location.

Interestingly, in October 2017 the same deeper sequence repeated, detected using the same templates and when relocated, the locations were the same. The sequence repeated as a mainshock-aftershock series with mainshock of M_L 2.1 and its short aftershock sequence. For this mainshock no focal mechanism exists, but since the detection was obtained by same templates as were used for the 2010 sequence, solutions must be similar if not the same.

Epicentres from NE towards SW follows at latitude longitude 45.601, 14.262, 45.563, 14.269 and 45.539, 14.264.

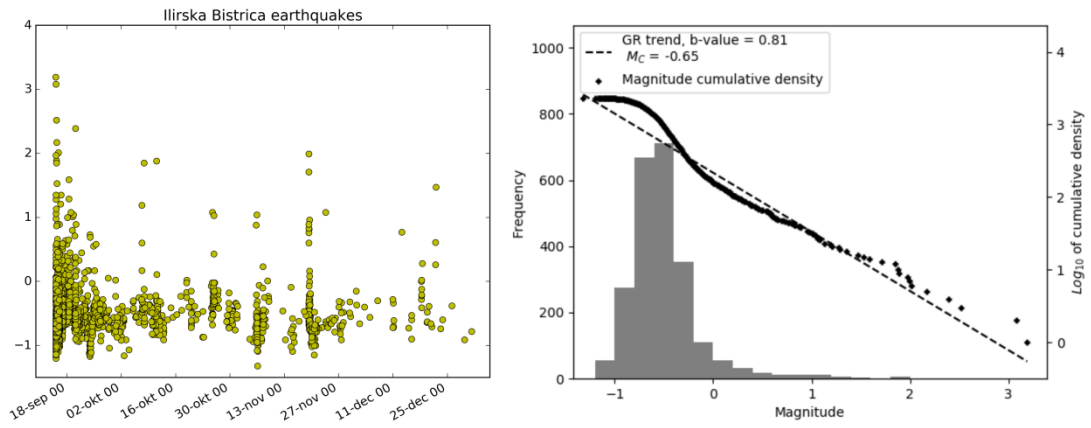

Figure 41: Magnitude vs time distribution (left) of the detected events for 2010 Ilirska Bistrica series. Mc and b-value of the whole series (right).

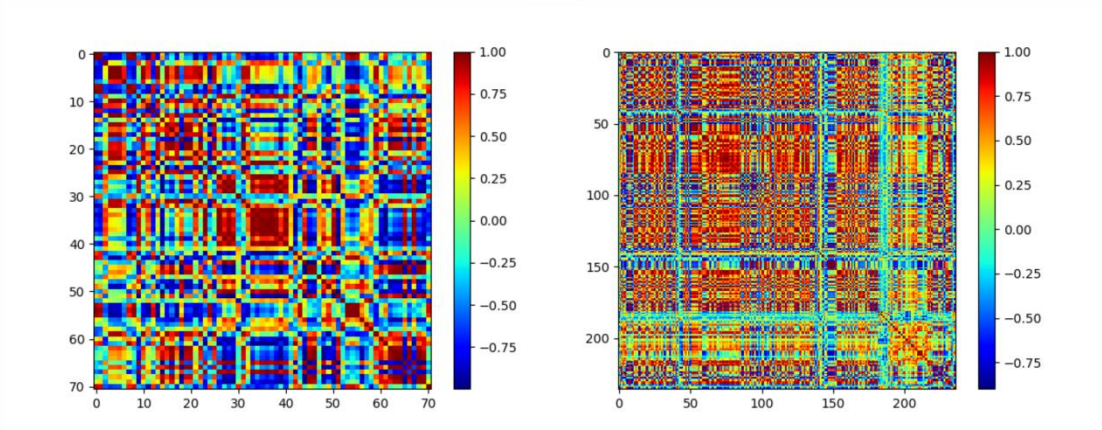

Figure 42: Correlation values of the selected templates around P arrival (left) and correlation values of detections around S arrival (right). On detection correlation figure, 3 distinguish families of detections are present.

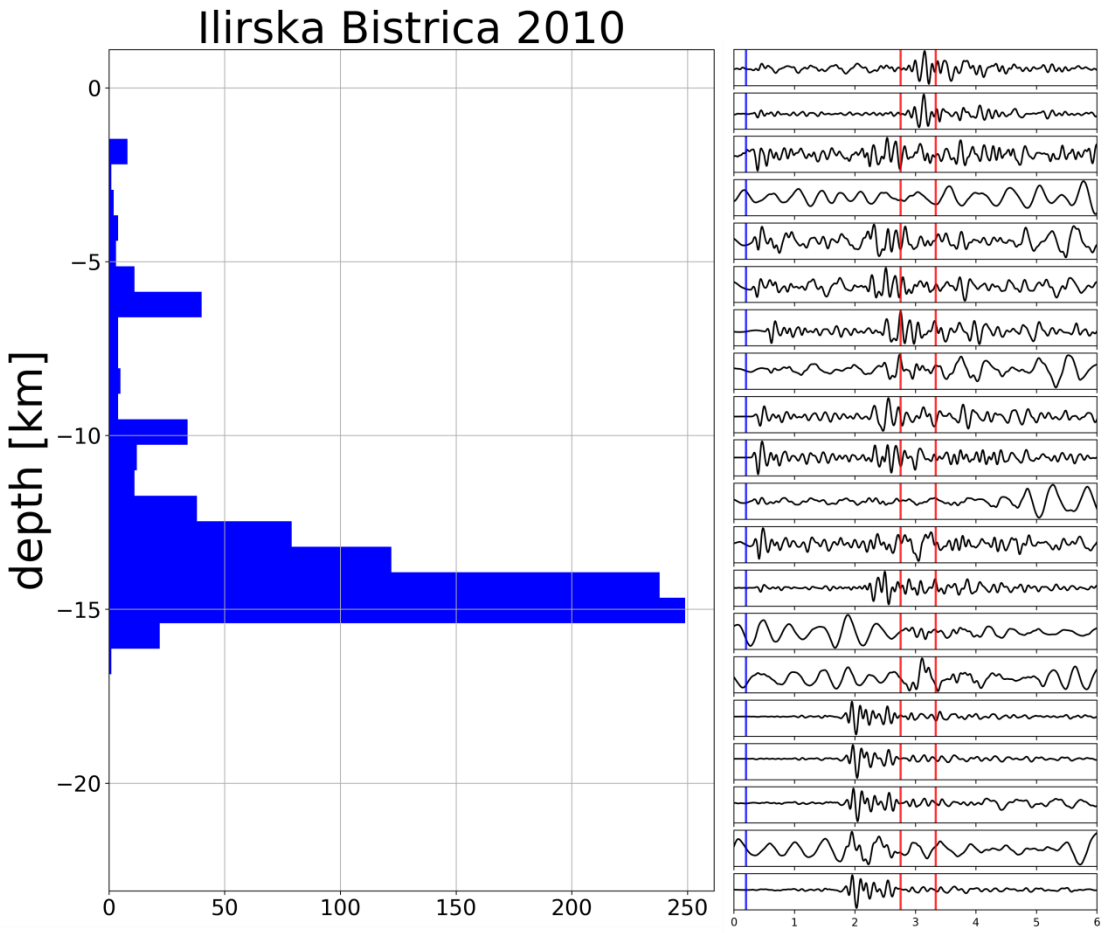

Figure 43: Depth distribution between 5 and 15 km for the Ilirska Bistrica sequence (left). Separation on 3 sub-clusters is observed at the depths 5, 10 and between 13 and 15km. On the right figure we can observe changes around S window after aligning the detections on P arrival time. Changes come from different locations and depth of the earthquakes.

4.1.4 Knežak 2014 mainshock-aftershock series

The strongest earthquake along the active faults IFS that happened after the 1998 and 2004 M 5.7 and M 5.4 earthquakes, happened on 22nd of April 2014 in the southern part of the studied area. The mainshock had a M_W 4.5 and was later followed by numerous aftershocks, lasting through 2014 into the 2016. In the 2013 and 2014, prior to the mainshock, no earthquakes were found in near vicinity of the epicentral area. Two small, M_L 1.5 earthquakes happened close by in 2011 and 2012 but we were unable to compute any focal solutions for them. Epicentral area is 13.9 km² big, extending in NW-SE direction, the same direction as the leading active faults of the region. Completeness of

the catalogue is set at -0.63, with b-value at 0.81 (Figure 44 - right). Focal solutions of the mainshock were calculated with waveform inversion by OGS and from first arrivals of P phases by ARSO. Both solutions agree on a pure vertical strike slip mechanism.

Majority of the earthquakes were relocated to the depths between 18 and 20 km (Figure 46), making this sequence the deepest earthquake sequence along the IFS. The temporal distribution of the earthquakes is clearly different from previous swarms and triple mainshock-aftershock series with sharp decay of earthquake rates soon after the mainshock.

The S window comparison show that S wave is gaining on similarity from initial mainshock towards the last detected event, probably due to the fact, that mainshock and first stronger aftershocks are of quite higher magnitude then all the rest of the aftershocks (Figure 45).

Observing aligned P arrivals and S windows, we can see slight migration of the S window (Figure 46 - right).

Epicentral area is at 45.651, 14.255.

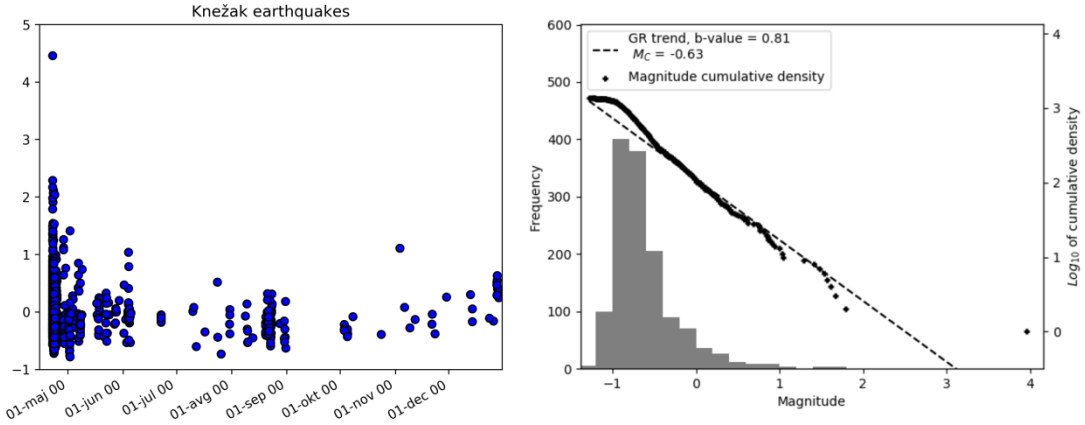

Figure 44: Magnitude vs time distribution (left) of the detected events for 2014 Knežak mainshock sequence. Mc and b-value of the sequence (right).

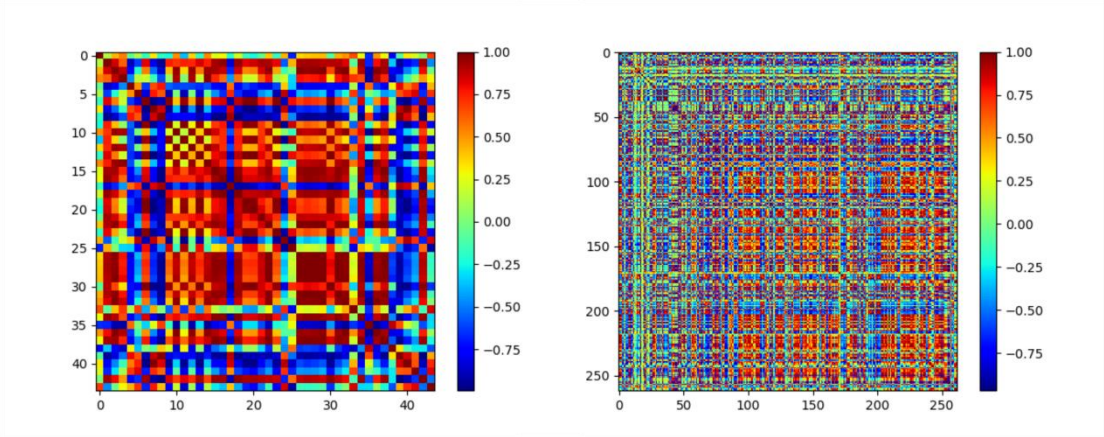

Figure 45: Correlation values of the selected templates around P arrival (left) and correlation values of detections around S arrival (right). Normally, higher magnitude earthquakes show different waveforms than their aftershocks, due to the rupturing process and different location.

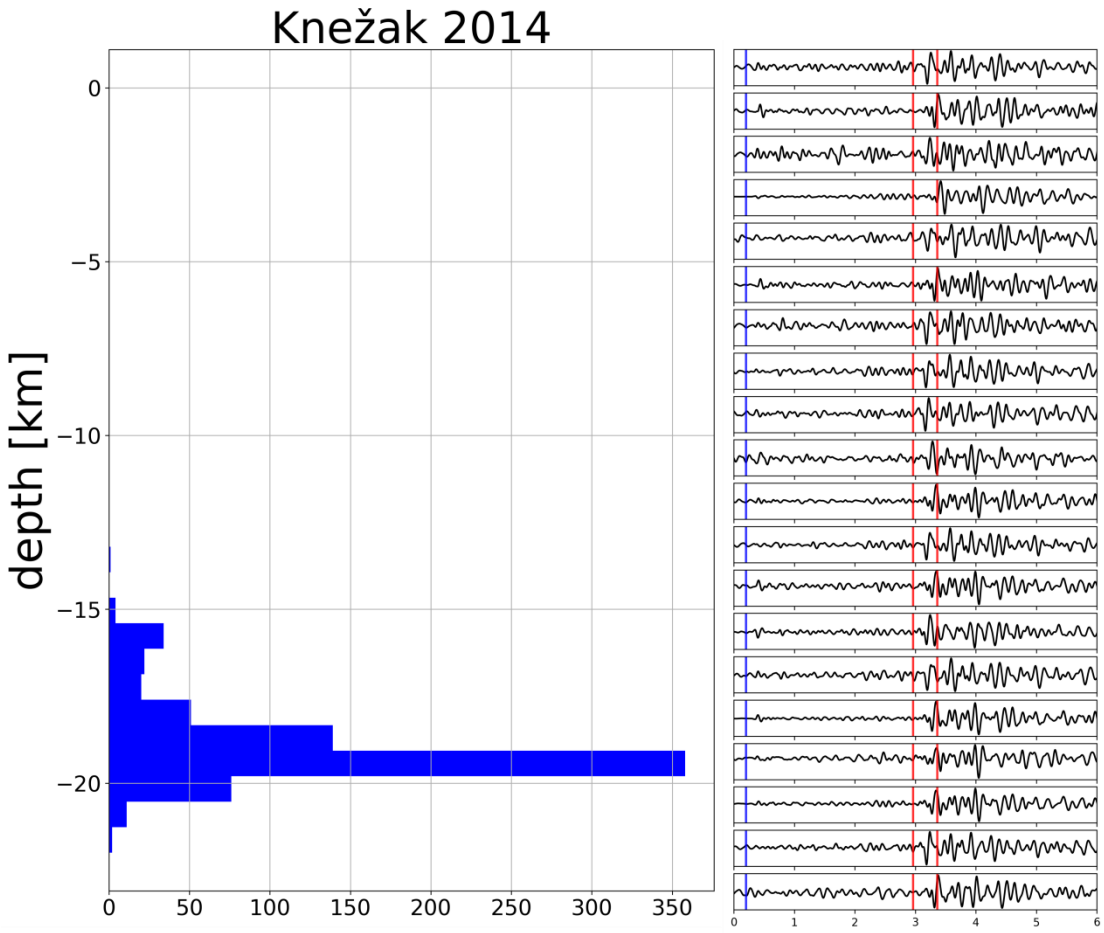

Figure 46: Depth distribution between 18 and 20 km for the Knežak sequence (left). On the right figure we can observe slight changes around S window after aligning the detections on P arrival time. Changes come from different locations and depth of the earthquake.

4.1.5 Bovec area 2007-2017

Micro earthquakes and sometimes burst of micro earthquake activity are quite constant in the region of Bovec, in the northernmost part of the NW External Dinarides, specially along the Ravne fault, which is a casual fault of 1998 and 2004 M 5.7 and 5.4 earthquakes and still remains the most active fault in the IFS in the studied time period. Ravne fault lies in the area, where NW-SE trending strike slip faults change direction towards W-E trending thrust faults of the Southern Alps domain.

In this study 1874 earthquakes were detected in the Bovec area (along Ravne, N tip of Idrija and some unknow faults towards SW of Bovec) in the period between 2006 and 2017 with M_L between -1.0 and 4.1 that happened in August 2015 (Figure 47).

Along the N tip of Idrija fault, around 200 earthquakes were detected, making Idrija much less active than the Ravne fault. Most active part of the Ravne fault is its northernmost part, where repeating earthquakes are extremely common, with 576 detected events in the time between 2006 and 2017.

From the end of 2009 through 2010 Bovec area was affected by an elevated rate of micro earthquakes in a sequence that happened all along the Ravne fault, migrating in a general direction from NW towards SE, finally jumping towards N part of Idrija fault at the end of the sequence (Figure 48).

2009 - 2010 episode consists of 4 smaller sequences on 3 different locations together combined into a few months long Bovec swarm. Swarm started at the end of October 2009 with M_L 1.0 earthquake. This earthquake was followed by micro earthquakes and another M_L 1.5 earthquake on 15th of November 2009. On 26th of December first of the mainshock-aftershock series comprising the Bovec swarm happened with mainshock of M_L 1.8. Next mainshock-aftershock series happened on 14th of February 2010 with the strongest earthquake of the Bovec swarm with M_L 1.9. This earthquake was preceded by few micro pre-shocks.

Next bigger earthquake happened on 1st of April 2010 and was preceded by micro pre-shocks and followed by an aftershock series.

Finally, swarm finished with 3 slightly stronger earthquakes of M_L 1.3 on 12th of May 2010, M_L 1.0 on 30th of May 2010 and final M_L 0.6 earthquake on 18th of June 2010.

During this period of last 3 earthquakes, rate of microearthquake activity along Ravne fault, and not representing the aftershocks of these earthquakes, was slightly elevated.

In general, seismic activity along Ravne fault in the studied period consists of constant micro earthquakes with up to M_L 2 and one M_L 4.2 earthquake and its aftershock series that happened on 29th of August 2015. This mainshock happened in the same area as the most common repeating earthquakes probably directly connected to the rupture zones of 1998 and 2004 earthquakes and could represent their aftershock series.

For the Bovec area, automatically we were able to detect 196 earthquakes, while additional 709 earthquakes were added by waveform inspection. After template creation and scanning of the waveforms, we successfully added additional 969 earthquakes.

For the Bovec swarms no focal solutions exist, and no solutions were obtained from the first arrival analysis, due to the size of the events and the network geometry. The only focal solution in this time period exists for the 29th of August 2015 mainshock, computed using waveform inversion by OGS and first arrivals by ARSO. The solution is mostly dip-slip component with slight strike slip component.

Depth distribution for Ravne fault is shallow, down to 10 km, with majority at around 6 km, while clear clustering of depths at 15 km is visible for the events along northernmost tip of Idrija fault (Figure 49).

The completeness of catalogue is at -0.19 with b-value of 0.83 (Figure 47 - right).

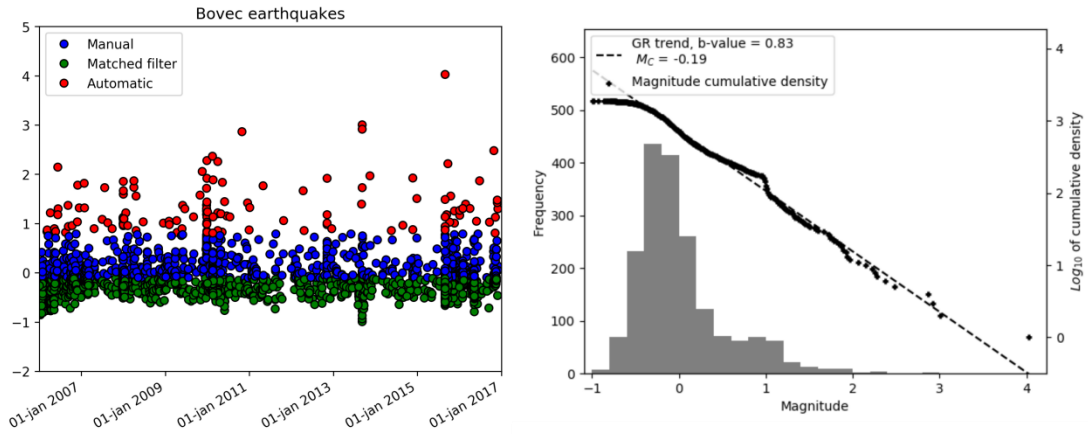

Figure 47: Magnitude vs time for the earthquake activity along Ravne fault. In red, detections obtained by automatic STA/LTA method are shown, blue dots represent events we were able to detect and relocate manually. Green dots represent events, that were only detected by matched filter detection algorithm. On the right figure b-value and Mc are shown.

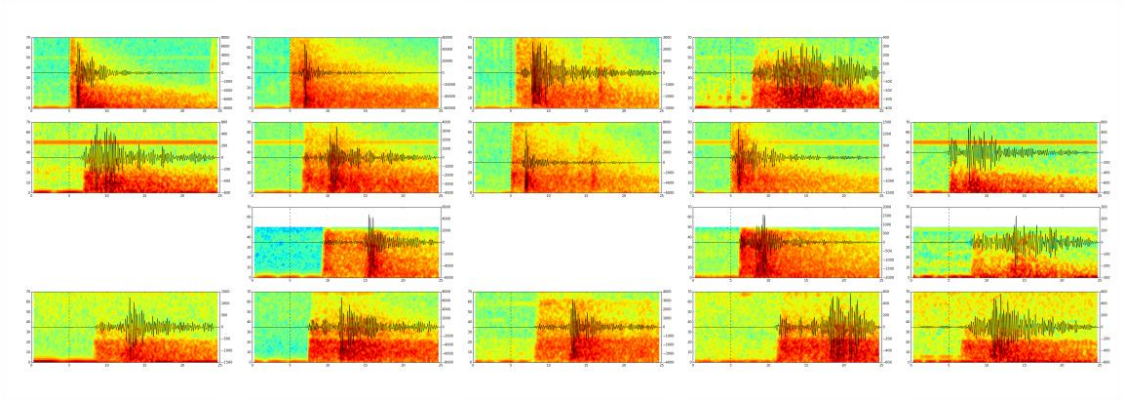

Figure 48: Spectrograms of 5 different families (vertical) of repeating earthquakes happening along Ravne fault. Columns represent one family, on 4 different stations (always ordered as CADS, ROBS, VINO, GORS). What defines a family of earthquakes are changes of hypocentre and/or focal solution. By just looking at the first station (CADS) we can see, that difference between P and S arrival time changes regarding the distance between the receiver and source.

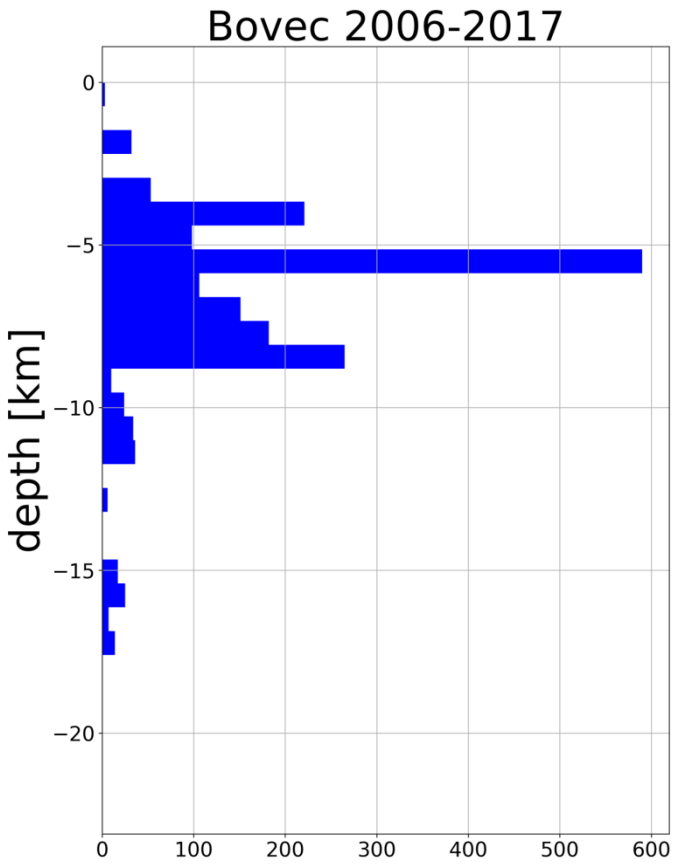

Figure 49: Depth distribution along NW IFS. Shallow events are happening along Ravne fault, while earthquakes at the depths below 15km are located along the NW tip of Idrija fault.

4.1.6 Selce 2017 swarm

On 9th of June 2017 a swarm sequence started in the central area of S part of IFS. The swarm was one of the smaller swarms as in magnitude and short longevity in the studied time period, but was well recorded by the local network. The swarm lasted for 6 days, finishing on 15th of June 2017. It started with a M_L -0.02 earthquake and finished with a M_L 0.01 earthquake with 274 earthquakes with 7 earthquakes of M_L between 0.7 and 1.4. The strongest earthquake happened on 12th of June, 3 days after the initiation of the swarm.

Magnitude of completeness was 0.4 with high b-value of 1.4. Majority of earthquakes happened at the depth between 9 and 10 km. In contrary with earthquakes happening in this region it shows normal focal mechanism as computed from first arrivals. Similarity of the detected events is high, with only subtle changes separating the events into two groups. Change happened somewhere in the middle of the swarm activity.

Epicentral area is at latitude longitude 45.715, 14.16.

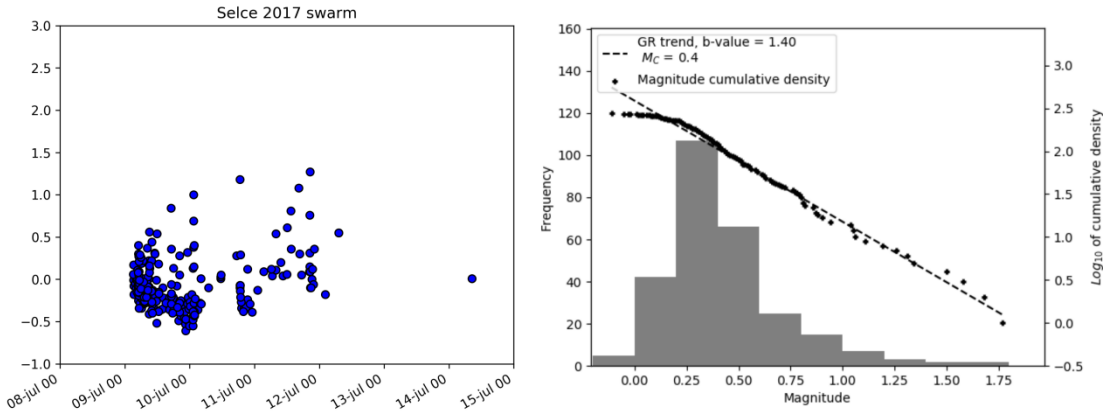

Figure 50: Magnitude vs time distribution (left) of the detected events for 2017 Selce swarm. Mc and b-value of the sequence (right).

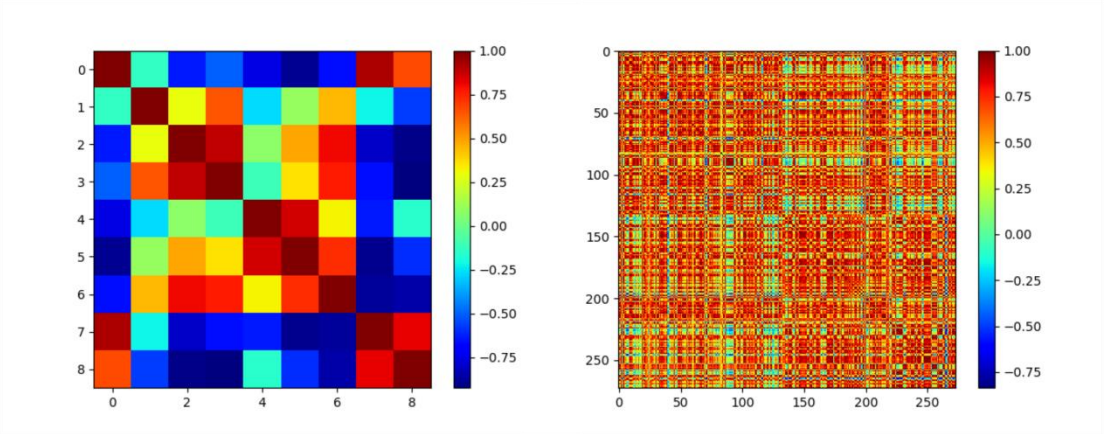

Figure 51: Correlation values of the selected templates around P arrival (left) and correlation values of detections around S arrival (right). Slight grouping into two families is observed on the right figure, which could maybe be present due to the change in magnitudes from very small in the first few days, to small in the next 3 days.

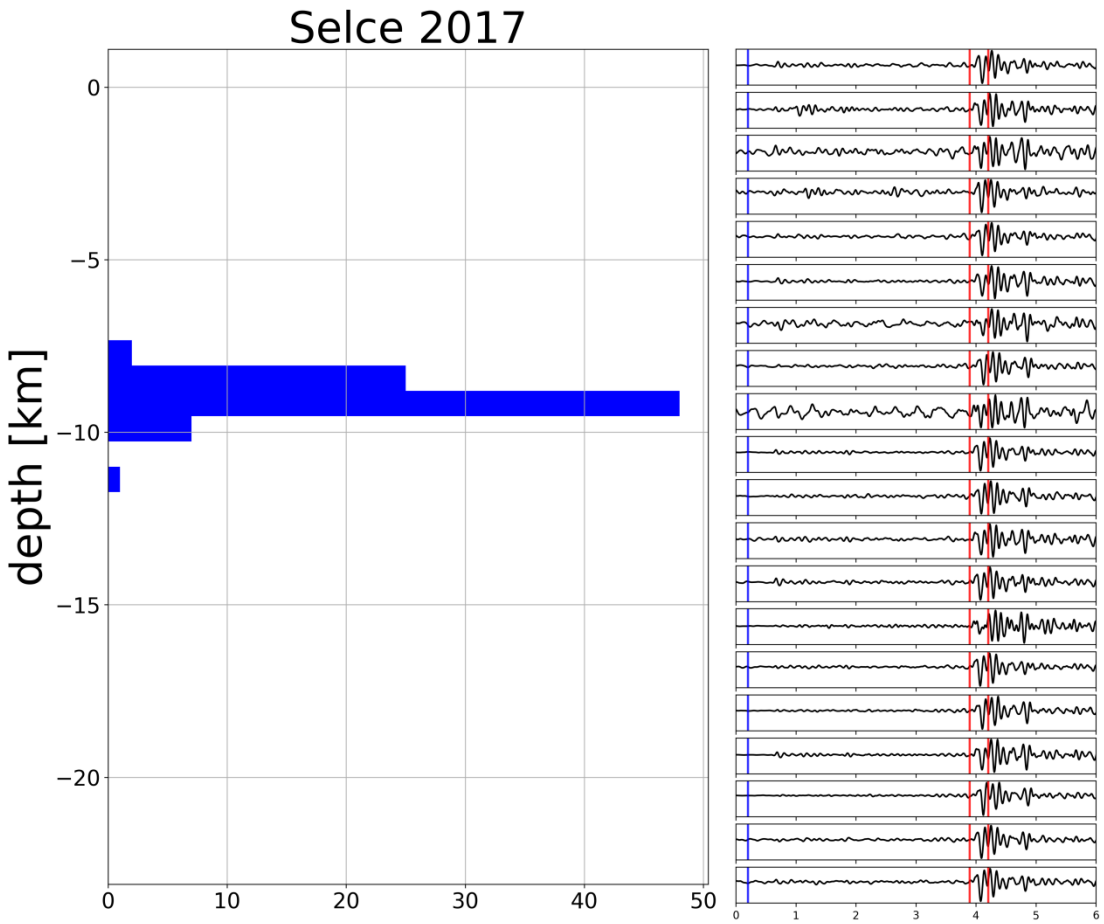

Figure 52: Depth distribution between 8 and 10 km for the Selce sequence (left). On the right figure we can observe slight changes around S window after aligning the detections on P arrival time. Changes come from different locations and depth of the earthquake

4.1.7 Rijeka (Croatia) 2017 sequence

Close to the town Rijeka, Croatia, major earthquake sequence took place from June until middle of October (in the time of writing) 2017. It consisted of two hypocentral areas, first northern and shallower sequence and southern, deeper sequence, both consisting of numerous detected events.

First, northern sequence is a swarm earthquake sequence, lasting for few days, from 6th to 11th of June, when it suddenly stops. The quiescence lasted until 9th of September when the 2nd part of the swarm started and lasted until 21st of October (Figure 53).

The strongest earthquake of the first part of the swarm sequence was M_L 1.1 earthquake, while in the 2nd part, the strongest earthquake had a M_L 2.2. No focal solution for the strongest 2.1 earthquake exists, due to the small magnitude and poor spatial coverage, with only one really near fault station, which exhibits a lot of noise, corrupted data and has much smaller sampling rate (50 Hz) than other stations, north of the town Rijeka. Spatial distribution of the relocated earthquakes shows slightly different then NW-SE Dinaric orientation, but this could easily be contributed to the error in the locations of the events, due to poor station coverage.

Magnitude of completeness of this swarm is 0.34 with b-value 1.0 (Figure 53). The depth distribution is worse than in previous cases, ranging between 6 and 12 km (Figure 55), with majority at 9 km. Cross-correlation values of templates as well as detections show slight grouping that corresponds to the two temporal groups of activity of the swarm.

Second, southern sequence was the strongest sequence in the southern part of IFS after the 2014 Knežak mainshock. The sequence started on 7th of August 2017 with 5 pre-shocks with M_L between 0.7 and 1.3. On 8th of August, first of 6 $M_L > 3.0$ earthquakes happened with M_L 3.8. It was followed by few aftershocks and the strongest M_L 4.0 earthquake at the end of 8th of August. On 9th of August, three more stronger earthquakes happened with M_L 3.8, 3.0 and 3.6. The sequence could be described as a very short-lived swarm-like sequence or a sequence consisting of 4 mainshock-aftershock sequences. The sequence ended on 15th of October 2017 (Figure 56).

Focal solutions from first arrivals are not well constrained, due to the same problem of poor network coverage (stations only on the northern part) but they do agree with poorly

constrained waveform inversion solutions that show strike slip faulting with dip-slip component.

Depth distribution of the events is deeper than for the northern swarm, with events between 14 and 19 km depth, with majority at 17 km (Figure 58). Magnitude of completeness of this sequence is 1.03 with b-value of 0.78 (Figure 56). Such low Mc is due to the distance from the closest station and fact, that the station is not useful for the detection of really micro earthquakes.

Cross-correlation of the detected earthquakes is very low (same problem of the stations) while cross-correlation values of templates show differences in templates.

Northern sequence:

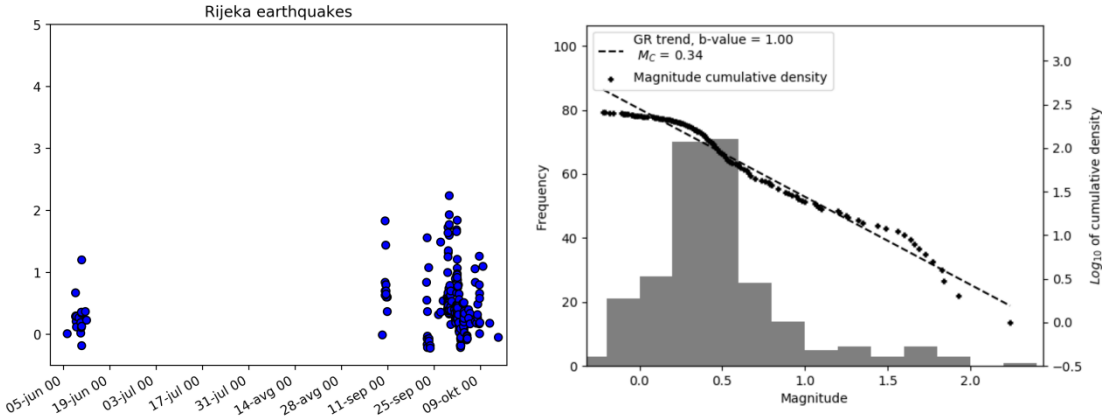

Figure 53: Magnitude vs time distribution (left) of the detected events for 2017 northern Rijeka swarm-like sequence. Mc and b-value of the sequence (right).

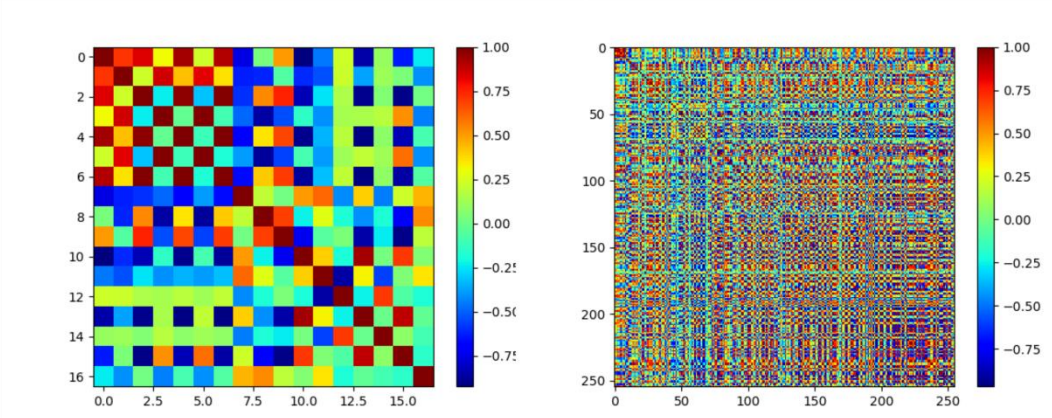

Figure 54: Correlation values of the selected templates around P arrival (left) and correlation values of detections around S arrival (right).

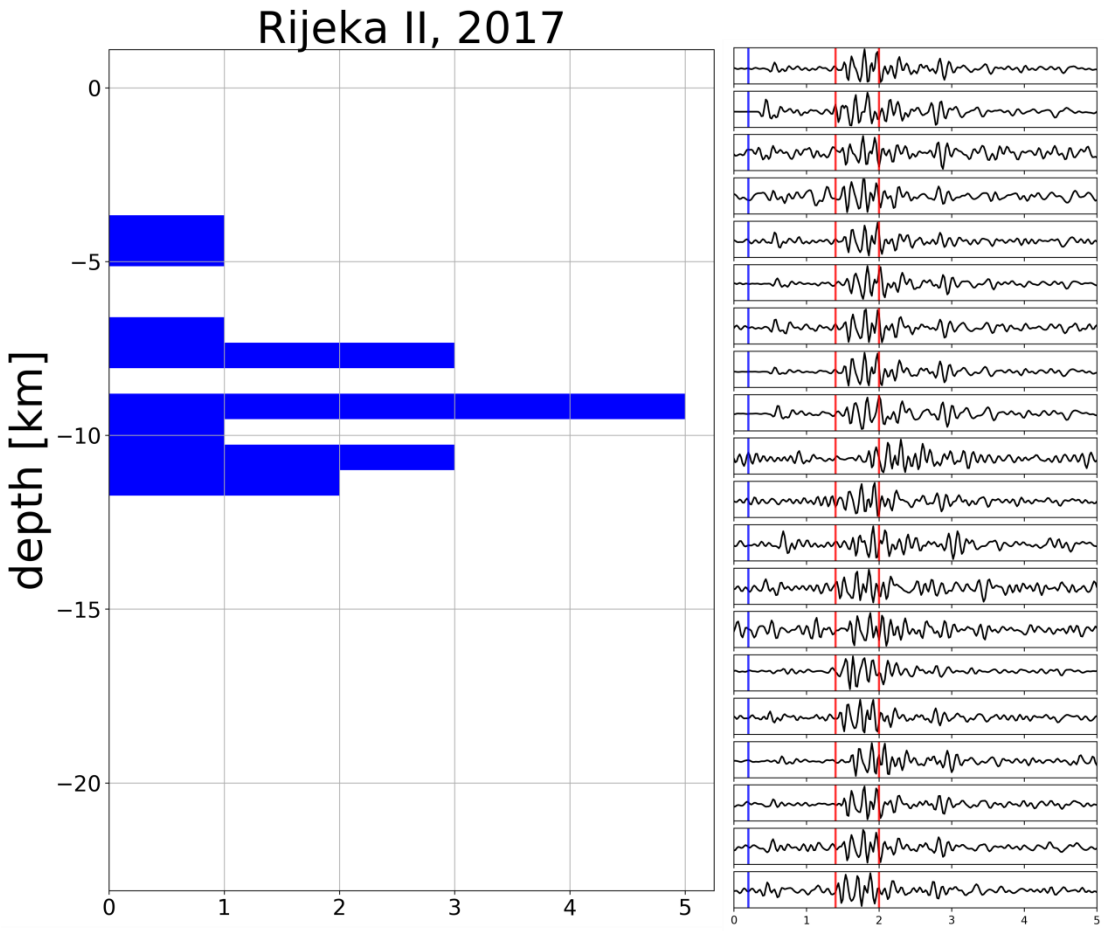

Figure 55: Depth distribution between 4 and 12 km for the northern Rijeka swarm (left). On the right figure we can observe slight changes around S window after aligning the detections on P arrival time. Changes come from different locations and depth of the earthquake.

Southern sequence

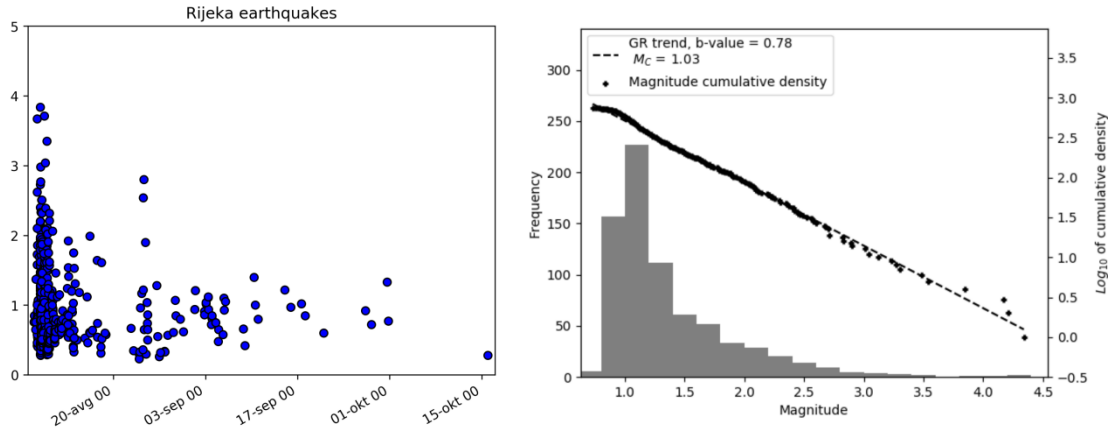

Figure 56: Magnitude vs time distribution (left) of the detected events for 2017 Rijeka mainshock sequence. Mc and b-value of the sequence (right).

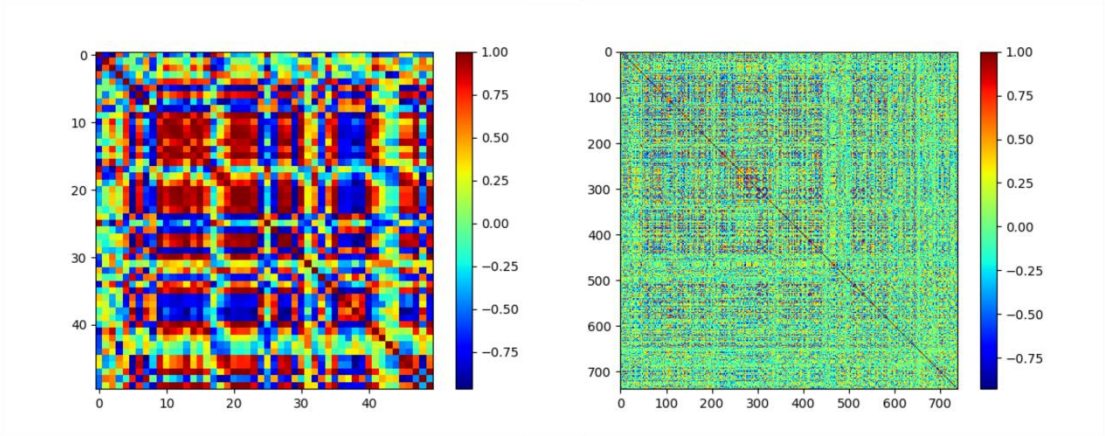

Figure 57: Correlation values of the selected templates around P arrival (left) and correlation values of detections around S arrival (right).

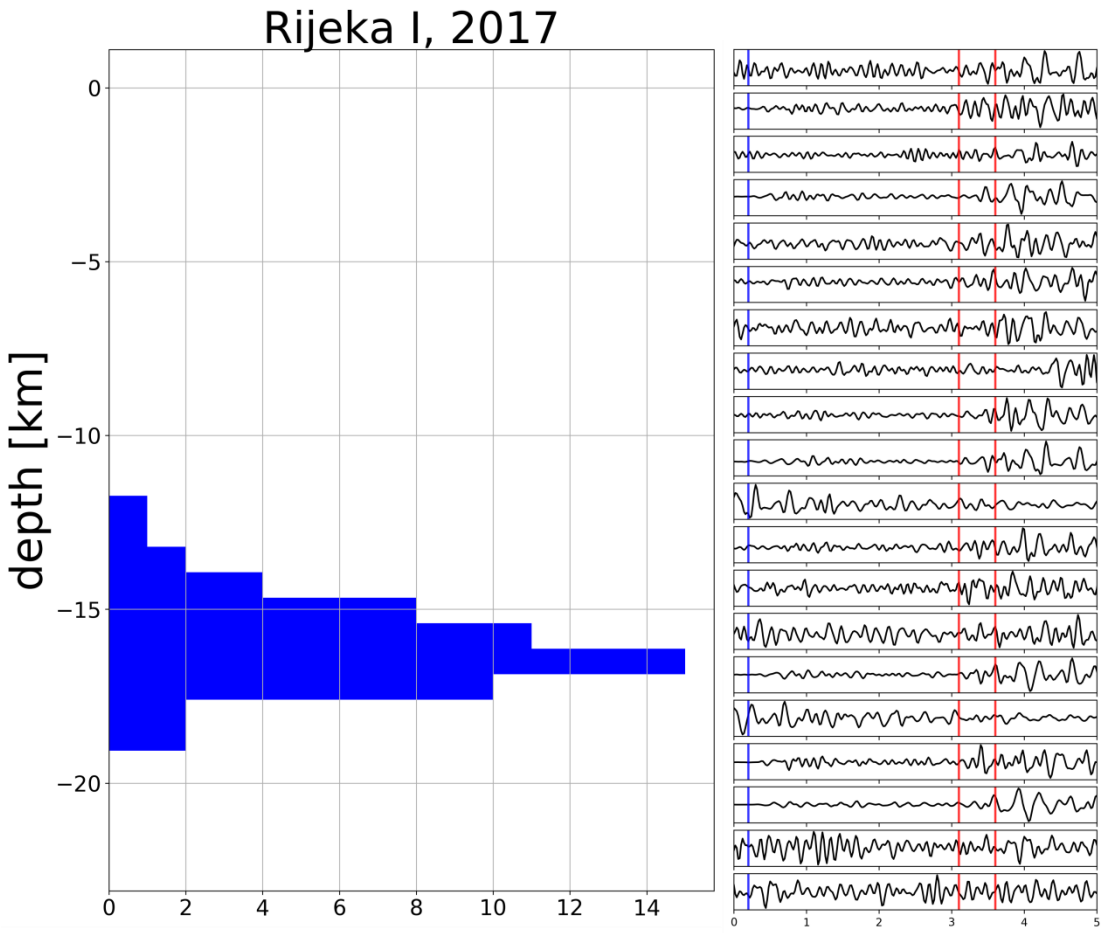

Figure 58: Depth distribution between 12 and 18 km for the southern Rijeka sequence (left). On the right figure we can observe slight changes around S window after aligning the detections on P arrival time. Changes come from different locations and depth of the earthquake

4.1.8 Ilirska Bistrica 2017

On the 15th of August 2017 a short-lived swarm took place in the southern part of the IFS on the border between Slovenia and Croatia. Swarm begun with a M_L 0.0 earthquake and finished on 30th of August with a M_L 1.7 earthquake (Figure 59). The swarm consist of small number of events, all together 28, but no mainshock is present. Majority of events was below M_L 0.5 with only 3 above 1.5. No focal solutions are available for these events.

Sequence was very shallow, with depth distribution between 3 and 5 km (Figure 61), magnitude of completeness was -0.2 with very low b-value of 0.49 (Figure 59).

Similarity of templates is quite high, while similarity of detections does show repetitions of high similarity and low similarity. Due to poorly covered area and small size of the earthquakes and small number of them, not much can be said about the distribution of them, although a variation around S window does show differences in the location of earthquakes (Figure 60).

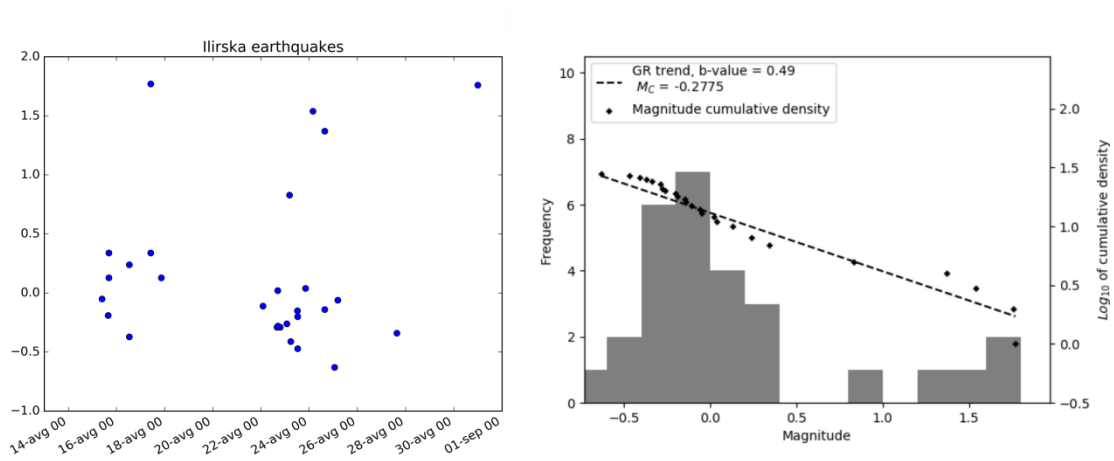

Figure 59: Magnitude vs time distribution (left) of the detected events for 2017 Ilirska Bistrica swarm. Mc and b-value of the sequence (right).

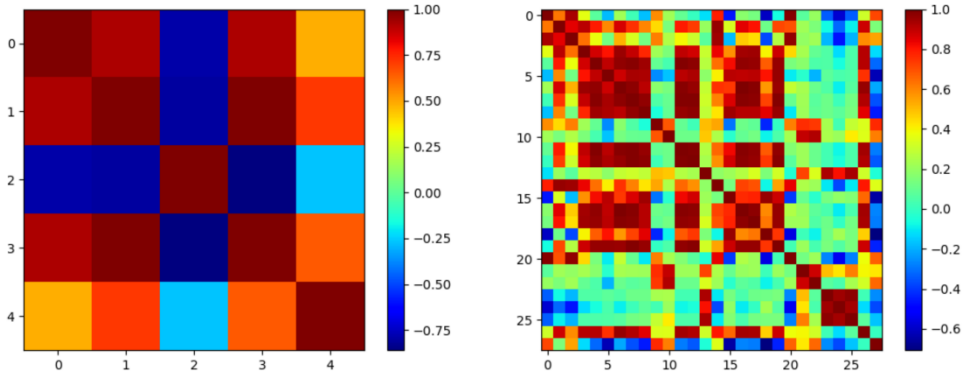

Figure 60: Correlation values of the selected templates around P arrival (left) and correlation values of detections around S arrival (right).

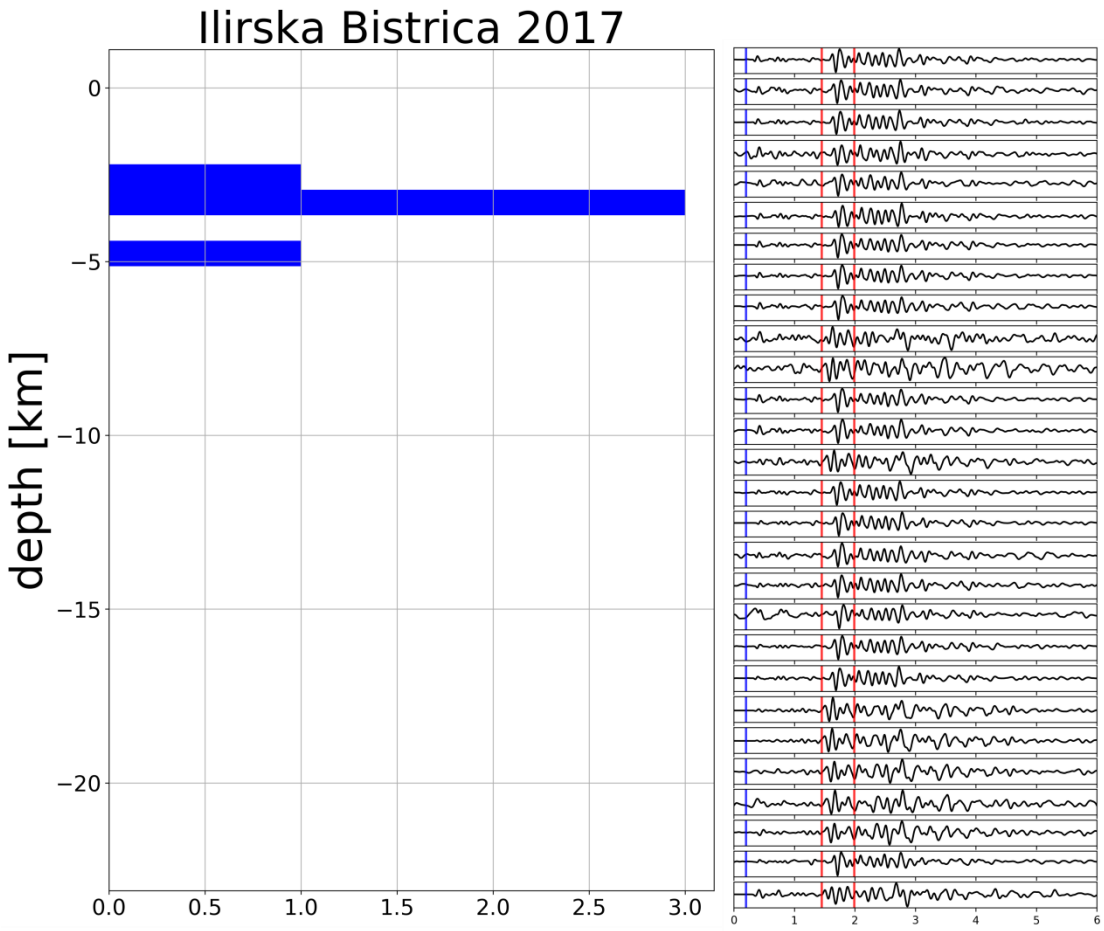

Figure 61: Depth distribution between 3 and 5 km for the Ilirska Bistrica swarm (left). On the right figure we can observe slight changes around S window after aligning the detections on P arrival time. Changes come from different locations and depth of the earthquake

4.1.9 Snežnik 2017

On 8th of October 2017, a small mainshock-aftershock sequence happened in the S part of IFS. The mainshock was preceded by two small M_L 0.0 that happened few hours before. Mainshock was a M_L 2.4 earthquake, that was followed by normal aftershock sequence that finished on 9th of October 2017. There were altogether 268 detected earthquakes with magnitude of completeness at -0.18 and b-value of 0.96.

Focal solutions were obtained from first arrivals and show strike slip faulting with NW-SE or NE-SW direction. The depth distribution of the earthquakes is between 11 and 14 km, with majority at 12 km.

The similarities of both, templates and aftershocks show high values with diminishing values toward the end of the sequence. Also aligned waveforms show only small variations along the S window.

Epicentral area is at latitude longitude 45.612 14.385.

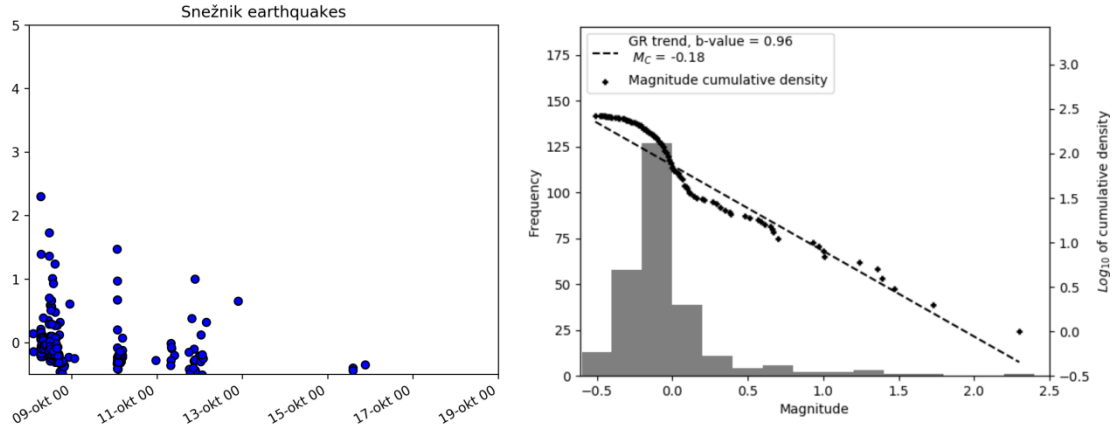

Figure 62: Magnitude vs time distribution (left) of the detected events for 2017 Snežnik mainshock sequence. Mc and b-value of the sequence (right).

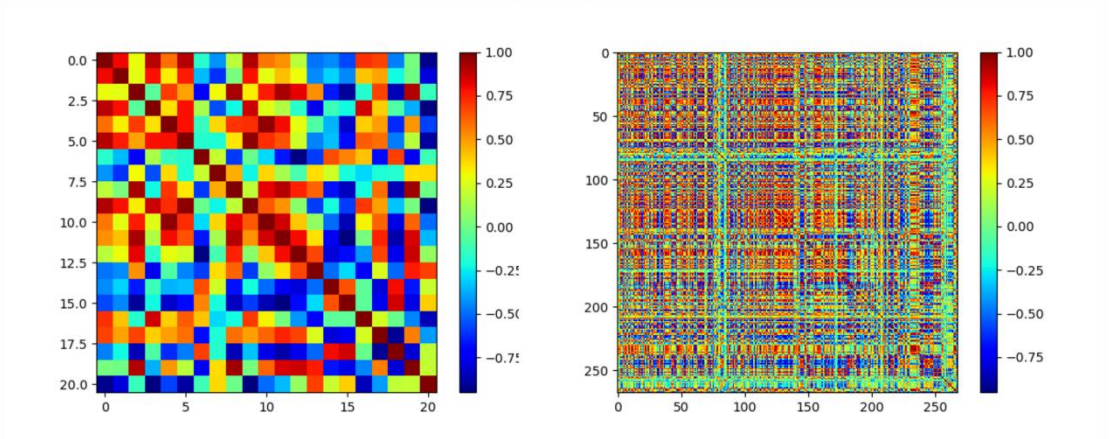

Figure 63: Correlation values of the selected templates around P arrival (left) and correlation values of detections around S arrival (right).

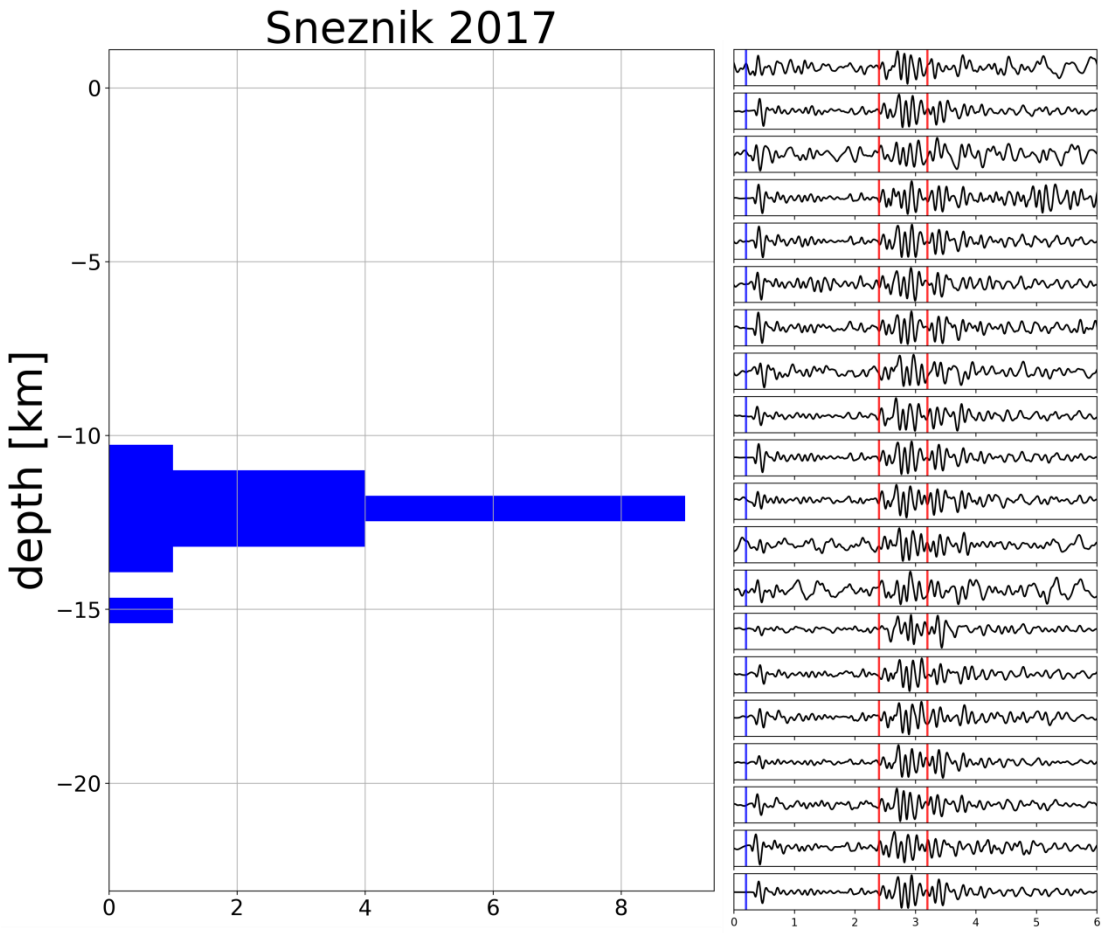

Figure 64: Depth distribution between 10 and 15 km for the Snežnik sequence (left). On the right figure we can observe slight changes around S window after aligning the detections on P arrival time. Changes come from different locations and depth of the earthquake.

5. Discussion

Considering the relocated earthquakes using relative relocation methods together with the new, 3D velocity model obtained from the surface wave analysis, a detailed geometry of active faults in the NW External Dinarides can be proposed, which can be used in hazard studies of the area. In the first part of this chapter, a model of active faults will be given and compared with previous structural knowledge of the same area.

In second part, an idea of temporal and spatial clustering of the earthquake activity in the NW External Dinarides will be explored together with the data of Postojna cave extensometer in the time limit between 2006 and end of 2017. A physical model of earthquake triggering during these episodes will be proposed and explored.

5.1 Idrija fault system model

So called Dinaric faults (Vrabec and Fodor 2006) show clear surface and morphological expressions in the NW External Dinarides and can be more than 100 km long (Idrija fault) (Figure 1). Geological mapping of Western Slovenia showed that area is strongly faulted (Buser 2009), but rare evidences of active faulting exist except along the major faults of the Dinaric system, namely Ravne, Idrija, Predjama and Raša fault (Cunningham et al., 2006; Kastelic et al., 2008; Moulin et al., 2014, 2016, Foroutan et al., 2018). Documented past earthquakes are rare (Bajc et al., 2001; Bavec et al, 2013; Fitzko et al., 2005), but they do show recent activity in the region. Although earthquake activity in the years since 2006 shows trends of happening close to these geological faults, it is hard to connect single earthquakes to these faults, especially due to their small sizes, which do not enable us to compute focal mechanism of the earthquake or, if focal mechanisms are successfully obtained, maybe do not show actual tectonic regime. Due to these restrains, high resolution relocation of earthquakes helped in the mapping and correlating earthquakes to the geological faults and their (in)activity in the period from 2006. In this work, similar conclusions are obtained as in previous works, that Ravne, Idrija, Predjama and Raša faults are indeed currently most active faults of the NW External Dinarides and represent recent active faults of Idrija fault system.

As already discussed in the Chapter 4.1, earthquake activity in W Slovenia can be divided roughly into 3 regions, norther area on the junction between NW External Dinarides and Southern Alps, with most active Ravne and Idrija fault and continuation of Predjama and Raša fault (due to the segmentation of the faults, this could be completely different faults and not their continuations), central part with Idrija, Predjama and Raša fault and southern part with Idrija, Predjama, Selce and Raša faults. In the N part, activity is most abundant along Ravne fault, followed by activity along Idrija fault and activity along Predjama and Raša continuations. The central part was the least active part in the time span of this thesis, with most earthquakes happening along Raša fault, followed by Predjama fault and Idrija fault. There are also some earthquakes between Predjama and Idrija fault, but their size was too small to obtain focal solutions, which maybe could tell if these earthquakes happened along some minor transfer faults between Idrija and Predjama fault or not. Southern part is the most active along Selce fault, followed by Raša and Predjama fault, with only rare earthquakes happening along what could be Idrija fault.

5.1.1 Focal mechanisms

Only few earthquakes with $M_L > 2.0$ were used in this study whose focal mechanisms are known or were computed during the work of this thesis, which could be used in modelling of the fault system (Figure 65 and 66). Bigger events whose focal mechanisms were obtained by OGS with waveform inversion (Sarao, 2013, 2016) agree with first arrival mechanism obtained by ARSO and show mostly strike-slip faulting except for the 2015 Ravne fault earthquake in the N part of the system, whose main component is reverse. For two smaller earthquakes focal mechanisms, computed during this thesis, were not constrained very precise and vary up to 10°. The two focal mechanisms were calculated for the M_L 1.5 earthquake inside 2017 Selce fault swarm, which interestingly shows normal focal mechanism, and for 2017 Snežnik M_L 2.3 mainshock aftershock series which shows pure strike-slip faulting. The focal solution of M_L 1.5 is not well resolved and probably does not represent the true slip response due to the regional stresses.

Focal mechanisms are in agreement with GPS studies (Caporali et al. 2008) that shows up to 4.6 mm/yr (2.6 ± 2.0 mm/yr) right-lateral strike-slip motion between Trieste and

Ljubljana stations, as well as geomorphological indicators of slip along the active faults and most likely show a right-lateral strike-slip faulting along the Idrija, Predjama, Selce and Raša fault and a thrusting event along the Ravne fault in the junction between External Dinarides and Southern Alps, where the transition from strike-slip to thrusting happens.

Cross-sections, perpendicular to the strike of main faults, over northern, central and southern part of the system show flower-like structure with shallower earthquakes along the Ravne fault in N and along Raša fault in the S, while earthquakes along central part of Raša, Selce and Predjama faults are slightly deeper (depths down to 20 km). Idrija fault seem active only in the N part, with deepest earthquakes not happening beneath 18 km.

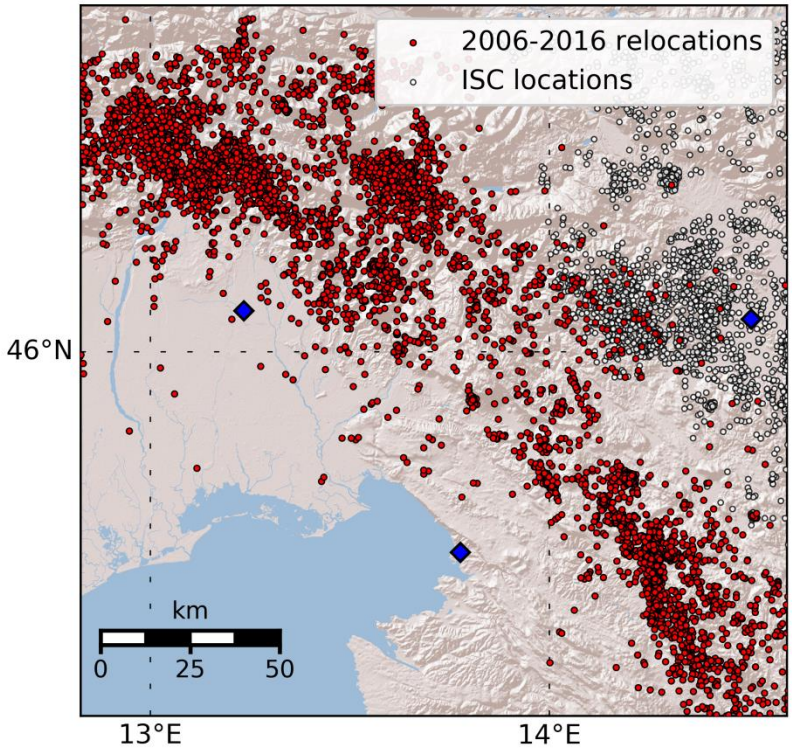

Figure 65: All the detected and relocated earthquakes from 2006 to 2016 in red. White dots represent earthquakes that happened in the same time period (International Seismological Centre 2014) *and are not part of faulting along IFS.*

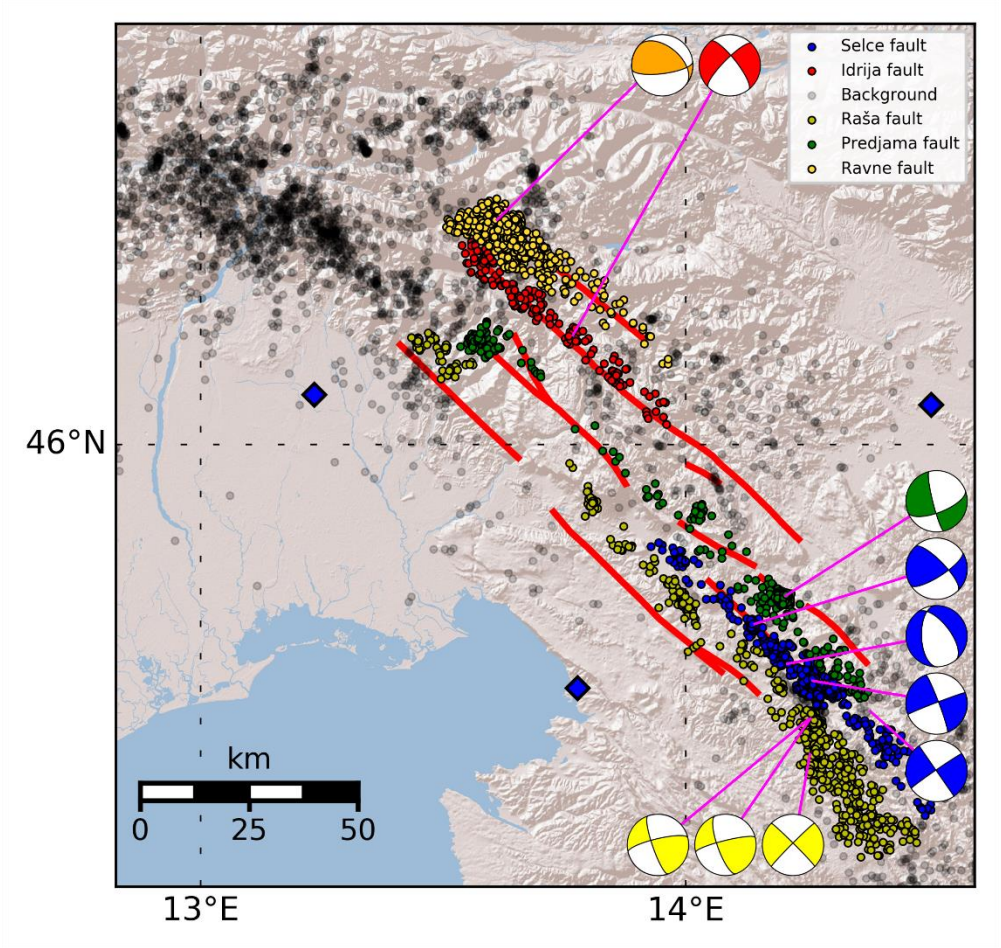

Figure 66: Earthquakes associated with causative faults and focal solutions of stronger earthquakes since 2006.

5.1.2 Geometry of the fault system

As observed in the 3D surface wave velocity model (Guidarelli et al., 2017), Idrija fault is near vertical (80º) leading structure along which shorter faults with similar strike exist and either connect to it at depth or are individual structures with smaller footprint then Idrija fault.

Resolution of earthquake locations along the Ravne fault (Figure 68, A) is not resolved enough to clearly observe the geometry of the fault, but seemingly it dips toward SE, connecting to the Idrija fault at around 10 km depth while its northern part probably exhibits change of strike and dip to somewhat more South Alpine thrusting (focal solutions).

Predjama fault (or different segments of the fault) can be traced along all three subareas (Figure 67). Relative relocations were performed along the Predjama fault in the S part, in the swarm sequence that happened there between the end of 2009 and beginning of 2011. For the central and N part, relative relocations do not show any significant change from the manual, non-linear locations. The earthquakes along Predjama fault seem to follow constant strike as visible in cross-sections.

Earthquakes connected with the Selce fault, with surface expression visible in the central and S part, are happening between 8 and 20 km, depending on the sequence. It seems that stronger earthquakes (2008 M_L 3.0 and 2014 M_L 4.7) nucleate deeper while smaller magnitude sequences and 2017 swarm sequence are shallower.

Raša fault can be traced in the central and S (Figure 68, B, C, D) part of the system. Like Selce fault, earthquake activity is distributed between 4 to 18 km. Earthquakes connected to the Raša fault are clearly illuminating a fault going from sub vertical in the shallow part towards dipping fault at the depth both in central part of the system, while in the southern part earthquake activity is not clearly resolved (Figure 68, C and D). Either the earthquake locations of sub-clusters incorporate higher errors in such way, that clusters dip towards SW, seemingly illuminating Raša fault (all 3 sub-clusters) but with reactivated branches of damaged zones under angle towards main fault where the aftershocks are taking place or the strike of the "Raša" fault completely changes the strike from Dinaric to a fault with N161 strike, which agrees better with the focal solutions obtained from the two M_W 3.5 earthquakes that happened inside bigger and deeper mainshock–aftershock sequence.

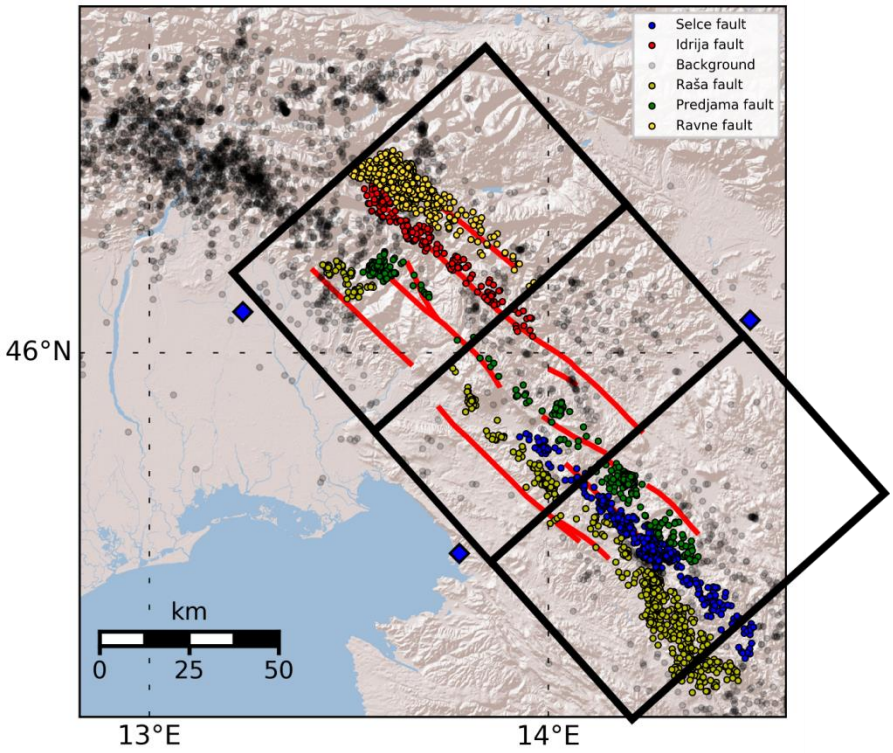

Figure 67: Division of the area into northern (1), central (2) and southern (3) part that correspond to selected cross sections perpendicular to the strike of IFS.

As a structure of the active faults of IFS, we propose a series of parallel strike-slip faults with dip-slip component, with Idrija fault being the leading fault, sampling all the crust with near vertical dip while other faults exist in the upper crust and are dipping towards Idrija fault.. The Ravne fault in the N part of the system is dipping towards the Idrija fault (towards SW) and connects to the Idrija fault at around 10 km depth. Predjama and Selce fault are sub vertical down to much greater depths, with Selce fault probably connecting to Raša fault, which represent the westernmost fault of the fault system. The geometry of Raša fault is resolved at shallow part where the fault is sub vertical (Foroutan et al., 2018) and dipping towards NE at greater depths. It is not known if the fault connects with Idrija fault even deeper either at some angle or as a flat decollement or it is its own structure.

Proposed model for the central part agrees with the model of Idrija, Predjama and Raša fault, proposed by Placer et al. (2010) relatively well. Placer's model suggests that Raša, Predjama and Idrija faults are al sub-vertical faults, probably connecting to older inactive detachment plain somewhere at depth.

Model, proposed by Moulin et al. (2016), defines the system as a flower-like structure with flat parts of the faults relatively shallow, completely ignoring the earthquake activity and their locations. Except of the near surface geometry, our proposed model disagrees with the one proposed in Moulin et al. (2016).

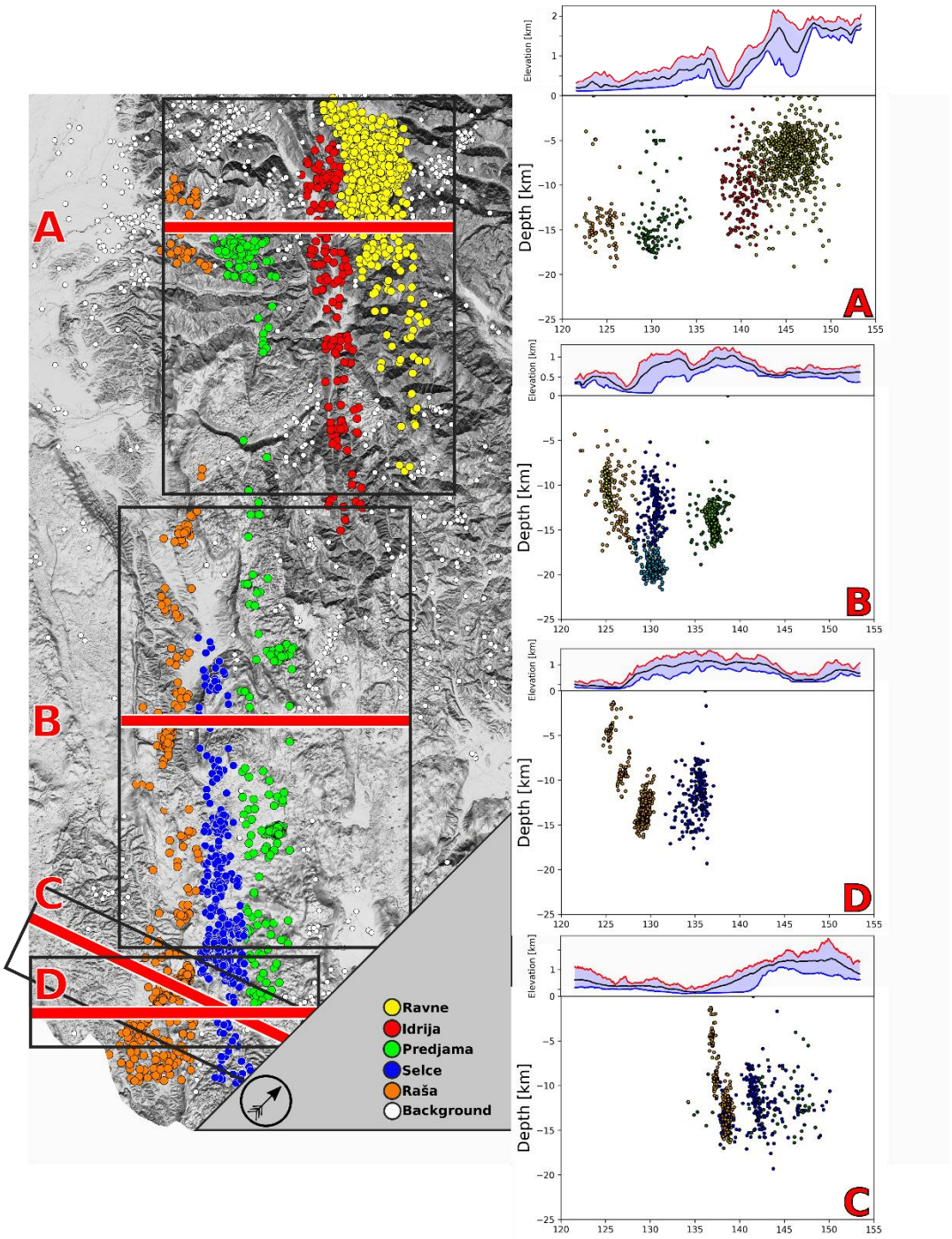

Figure 68: Cross section northern (A, central (B) and southern (C, D) area, perpendicular (A, B, C) to the strike of IFS and with slightly different (70°) angle. Above cross sections, elevation profile of DEM over the area is shown, mean elevation (black), maximum elevation (red) and minimum elevation (red).

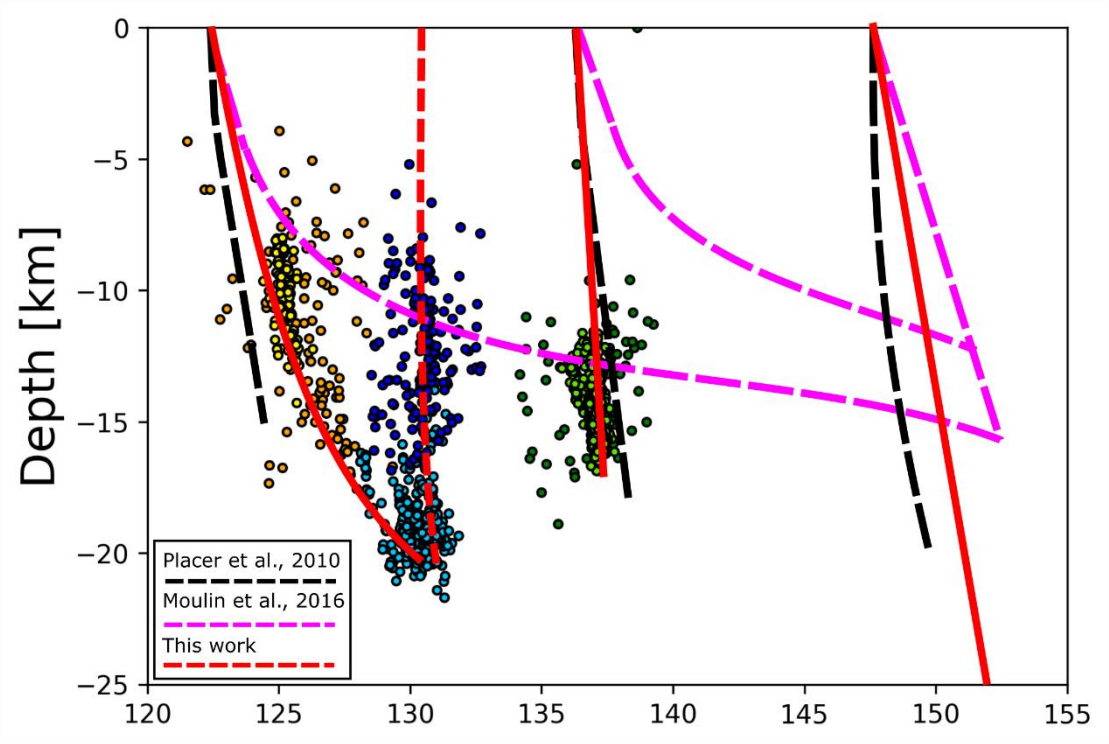

Figure 69: Proposed model perpendicular over the central part of IFS. Black dashed lines were obtained from Placer et al. (2010), pink dashed lines from Moulin et al. (2016). Red lines represent proposed model from this work. Idrija fault was defined from Guidarelli et al. (2017).

5.1.2.1 Southern extend of the Raša fault

As discussed in the previous sub chapter, we connected earthquakes in the southern part, whose epicentres are located few km NE away from what could be Raša fault at the surface, to the Raša fault itself. As discussed, Raša fault is changing to sub vertical geometry at the surface towards NE dipping structure parallel to Idrija fault or changes the strike from Dinaric to N160.

In the both cases of described geometry, seismogenic zone of Raša fault extends between 3 and 18 km, basically almost whole seismogenic zone of IFS (since the deepest earthquakes can be found at the depth of 20 km.).

Although 3 focal solution, computed for the 3 earthquakes that happened in the southern part of Raša fault all show sub vertical right-lateral strike slip solutions, the mechanisms do not contradict the first proposed model in sense that these earthquakes are small events

(M_L < 4.0) meaning their source area is very small with r < 300 m (Uchida et al. 2012). Since we do not have any information of the width of the Raša fault at depth, small earthquakes could be rupturing only small parts of the fault zone (combination of main fault together with the fractured zone), that is thicker than the source area itself. In this case, small earthquakes, happening along Raša fault are not giving us real picture of faulting during big earthquakes (M_W > 6.0) where the much larger area of main fault zone would slip.

In the second proposed geometry of the "Raša" fault, aftershocks are showing much more vertical distribution which agrees with the focal solution of the two strongest earthquakes of the deeper cluster, but fails to explain the 3rd computed focal solution of the intermedium cluster, which shows vertical strike-slip faulting with Dinaric direction.

The geometry of the Raša fault in its most southern extend of the studied area is so not completely resolved, with two different possibilities. Due to the slightly less resolved relocation of these 3 clusters (no useful stations to the south) our proposal for the geometry in this part is slightly biased towards similar geometry of the fault as in the central part – sub vertical fault at the surface with NE dipping part at the depth. Until our resolving power in this part changes, no clear picture can be presented.

5.2 Transient

As was shown in the chapter 4, Idrija fault system exhibited two temporal clusters of earthquake activity in the years between 2006 and mid-2018 (at the time of writing). System wide clustering happened in 2009-2010 with elevated earthquake activity along northern part of IFS, mostly along Ravne fault in swarm like series lasting few months. At the same time period, swarm-like earthquake series happened along Predjama fault, close to the town of Postojna, Slovenia in a more than a yearlong sequence. Few months later, a triple mainshock–aftershock series, migrating from N towards S and from deeper portion to the shallower portion of Raša fault, happened in the southern part of the IFS, finishing the 2009-2010 transient series of IFS.

After the 2010, only 3 stronger earthquakes happened along the IFS; M_W 4.5 earthquake on 22nd April 2014 in the southern part of IFS, along Selce fault, a M_W 3.6 earthquake on 29th May 2014 on the northern part of IFS, along Idrija fault itself, and a M_W 4.1 earthquake on 29th August 2015 along Ravne fault in the northern part of IFS.

In June 2017 a new temporal and spatial cluster of elevated earthquake activity started in the southern part of IFS, in the southern extend of Raša fault and its continuation towards south, towards the Vinodol – Rijeka fault (Basili et al., 2013). Sequence consisted of mainshock–aftershock series and swarms, both short lived and few months long swarm sequences.

In this chapter insight on the 2009 – 2010 transient behaviour and its underlying physics will be discussed. The 2017 sequence will not be discussed in detail since no other data exists and only seismological aspect of the transient was explored.

5.2.1 2009–2010 Idrija fault system wide transient episode

The 2009 – 2010 Idrija fault system transient was observable all along the IFS – as a series of mainshock–aftershock sequences forming a few months long swarm along the northern part of the system, mostly along the Ravne fault, as a yearlong swarm sequence along the Predjama fault in the central part of the system, and a triple mainshock–aftershock series along Raša fault in the south of the system.

The elevated earthquake activity, described in this thesis as a transient happening along

IFS first started in July 2009, close to the city of Postojna, Slovenia, along the Predjama fault. This was a short-lived sequence of microearthquake activity, few km NW from the place, where in December 2009 the Postojna swarm started. After July earthquakes along Predjama fault, there was few months of low activity along IFS, except of a small sequence W of the Predjama earthquake series, along the Raša fault. This quiescence lasted until mid-November when the swarm-like sequence of northern IFS started. The maximum of the northern IFS earthquake activity was reached at the end of December and lasted until April 2010, followed by the decay of activity until the August 2010. At exactly the same time, Postojna swarm started along Predjama fault. It lasted until August 2010, with some smaller aftershocks lasting until early 2011. In September, the earthquakes migrated towards the southern part of the system, where triple mainshock sequence happened along the Raša fault.

Interestingly, at the same time period, between October 2009 and August 2010, extensometer in the Postojna cave (Gosar et al., 2011) shows extreme changes along vertical Z axis (Figure 70). Extensometer, which is placed on Predjama fault planes, measured almost 0.08 mm of subsidence of the NE block. This effect lasted for 4 months without any major changes, then suddenly dropped back to much lower value, signalling uplift of the NE block to almost the same position as before the transient deformation, with cumulative displacement of 0.02 mm. After this deformation episode, extensometer stayed at approximately the same level until mid-2013.

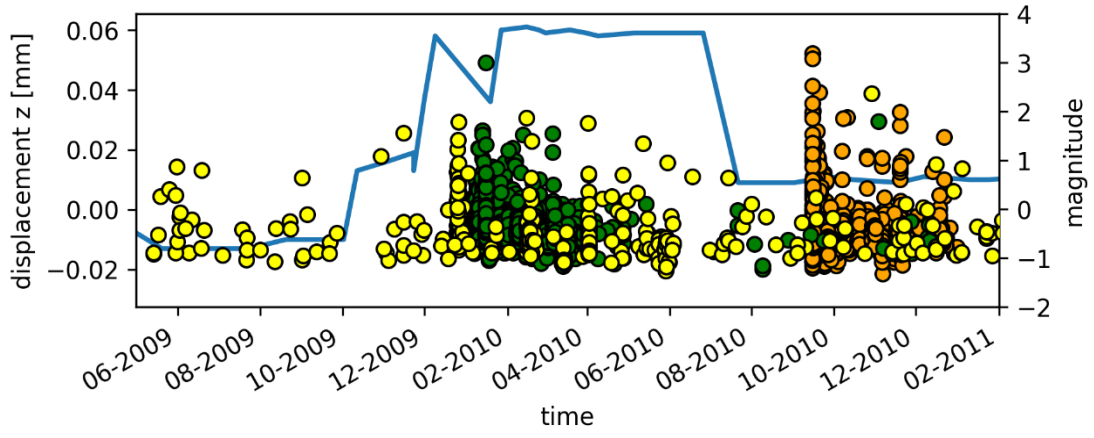

Figure 70: Earthquake activity and changes on vertical axis of the Postojna cave extensometer. Yellow dots are earthquakes along Ravne fault in the N, green are the earthquakes of Postojna swarm and orange are earthquakes of the triple mainshock-aftershock sequence in the S of IFS. Good correlation between earthquake activity and changes on extensometer is observed.

To obtain possible insight into the physics of the extensometer changes and earthquake triggering, Coulomb stress change modelling was performed (personal communication with Farhan Javed).

Assuming a simple Coulomb friction model for earthquakes, change of Coulomb failure stress will increase or decrease the potential for nucleation of earthquake, as defined by

$$\Delta CFS = \Delta\tau + \mu(\Delta\sigma_n + \Delta p) \quad 20$$

where $\Delta\tau$ is the shear stress change resolved in the preferred slip direction, $\Delta\sigma_n$ and Δp are the normal stress change (positive for unclamping on the fault) and pore pressure change on the fault, and μ is the coefficient of friction. It appears that ΔCFS as low as 0.1 bar can trigger the seismic activity (King et al., 1994; Reasenberg & Simpson, 1992). According to Rice and Cleary (1976), pore pressure can be related to normal stress using the following equation:

$$\Delta p = B\,\Delta\sigma_{kk}/3 \quad 21$$

where B is the Skemption's coefficient and its value varies from 0 to 1. It means that any sudden change in the normal stress in a saturated porous medium causes a change in pore pressure. The pore pressure change will then tend to diminish by fluid diffusion at the rate determined by the local diffusivity of the system. Thus, fault clamping and unclamping, which strengthens and weakens the faults respectively, will change according to the changes in normal stresses or pore pressure changes. Fault unclamping will hence promote the earthquake activity along the unclamped fault, and clamping will suppress it.

We modelled the transient deformation using the geometry of the fault system and slip rates of the fault system as derived from our understanding of the fault system. The best model explaining the elevated earthquake activity and changes along the extensometer in Postojna cave was contributed to the tectonic transient happening along the leading fault of the system – Idrija fault.

As derived from InSAR studies and seismogenic depth of the IFS as observed in this work, Idrija fault system is locked down to 18 km and accumulates strain at the rate of 2 mm/yr along both strike and dip direction. It is possible, that portion of the fault between 18 and 45 km, which undergoes creeping, exhibits transient deformation during the observed period, which would explain IFS wide elevated earthquake activity. To test this

hypothesis, changes in stress state and comparison with the spatial extend of the earthquake activity was estimated.

For the model, changes of shear, normal and Coulomb stresses at the depth of 15 km were estimated. ΔCFS was computed assuming the $\mu = 0.4$ and $\mu = 0.8$. The $\Delta CFS > 0.01$ bar was estimated for the central part of the system, thus $\Delta CFS > 0.01$ bar/year was estimated for the creep rate of Idrija fault set at 2 mm/yr. Assuming the constant creep rate, ΔCFS becomes greater than 0.1 bar after a decade. Figure 71 depicts shear and normal stress changes at the location of the Postojna cave extensometer and surrounding region, indicating unclamping of the faults is the most favourable mechanism for the overall seismic activity. This is also evident from the cross sections on Figure 72.

The subsidence and later uplift of the Postojna cave extensometer could be the result of the downward and upward motion of the block between Predjama fault and Idrija fault. The downward motion is a consequence of the increase in vertical stresses ($\sigma_v - \Delta p_h$) due to the extraction of fluids at the depth, in which $\sigma_v = \rho g h$ and ΔP_h is the change in hydrostatic pressure. This would create a pressure gradient at the depth, increasing pore pressure in the regions where pore pressure decreased, coinciding with the earthquake swarm activity, beneath the Postojna block. Finally, the pore pressures would diminish, and vertical stresses would decrease with time, reaching the equilibrium followed by the uplift of Predjama block. A diagram is shown in Figure 73.

The model only covers the activity along the central part of the IFS, but the same mechanism is easily applied to the increase of activity along the Ravne fault (north) in the same time period and the activity along Raša fault (south) happening few months after the observable surface deformation seen on extensometer.

Earthquakes along Ravne fault are shallower than the earthquake activity along other faults of the IFS and are happening in the zone of the elevated normal stresses (Figure 72) on the right of the Idrija fault in the shallow part. Similarly, earthquakes of Raša fault start with the deep mainshock–aftershock sequence, which is again in the area of elevated normal stresses (Figure 72– left side of Idrija fault at bigger depths). Due to the unclamping of the Raša fault, whole fault exhibits elevated earthquakes rate period as a migration of earthquakes from N towards S and from bigger depths towards the shallow portion of the fault.

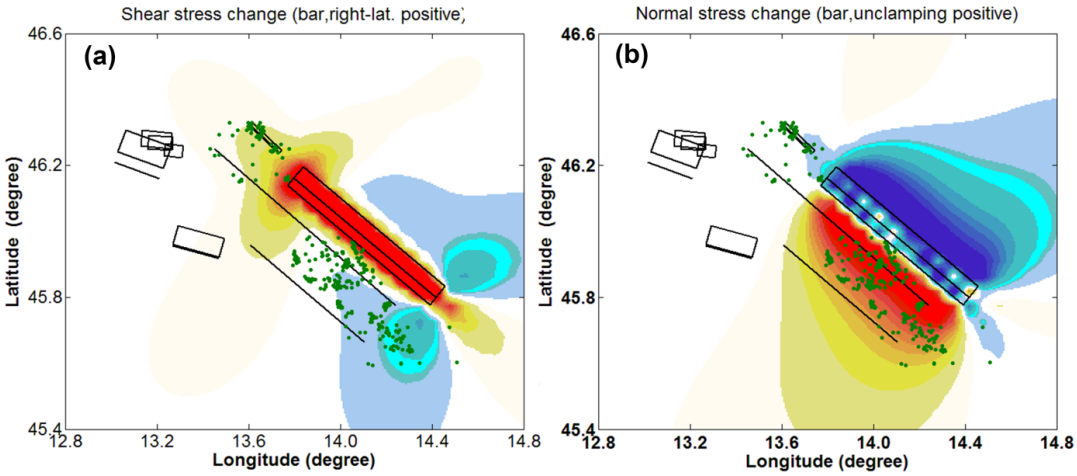

Figure 71: Shear stress (a) and normal stress (b) changes as modelled along IFS for the period of 10 years with constant 0.01 bar/year loading at the depth of 15 km. As we can see on the figures, shear stress changes cannot explain fault unclamping, while normal stress changes can.

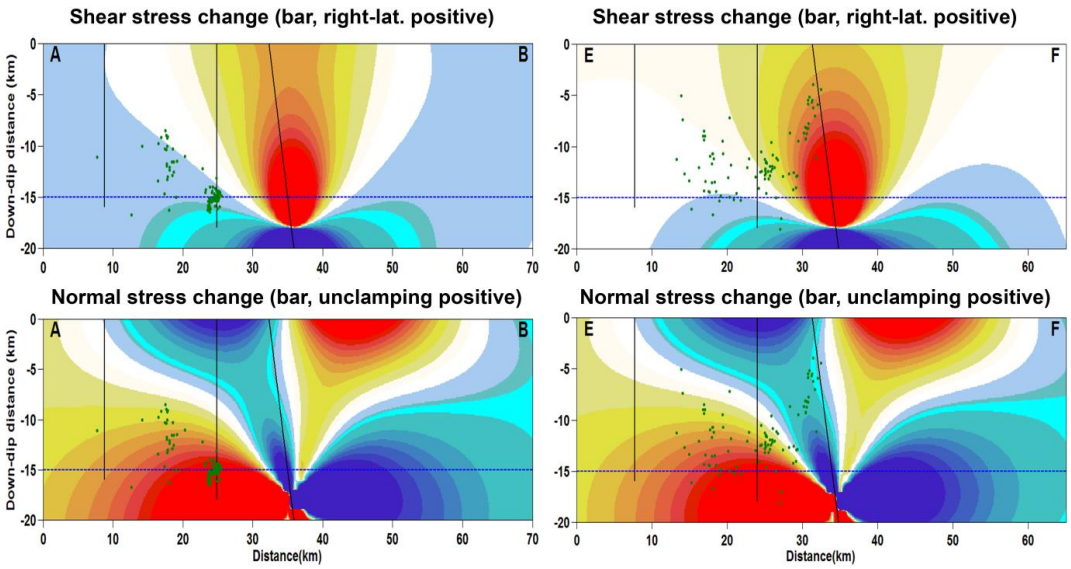

Figure 72: Same as Figure 71, but in cross section, perpendicular to the IFS.

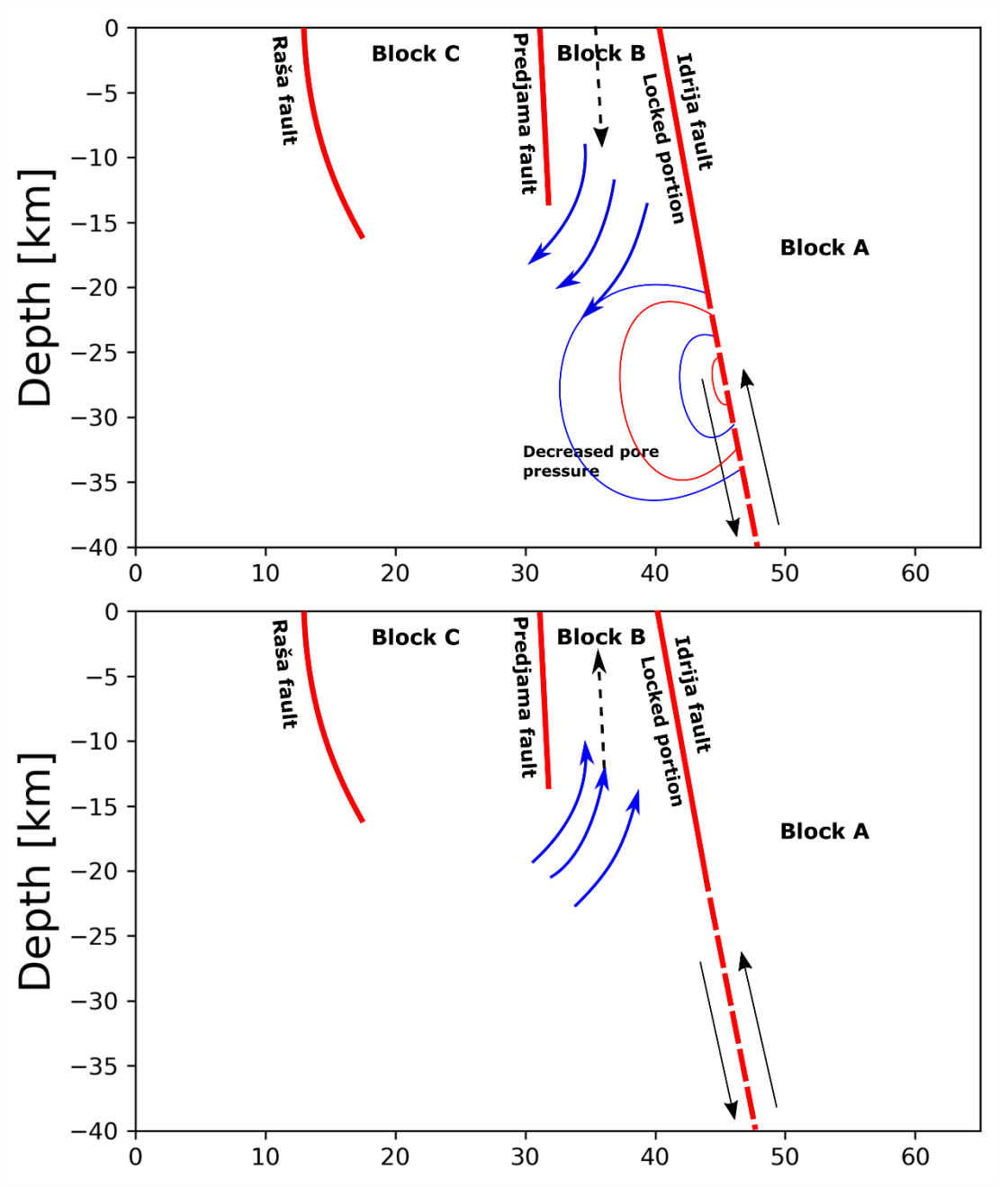

Figure 73: Proposed model of the aseismic transient in the 2009-2010 episode. Due to the slightly elevated creep rates beneath the locked portion of Idrija fault, fluids will first migrate away from the Block B due to the decreased pore pressures at depths and later migrate back promoting swarm activity along Predjama fault. Due to the migration of fluids, the Block B will first subside and after the return uplift to previous state.

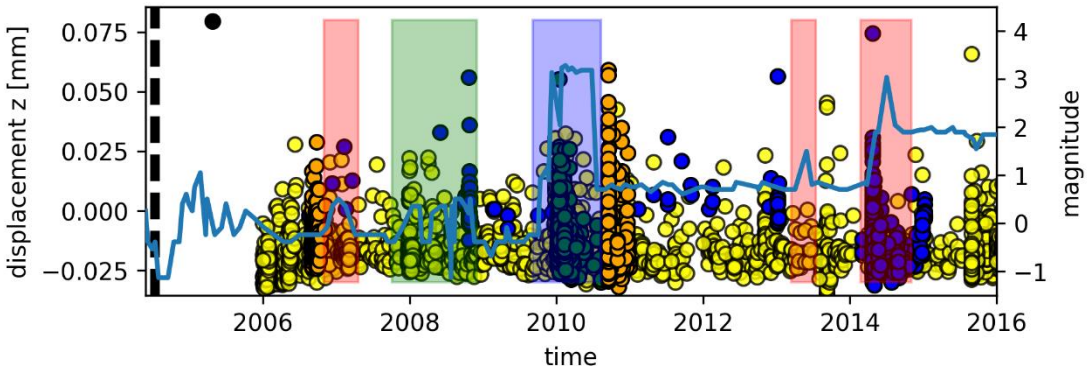

Figure 74: Changes in vertical axis of the Postojna extensometer. The 2009-2010 episode shows much bigger changes then other, except in the 2014, when a local M_W 4.5 happened some 20 km SW of the Postojna cave. Red rectangles show vertical changes after local earthquake activity, green show changes happening before the earthquake activity and blue at the same time as local earthquakes.

Similar episodes of the vertical changes along the Postojna cave extensometer, as the one that happened in the 2009 – 2010 can be observed also on the longer time scale – seemingly always connected to the local earthquakes (Gosar et al., 2009), either in the form of swarms or mainshock – aftershock activity. If we apply our proposed model of changes along the extensometer due to the pore pressure changes at the depth, we can observe a correlation between the fault causing the earthquakes regarding to the Postojna cave extensometer. Transient originating at Raša fault would cause migration of the fluids as observed on the extensometer following the earthquake activity, while transient originating at Idrija fault (Figure 74) would cause the change along the extensometer prior to the earthquakes, since there is some lag time between the beginning of the transient deformation and earthquake triggering. This is observed on Figure 74 as the coloured rectangles. In the last case of vertical change, longer duration of transient is most likely not a case, since the change on the extensometer is induced by a local M_W 4.5 earthquake and the response of fluids to sudden stress changes or migration of the fluids away from the Predjama fault due to the opening of cracks at the hypocentral area of the earthquake.

5.2.2 Driving mechanism

With constant loading of the Idrija fault at 0.01 bar as was used in the modelling phase, we are unable to explain wide spread triggering of earthquake activity along IFS in less than 10 years, as observed in the time span between 2006 and mid-2018. If the earthquake activity along IFS is really caused by the unclamping of the faults, due to the constant stress loading along the main fault of the system, we could argue that such "unclamping episode" happened in 1998 and 2004, causing the magnitude 5.6 and 5.4 earthquakes in the northern part of IFS. With 0.01 bar stress loading next such episode should follow in 2014 but it happened in 2009-2010 and again in 2nd half of 2017 in the southern part of the IFS. It is possible, that an aseismic transient deformation is the driving mechanism behind widespread earthquake triggering along the IFS in sense of slightly elevated creep rate beneath the seismogenic zone along Idrija fault. Other swarms and mainshocks related to the changes along the extensometer could be unrelated to any kind of transient deformation but only associated with migration of the fluids at the seismogenic depths due to the elevated earthquake activity in form of swarms or deformations related to the mainshock-aftershock activity. Aseismic deformations are driving active fault deformation in many tectonic settings, such as subduction zones with slow slip events, in volcanic environments as a deformation related to the migration of fluids and also in the areas of strike slip faulting, such as San Andreas fault in USA, Alpine fault in New Zealand and Great Anatolian fault in Turkey where repeating earthquakes show slight changes in the slip rate, as described in the previous chapter. Better understanding of the behaviour of the deformations related to the transient forcing along IFS can only be obtained with better knowledge of the physical properties of active faulting. Important step in the observation of IFS would bring dense network of continuous GPS stations perpendicular to the fault system, which would give us better constrains on possible periodic elevated slip rates over the faults and also better understanding of slip rate distribution over and between the faults comprising IFS.

With only limited knowledge obtained with high resolution relocation of micro earthquake activity and observations from the extensometer in Postojna cave, it is not possible to exactly define main style of transient deformation along IFS. Most likely, transient fluid migration can be ruled out, since the area is far away from any active volcanic system – deformation on the extensometer is indeed due to the migration of the

fluids, but this migration happens in the shallower part of the system as a response to pore pressure changes, related to the transient push. Slow slip event seems more reasonable since the transient most likely originates from the elevated slip rates beneath the seismogenic zone, deeper than 15 km along Idrija fault.

In this case, most likely candidate for transient deformation should be kind of a slow slip event, but at much smaller scales than what we can easily observe at the subduction zones and major strike slip faults around the world. Idrija fault itself is a slow slipping fault (2 mm/yr both combined in horizontal and dip component) at the depths, and the slow slip episode should not elevate the slip rate much. Such a mechanism could only be observed from space born geodetic observation on longer time scales with GPS monitoring both on the near fault and at the longer wavelengths which would enable us to sample deeper portion of the fault.

6. Conclusions

- To obtain as precise locations as possible we manually repicked all the automatically detected phases in the catalogue. By manually reviewing of all the available data we added additional micro earthquakes to the catalogue and by performing the cross correlation detection the final catalogue holds almost 12000 detected earthquakes from initial (automatic and manual) 8000.

- Idrija fault system is a system of right lateral strike slip active faults as was shown from relocation of the micro earthquake activity in the period between 2006 and mid-2018. Focal solutions of the earthquakes happening in this time scale mostly agree with the right lateral strike slip component observed from the geologic mapping of the area except of the Selce swarm sequence that happened in 2017 which shows extensional deformation but with the same strike. Relocated earthquake sequences agree are illuminating all the major active faults observed on the surface, namely Raša, Selce, Predjama, Idrija and Ravne fault.

- Geometry of the faults is partially observable from the relocated sequences. Raša fault is clearly defined in its central part, where clear trend from sub vertical fault at the surface to NE dipping fault at the depth is observed. In its southern part, where its geological extend is not clearly defined, the fault could either continue with approximate same geometry, or the relocated earthquakes illuminate a fault, striking under the angle to Raša fault. In the northern extend of the Raša fault, we were not able to obtain clear geometry. The earthquakes located in its northern part could be also contributed to other faults (Cividale) with termination of Raša fault at the northern part of central area.

Selce fault, fault located few km E of Raša fault is clearly visible from the relocation of the earthquakes in the central and southern part of the system. The fault can be traced along the surface in its central part in the Pivka basin, close to the town of Idrija.

Predjama fault is clearly geologically defined in Moulin et al. (2016) but not so clearly defined from the relocation of earthquakes. The broader area around Predjama fault is affected by earthquake activity, but only one swarm like sequence that happened in 2009 – 2011 can be directly connected to it.

Idrija fault is the biggest fault of IFS and is nicely expressed on the surface and

observable on DEM. Interestingly, earthquake activity only affects Idrija fault at its northern extend with no earthquakes in its central and southern extend. Since the seismic network has the same coverage in all the parts, seismic quiescence can't be contributed to missed earthquakes. It seems that the Idrija fault is locked in its central and southern extend, which coincide with the InSAR observations by Wang et al. (2018).

Ravne fault is the most active fault of the IFS with majority of the earthquakes happening in its northern part and some in the central part. The geometry of the fault is not well constrained, but most likely it is sub vertical at the surface and joining with Idrija fault at around 10 km of depth. In its northernmost part, Ravne fault also represent the change to Southern Alps thrusting tectonic regime which is observed in the focal mechanisms of some earthquakes. The earthquake activity along Ravne fault probably does not represent only the aftershocks of 1998 and 2004 earthquakes, since the activity, especially in its northernmost part does not show any strong decay valid for aftershock sequences.

- We observed that IFS exhibit temporal clustering of earthquake activity along the system. In the observed time period, two clusters were observed, a system wide cluster of mainshock–aftershock series and swarms in 2009–2011 and a spatially smaller but seismically more intense clustering in the southern part of the system in the second half of 2017.

The 2009 – 2011 event was modelled as a tectonic transient along Idrija fault along the deeper portion of the fault, beneath seismogenic zone. In this part, the fault is presumably freely creeping at approximately 2 mm/yr while during the tectonic transient the slip rate is slightly elevated. Elevated slip rate is enough to cause system wide unclamping of the faults and related earthquake activity. Transient was also observed at the surface on the extensometer in the Postojna cave along its vertical axis. The response of the extensimeter was contributed to the migration of fluids in the shallower parts of the crust, due to the pore pressure changes at the deeper portions, which are related directly to the tectonic transient.

- For better understanding of the behaviour of the IFS our knowledge of geology, seismology, paleoseismology and geodetic observations should be widened. Multidisciplinary monitoring of the system should be continuing with extending the seismic network in order to detect even smaller earthquakes and possible low frequency earthquakes and tectonic tremor typical for deep seated major faults. Paleoseismological

studies should be extended over all the active faults and better GPS network should be built in the area, giving us the ability to constrain better slip rates over the system and over individual faults and possible to detect future tectonic transients in shape of slow slip events.

References

Ambraseys, Nicholas N. 1976. *He Gemona Di Friuli Earthquake of 6 May 1976*.

Anderson, Helen and James Jackson. 1987. "Active Tectonics of the Adriatic Region." *Geophysical Journal of the Royal Astronomical Society* 91(3):937–83.

Aoudia, A., A. Saraò, B. Bukchin, and P. Suhadolc. 2000. "The 1976 Friuli (NE Italy) Thrust Faulting Earthquake: A Reappraisal 23 Years Later." *Geophysical Research Letters* 27(4):573–76.

Bajc, J., A. Aoudia, A. Sarao, and P. Suhadolc. 2001. "The 1998 Bovec-Krn Mountain (Slovenia) Earthquake Sequence." *Geophysical Research Letters* 28(9):1839–42.

Basili, R. et al. 2013. "The European Database of Seismogenic Faults (EDSF) Compiled in the Framework of the Project SHARE." *URL: Http://diss. Rm. Ingv. It/share-Edsf*.

Basili, Roberto et al. 2008. "The Database of Individual Seismogenic Sources (DISS), Version 3: Summarizing 20 Years of Research on Italy's Earthquake Geology." *Tectonophysics* 453(1):20–43.

Bavec, M and Atanackov, J and Celarc, B and Hajdas, I and Jamsek Rupnik, P and Jez, J and Kastelic, V and Milanic, B and Novak, M and Skaberne, D.and others. 2013. *Evidence of Idrija Fault Seismogenic Activity during the Late Holocene Including the 1511 Mm 6.8 Earthquake*.

Bechtold, M., M. Battaglia, D. C. Tanner, and D. Zuliani. 2009. "Constraints on the Active Tectonics of the Friuli/NW Slovenia Area from CGPS Measurements and Three-Dimensional Kinematic Modeling." *Journal of Geophysical Research* 114(B3):B03408. Retrieved (http://doi.wiley.com/10.1029/2008JB005638).

Benedetti, Lucilla, Paul Tapponnier, Geoffrey C. P. King, Bertrand Meyer, and Isabelle Manighetti. 2000. "Growth Folding and Active Thrusting in the Montello Region, Veneto, Northern Italy." *Journal of Geophysical Research: Solid Earth* 105(B1):739–66.

Beyreuther, Moritz et al. 2010. "ObsPy: A Python Toolbox for Seismology." *Seismological Research Letters* 81(3):530–33.

Di Bona, Massimo. 2016. "A Local Magnitude Scale for Crustal Earthquakes in Italy." *Bulletin of the Seismological Society of America* 106(1):242–58.

Borghi, Alessandra, Abdelkrim Aoudia, Riccardo E. M. Riva, and Riccardo Barzaghi. 2009. "GPS Monitoring and Earthquake Prediction: A Success Story towards a Useful Integration." *Tectonophysics* 465(1–4):177–89.

Bragato, Pier Luigi et al. 2014. "The Central and Eastern European Earthquake Research Network-CE3RN." in *EGU General Assembly Conference Abstracts*, vol. 16.

Bressan, Gianni, Stefano Kravanja, and Gianlorenzo Franceschina. 2007. "Source Parameters and Stress Release of Seismic Sequences Occurred in the Friuli-Venezia Giulia Region (Northeastern Italy) and in Western Slovenia." *Physics of the Earth and Planetary Interiors* 160(3–5):192–214.

Briestensky, Miloš et al. 2015. "Evidence of a Plate-Wide Tectonic Pressure Pulse Provided by Extensometric Monitoring in the Balkan Mountains (Bulgaria)." *Geologica Carpathica* 66(5):427–38.

Burrato, Pierfrancesco et al. 2008. "Sources of M W 5+ Earthquakes in Northeastern Italy and Western Slovenia: An Updated View Based on Geological and Seismological Evidence." *Tectonophysics* 453(1):157–76.

Buser, Stanko. 2009. "Geological Map of Slovenia 1:250.000."

Caporali, A. et al. 2008. "Geokinematics of Central Europe: New Insights from the CERGOP-2/Environment Project." *Journal of Geodynamics* 45(4–5):246–56.

Caporali, A., F. Neubauer, L. Ostini, G. Stangl, and D. Zuliani. 2013. "Modeling Surface GPS Velocities in the Southern and Eastern Alps by Finite Dislocations at Crustal Depths." *Tectonophysics* 590:136–50.

Chamberlain, Calum J., Carolin M. Boese, and John Townend. 2017. "Cross-Correlation-Based Detection and Characterisation of Microseismicity Adjacent to the Locked, Late-Interseismic Alpine Fault, South Westland, New Zealand." *Earth and Planetary Science Letters* 457:63–72.

Chamberlain, Calum J., David R. Shelly, John Townend, and Tim A. Stern. 2014. "Low-Frequency Earthquakes Reveal Punctuated Slow Slip on the Deep Extent of the Alpine Fault, New Zealand." *Geochemistry, Geophysics, Geosystems* 15(7):2984–99.

Cheloni, Daniele et al. 2017. "Aseismic Transient during the 2010–2014 Seismic Swarm: Evidence for Longer Recurrence of M ≥ 6.5 Earthquakes in the Pollino Gap (Southern Italy)?" *Scientific Reports* 7(1):576. Retrieved (http://www.nature.com/articles/s41598-017-00649-z).

Cunningham, Dickson, Stephen Grebby, Kevin Tansey, Andrej Gosar, and Vanja Kastelic. 2006. "Application of Airborne LiDAR to Mapping Seismogenic Faults in Forested Mountainous Terrain, Southeastern Alps, Slovenia." *Geophysical Research Letters* 33(20).

Čarman, Martina. 2011. *Earthquakes Near Ilirska Bistrica in 2010*.

Dewey, James W. 1971. "Seismicity Studies with the Method of Joint Hypocenter Determination." Retrieved (http://bssaonline.org/cgi/content/abstract/62/6/1711).

Dieterich, James H. and Brian D. Kilgore. 1994. "Direct Observation of Frictional Contacts: New Insights for State-Dependent Properties." *Pure and Applied Geophysics PAGEOPH* 143(1–3):283–302.

Dodge, D. A. and W. R. Walter. 2015. "Initial Global Seismic Cross-Correlation Results: Implications for Empirical Signal Detectors." *Bulletin of the Seismological Society of America*.

Dragoni, Michele, Maurizio Bonafede, and Enzo Boschi. 1984. "On the Interpretation of Slow Ground Deformation Precursory to the 1976 Friuli Earthquake." *Pure and Applied Geophysics PAGEOPH* 122(6):781–92.

Dreger, D. S. 1994. "Empirical Green's Function Study of the January 17, 1994 Northridge, California Earthquake." *Geophysical Research Letters* 21(24):2633–36.

Dreger, Douglas, Robert M. Nadeau, and Angela Chung. 2007. "Repeating Earthquake Finite Source Models: Strong Asperities Revealed on the San Andreas Fault." *Geophysical Research Letters* 34(23).

Evangelidis, C. P., K. I. Konstantinou, N. S. Melis, M. Charalambakis, and G. N. Stavrakakis. 2008. "Waveform Relocation and Focal Mechanism Analysis of an Earthquake Swarm in Trichonis Lake, Western Greece." *Bulletin of the Seismological Society of America* 98(2):804–11.

Fitzko, F., P. Suhadolc, A. Aoudia, and G. F. Panza. 2005. "Constraints on the Location and Mechanism of the 1511 Western-Slovenia Earthquake from Active Tectonics and Modeling of Macroseismic Data." *Tectonophysics* 404(1):77–90.

Galadini, F., M. E. Poli, and A. Zanferrari. 2005. "Seismogenic Sources Potentially Responsible for Earthquakes with M≥ 6 in the Eastern Southern Alps (Thiene-Udine Sector, NE Italy)." *Geophysical Journal International* 161(3):739–62.

Gibbons, Steven J. and Frode Ringdal. 2006. "The Detection of Low Magnitude Seismic Events Using Array-Based Waveform Correlation." *Geophysical Journal International* 165(1):149–66.

Giuliana Rossi, Maria Zadro. 1997. "Long-Term Crustal Deformations in NE Italy Revealed by Tilt-Strain Gauges." *Physics of the Earth and Planetary Interiors* 97(1–4):55–70.

Gosar, Andrej, Stanka Šebela, Blahoslav Košťák, and Josef Stemberk. 2011. "On the State of the TM 71 Extensometer Monitoring in Slovenia: Seven Years of Micro-Tectonic Displacement Measurements." *Acta Geodyn Geomater* 8(4):389–402.

Gosar, Andrej, Stanka Šebela, Blahoslav Koštak, and Josef Stemberk. 2009. "Surface Versus Underground Measurements of Active Tectonic Displacements with TM 71 Exstensometers in Slovenia." *Acta Carsologica* 38(2–3).

Grenerczy, Gyula, Ambrus Kenyeres, and István Fejes. 2000. "Present Crustal Movement and Strain Distribution in Central Europe Inferred from GPS Measurements." *Journal of Geophysical Research: Solid Earth* 105(B9):21835–46.

Guidarelli, Mariangela, Abdelkrim Aoudia, and Giovanni Costa. 2017. "3D Structure of the Crust and Uppermost Mantle at the Junction between the Southeastern Alps and External Dinarides from Ambient Noise Tomography." *Geophysical Journal International*.

Gutdeutsch, R and Lenhardt, W. 1996. "Seismological Interpretation of the South Alpine Earthquake of January 25th, 1348." *ESC General Assembly Reykjavik Abstract W*.

Handy, Mark R., Stefan M. Schmid, Romain Bousquet, Eduard Kissling, and Daniel Bernoulli. 2010. "Reconciling Plate-Tectonic Reconstructions of Alpine Tethys with the Geological-Geophysical Record of Spreading and Subduction in the Alps." *Earth-Science Reviews* 102(3–4):121–58.

Hutton, L. K. and David M. Boore. 1987. "The ML Scale in Southern California." *Bulletin of the Seismological Society of America* 77(6):2074–94.

Igarashi, Toshihiro, Toru Matsuzawa, and Akira Hasegawa. 2003. "Repeating Earthquakes and Interplate Aseismic Slip in the Northeastern Japan Subduction Zone." *Journal of Geophysical Research: Solid Earth* 108(B5).

International Seismological Centre. 2014. "On-Line Bulletin."

Kao, Honn et al. 2005. "A Wide Depth Distribution of Seismic Tremors along the Northern Cascadia Margin." *Nature* 436(7052):841–44. Retrieved (http://www.nature.com/doifinder/10.1038/nature03903).

Kastelic, V., M. Vrabec, D. Cunningham, and A. Gosar. 2008. "Neo-Alpine Structural Evolution and Present-Day Tectonic Activity of the Eastern Southern Alps: The Case of the Ravne Fault, NW Slovenia." *Journal of Structural Geology* 30(8):963–75.

Kastelic, V., M. Živčić, J. Pahor, and A. Gosar. 2004. "Seismotectonic Characteristics of the 2004 Earthquake in Krn Mountains." *Potresi v Letu* 78–87.

Kastelic, Vanja and Michele Carafa. 2012. "Fault Slip Rates for the Active External Dinarides Thrust-and-Fold Belt." *Tectonics* 31(3).

Kennet, B. L. N. 1991. "IASPEI 1991 Seismological Tables." *Terra Nova* 3(2):122.

King, Geoffrey, C. P. King, Ross S. Stein, and Jian Lin. 1994. "Static Stress Changes and the Triggering of Earthquakes." *Bulletin of the Seismological Society of America* 84(3):935–53.

Lenhardt, W., Pesaresi, D., Živčić, M., Costa, G., Kuk, K., Bondár, I., Duni, L., Spacek, P., Dimitrova, L., and Popa, M. 2016. "The Central and East European Earthquake Research Network (CE3RN): Current Status and Future Perspectives."

Lippitsch, Regina. 2003. "Upper Mantle Structure beneath the Alpine Orogen from High-Resolution Teleseismic Tomography." *Journal of Geophysical Research* 108(B8):2376. Retrieved (http://doi.wiley.com/10.1029/2002JB002016).

Lomax, A. 2011. "NonLinLoc: Probabilistic, Non-Linear, Global-Search Earthquake Location in 3D Media."

Main, Ian. 1996. "Statistical Physics, Seismogenesis, and Seismic Hazard." *Reviews of Geophysics* 34(4):433.

Massin, Frédérick, Jamie Farrell, and Robert B. Smith. 2013. "Repeating Earthquakes in the Yellowstone Volcanic Field: Implications for Rupture Dynamics, Ground Deformation, and Migration in Earthquake Swarms." *Journal of Volcanology and Geothermal Research* 257:159–73.

Mazzotti, Stéphane and John Adams. 2004. "Variability of near-Term Probability for the next Great Earthquake on the Cascadia Subduction Zone." *Bulletin of the Seismological Society of America* 94(5):1954–59.

Merchel, Silke et al. 2014. "Surface Exposure Dating of the Veliki Vrh Rock Avalanche in Slovenia Associated with the 1348 Earthquake." *Quaternary Geochronology* 22:33–42.

Mogi, Kiyoo. 1963. “Some Discussions on Aftershocks, Foreshocks and Earthquake Swarms: The Fracture of a Semi-Infinite Body Caused by an Inner Stress Origin and Its Relation to the Earthquake Phenomena (Third Paper).” *Bulletin of the Earthquake Research Institute* (41):615–18.

Moulin, Adrien et al. 2014. “Determining the Present-Day Kinematics of the Idrija Fault (Slovenia) from Airborne LiDAR Topography.” *Tectonophysics* 628:188–205.

Moulin, Adrien et al. 2016. “The Dinaric Fault System: Large-Scale Structure, Rates of Slip, and Plio-Pleistocene Evolution of the Transpressive Northeastern Boundary of the Adria Microplate.” *Tectonics* 35(10):2258–92.

Nadeau, R. M. 2005. “Nonvolcanic Tremors Deep Beneath the San Andreas Fault.” *Science* 307(5708):389–389. Retrieved (http://www.sciencemag.org/cgi/doi/10.1126/science.1107142).

Nocquet, Jean-Mathieu. 2012. “Present-Day Kinematics of the Mediterranean: A Comprehensive Overview of GPS Results.” *Tectonophysics* 579:220–42.

Nur, Amos and John R. Booker. 1972. “Aftershocks Caused by Pore Fluid Flow?” *Science* 175(4024):885–87. Retrieved (http://www.ncbi.nlm.nih.gov/pubmed/17781062).

O’Brien, P. J. 2001. “Subduction Followed by Collision: Alpine and Himalayan Examples.” *Physics of the Earth and Planetary Interiors* 127(1–4):277–91.

Parotidis, M., E. Rothert, and S. A. Shapiro. 2003. “Pore-Pressure Diffusion: A Possible Triggering Mechanism for the Earthquake Swarms 2000 in Vogtland/NW-Bohemia, Central Europe.” *Geophysical Research Letters* 30(20):n/a-n/a. Retrieved (http://doi.wiley.com/10.1029/2003GL018110).

Perfettini, H. and J. P. Avouac. 2004. “Postseismic Relaxation Driven by Brittle Creep: A Possible Mechanism to Reconcile Geodetic Measurements and the Decay Rate of Aftershocks, Application to the Chi-Chi Earthquake, Taiwan.” *Journal of Geophysical Research: Solid Earth* 109(B2). Retrieved (http://doi.wiley.com/10.1029/2003JB002488).

Perfettini, Hugo and J. P. Avouac. 2007. “Modeling Aftership and Aftershocks Following the 1992 Landers Earthquake.” *Journal of Geophysical Research: Solid Earth* 112(7).

Placer, Ladislav. 1999. “Contribution to the Macrotectonic Subdivision of the Border Region between Southern Alps and External Dinarides.” *Geologija* 41(1998):223–55.

Placer, Ladislav. 2008a. “Principles of the Tectonic Subdivision of Slovenia.” *Geologija* 51(2):205–17.

Placer, Ladislav. 2008b. “Vipavski Prelom.” *Geologija* 51:101–5.

Placer, Ladislav, Marko Vrabec, and Bogomir Celarc. 2010. “The Bases for Understanding of the NW Dinarides and Istria Peninsula Tectonics.” *Geologija* 53(1):55–86.

Poljak, Marijan, Mladen Živčić, and Polona Zupančič. 2000. "The Seismotectonic Characteristics of Slovenia." Pp. 37–55 in *Seismic Hazard of the Circum-Pannonian Region*. Springer.

Reasenberg, P. a and R. W. Simpson. 1992. "Response of Regional Seismicity to the Static Stress Change Produced by the Loma Prieta Earthquake." *Science (New York, N.Y.)* 255(5052):1687–90.

Ribarič, Vladimir. 1982. *Seismicity of Slovenia; Catalogue of Earthquakes (792 AD--1981).* Seizmolo{š}ki zavod SR Slovenije.

Richter, Charles F. 1935. "An Instrumental Earthquake Magnitude Scale." *Bulletin of the Seismological Society of America* 25(1):1–32.

Rižnar, Igor, Božo Koler, and Miloš Bavec. 2007. "Recentna Aktivnost Regionalnih Geoloških Struktur v Zahodni Sloveniji." *Geologija* 50(1):111–20.

Sarao, A and Staff, Centro Richerche Sismologiche. 2013. "On Line Catalogue of Moment Tensor Solutions of Earthquakes Occured in NE Italy and Its Surroundings since 2009."

Sarao, A and Staff, Centro Richerche Sismologiche. 2016. "On Line Catalogue of Moment Tensor Solutions of Earthquakes Occurred in NE Italy and Its Surroundings in the Period 2014-2016."

Savage, Jc and Jl Svarc. 1997. "Postseismic Deformation Associated with the 1992 Mw = 7.3 Landers Earthquake, Southern California." *Journal of Geophysical Research: Solid …* 102(97):7565–77. Retrieved (http://onlinelibrary.wiley.com/doi/10.1029/97JB00210/full).

Schaff, David P. and Paul G. Richards. 2011. "On Finding and Using Repeating Seismic Events in and near China." *Journal of Geophysical Research: Solid Earth* 116(B3).

Scholz, CH H. 1968. "The Frequency-Magnitude Relation of Microfracturing in Rock and Its Relation to Earthquakes." *Bulletin of the Seismological Society of America* 58(1):399–415. Retrieved (http://www.bssaonline.org/cgi/content/abstract/58/1/399).

Shelly, David R., Gregory C. Beroza, and Satoshi Ide. 2007. "Non-Volcanic Tremor and Low-Frequency Earthquake Swarms." *Nature* 446(7133):305.

Shelly, David R., William L. Ellsworth, and David P. Hill. 2016. "Fluid-Faulting Evolution in High Definition: Connecting Fault Structure and Frequency-Magnitude Variations during the 2014 Long Valley Caldera, California, Earthquake Swarm." *Journal of Geophysical Research: Solid Earth* 121(3):1776–95.

Shemeta, Julie and Paul Anderson. 2010. "It's a Matter of Size: Magnitude and Moment Estimates for Microseismic Data." *The Leading Edge* 29(3):296–302.

Snoke, J.Arthur. 2003. "FOCMEC: Focal Mechanism Determinations." *International Handbook of Earthquake and Engineering Seismology* 85:1629–30.

Stampfli, G. M. et al. 1998. "Subduction and Obduction Processes in the Swiss Alps." *Tectonophysics* 296(1–2):159–204.

Stampfli, G. M. and G. D. Borel. 2002. "A Plate Tectonic Model for the Paleozoic and Mesozoic Constrained by Dynamic Plate Boundaries and Restored Synthetic Oceanic Isochrons." *Earth and Planetary Science Letters* 196(1–2):17–33.

Stein, Ross S. 1999. "The Role of Stress Transfer in Earthquake Occurrence." *Nature* 402(6762):605–9.

Stucchi, Max et al. 2013. "The SHARE European Earthquake Catalogue (SHEEC) 1000--1899." *Journal of Seismology* 17(2):523–44.

Sykes, Lynn R. 1970. "Earthquake Swarms and Sea-Floor Spreading." *Journal of Geophysical Research* 75(32):6598–6611.

Šebela, S. 2005. "Tectonic Sights of the Pivka Basin." *Acta Carsologica* 34(3).

Šebela, Stanka, Andrej Gosar, Blahoslav Košťák, and Josef Stemberk. 2005. "Active Tectonic Structures in the W Part of Slovenia--Setting of Micro-Deformation Monitoring Net." *Acta Geodyn. Geomater* 2(1):45–57.

Thurber, Clifford H. 1985. "Nonlinear Earthquake Location: Theory and Examples." *Bulletin of the Seismological Society of America* 75(3):779–90.

Uchida, Naoki et al. 2012. "Source Parameters of Microearthquakes on an Interplate Asperity off Kamaishi, NE Japan over Two Earthquake Cycles." *Geophysical Journal International* 189(2):999–1014.

Utsu, Tokuji, Yosihiko Ogata, Ritsuko S, and Matsu'ura. 1995. "The Centenary of the Omori Formula for a Decay Law of Aftershock Activity." *Journal of Physics of the Earth* 43(1):1–33. Retrieved (http://joi.jlc.jst.go.jp/JST.Journalarchive/jpe1952/43.1?from=CrossRef).

Vidrih, R and Cecic, I and Sincic, P. 1995. "The Ljubljana, Slovenia Earthquake on April 14th, 1895." *Geophysical Survey of Slovenia, Ljubljana*.

Vrabec, Marko and László Fodor. 2006. "Late Cenozoic Tectonics of Slovenia: Structural Styles at the Northeastern Corner of the Adriatic Microplate." *The Adria Microplate: GPS Geodesy, Tectonics and Hazards* 151–68.

Waldhauser, Felix. 2001. "hypoDD--A Program to Compute Double-Difference Hypocenter Locations (hypoDD Version 1.0-03/2001)." *US Geol. Surv. Open-File Rept. 01* 113.

Weber, John et al. 2010. "GPS-Derived Motion of the Adriatic Microplate from Istria Peninsula and Po Plain Sites, and Geodynamic Implications." *Tectonophysics* 483(3):214–22.

Wech, A. G., C. M. Boese, T. A. Stern, and J. Townend. 2012. "Tectonic Tremor and Deep Slow Slip on the Alpine Fault." *Geophysical Research Letters* 39(10).

Wells, Donald L. and Kevin J. Coppersmith. 1994. "New Empirical Relationships among Magnitude, Rupture Length, Rupture Width, Rupture Area, and Surface Displacement." *Bulletin of the Seismological Society of America* 84(4):974–1002.

Withers, Mitchell et al. 1998. "A Comparison of Select Trigger Algorithms for Automated Global Seismic Phase and Event Detection." *Bulletin of the Seismological Society of America* 88(1):95–106.

Yukutake, Yohei et al. 2011. “Fluid-Induced Swarm Earthquake Sequence Revealed by Precisely Determined Hypocenters and Focal Mechanisms in the 2009 Activity at Hakone Volcano, Japan.” *Journal of Geophysical Research: Solid Earth* 116(4).

Zupančič, P. et al. 2001. “The Earthquake of 12 April 1998 in the Krn Mountains (Upper Soča Valley, Slovenia) and Its Seismotectonic Characteristics.” *Geologija* 44(1):169–92.